**UNIVERSITÀ DEGLI STUDI DI MILANO**

**GRADUATE SCHOOL OF CLINICAL AND EXPERIMENTAL BIOMEDICAL SCIENCES**

***PhD Course in Experimental Pathology and Neuropathology***

**Cycle XXVIII Med/04**

# *The role of the sarcomeric protein myopalladin in skeletal and cardiac muscle structure, function, and disease*

**PhD Student:** *Maria Carmela Filomena*
**Identification number:** R10282

**Supervisor:** Prof. Massimo Locati
**Tutor:** Dr. Marie-Louise Bang

**Academic Year 2014/2015**

**UNIVERSITÀ DEGLI STUDI DI MILANO**

**Facoltà di Medicina e Chirurgia**

**Dipartimento di Biotecnologie Mediche e Medicina Traslazionale**

**Corso di Dottorato di Ricerca in**

**Patologia e Neuropatologia Sperimentali**

**Ciclo XXVIII Med/04**

# *Il ruolo della proteina sarcomerica miopalladina nella struttura, nella funzione e nella patologia del muscolo scheletrico e cardiaco*

**Dottoranda:** *Maria Carmela Filomena*
**Matricola:** R10282

**Relatore:** Prof. Massimo Locati
**Tutor:** Dr. Marie-Louise Bang

**Anno accademico 2014/2015**

# TABLE OF CONTENTS

**ABSTRACT**

**INTRODUCTION** ..... **1**

**1. INTRODUCTION TO MUSCLE TISSUE** ..... **1**

1.1 The origin of muscle tissue ..... 1

1.2 From whole striated muscle to sarcomere ..... 5

1.3 The organization of thin and thick filaments ..... 6

1.4 Muscle fiber types ..... 10

1.5 Muscle contraction ..... 12

1.6 Myofibrillogenesis ..... 13

**2. THE SARCOMERIC Z-LINE** ..... **14**

2.1 The structure and expression of Myopalladin and Palladin ..... 17

2.2 Interaction partners of Myopalladin and Palladin ..... 18

**3. THE SRF-MRTF SIGNALING PATHWAY** ..... **19**

3.1 The MRTFs ..... 23

**4. MYPN MUTATIONS IN SKELETAL AND CARDIAC DISEASES** ..... **25**

**AIM OF THE PHD THESIS** ..... **29**

**MATERIAL AND METHODS** ..... **31**

**1. *IN VIVO* METHODS** ..... **31**

1.1 Generation of Myopalladin knockout (MKO) mice ..... 31

1.2 Mouse procedures ..... 32

1.3 Treadmill running ..... 33

1.4 *In vivo* cardiac physiology ..... 33

**2. *EX VIVO* METHODS** ..... **34**

2.1 Mechanical analyses ..... 34

2.2 Isolation of adult ventricular cardiomyocytes (CMCs) ..... 36

2.3 Transmission Electron Microscopy (TEM) ..... 36

2.4 Histology and immunofluorescence ..... 37

**3. *IN VITRO* METHODS** ..... **38**

3.1 Cell culture ..... 38

3.1.1 Primary skeletal muscle cells ..... 38

3.1.2 C2C12 cells ..... 39

3.1.3 HEK293 cells ..... 39

3.2 SRF-luciferase reporter assay ..... 39

3.3 Co-Immunoprecipitation (Co-IP) ... 40
**4. Biochemistry and Molecular biology ... 41**
4.1 Plasmid constructs ... 41
4.2 Yeast techniques ... 42
4.2.1 Yeast two-hybrid screening ... 42
4.3 Actin assays ... 44
4.3.1 Protein expression and purification ... 44
4.3.2 Actin co-sedimentation assays ... 44
4.3.3. Fluorescence microscopy of actin filament bundles ... 45
4.3.4 Pyrene fluorescence assay ... 45
4.4 RNA analyses ... 45
4.4.1 RNA Extraction, RNA Reverse Transcription, and Quantitative Real-Time Polymerase Chain Reaction (qRT-PCR) ... 45
4.4.2 RNA sequencing ... 46
4.4.3 RNA sequencing analysis ... 46
4.5 Protein assays ... 47
4.5.1 Protein extraction ... 47
4.5.2 Determination of protein concentration ... 47
4.5.3 SDS-Polyacrylamide Gel Electrophoresis (SDS-PAGE) ... 47
4.5.4 Western blot analysis ... 49
**5. Statistical analysis ... 50**
**RESULTS ... 51**
**1. THE ROLE OF MYPN IN THE ORGANIZATION OF THE ACTIN CYTOSKELETON ... 51**
1.1 MYPN binds and bundles F-actin and promotes actin polymerization ... 51
1.2 MYPN binds to MRTFs and promotes MRTF-induced SRF signaling in C2C12 myogenic cells ... 53
**2. Generation of MYPN knockout (MKO) mice ... 54**
2.1 Skeletal muscle MKO phenotype ... 54
2.1.1 MKO mice are smaller compared to WT littermates and have reduced skeletal muscle fiber cross sectional area (CSA) ... 54
2.1.2 Progressive Z-line widening in MKO skeletal muscle ... 55
2.1.3 MKO mice are more susceptible to exercise-induced injury ... 56
2.1.4 Recovery following $BaCl_2$-induced skeletal muscle injury ... 57
2.1.5 Muscle denervation-induced atrophy ... 58
2.1.6 The absence of MYPN affects specific force and power output in EDL muscle (Collaboration with Prof. Marco Linari, University of Florence, Florence, Italy) ... 59
2.1.6.1 Effect of the absence of myopalladin on force per myosin motor ... 61

2.1.6.2 Force-pCa relation ..... 62
2.1.7 MYPN is expressed during myoblast differentiation ..... 63
2.1.8 Reduced myoblast differentiation rate in MKO mice compared to WT ..... 63
2.1.9 RNA-Sequencing (RNA-Seq) reveals abnormal SRF signaling in MKO mice ..... 64
2.1.10 No changes in protein synthesis and degradation in MKO muscle ..... 66
2.1.11 Upregulation of PAK1 in MKO skeletal muscle ..... 66
2.2 Cardiac Phenotype of MKO Mice ..... 68
2.2.1 Histological and ultrastructural analyses of MKO mouse hearts ..... 68
2.2.2 Echocardiographic analysis reveals progressive cardiac dilation and systolic dysfunction in MKO mice ..... 69
2.2.3 MKO mouse hearts develop chamber dilation and significantly reduced cardiac function following transaortic constriction (TAC) ..... 69
2.2.4 Activation of AKT and ERK in MKO mice following TAC ..... 70
**DISCUSSION ..... 72**
**REFERENCES ..... 75**

# ABSTRACT

Myopalladin (MYPN) is a striated muscle-specific sarcomeric protein belonging to the small palladin/myopalladin/myotilin family of actin-associated immunoglobulin-containing proteins [1]. Within the sarcomeric Z-line, MYPN binds to α-actinin, nebulin, and PDZ-LIM proteins [1, 2]. Furthermore, it is present in the nucleus and the I-band where it binds to the stress-inducible transcriptional cofactor CARP/Ankrd1, which, in turn, binds to the I-band region of titin, suggesting a role of MYPN in mechanosensing [1, 3]. The important role of MYPN in striated muscle is illustrated by the identification of *MYPN* mutations in human patients with dilated (DCM), hypertrophic (HCM), and restrictive (RCM) cardiomyopathy [4-6].

In our biochemical studies we demonstrated that MYPN, like PALLD, can bind and bundle filamentous actin (F-actin), thereby promoting actin polymerization. Moreover, we found that, similar to PALLD, MYPN interacts with MRTF-A and strongly increases MRTF-A-mediated activation of serum response factor (SRF) signaling, required for skeletal and cardiac muscle growth, maturation, and differentiation [7-11].

To determine the role of MYPN *in vivo*, we generated MYPN knockout (MKO) mice. MKO mice were significantly smaller compared to wildtype (WT) mice and had an about 30% reduction in skeletal muscle cross-sectional area (CSA) at all ages. Consistently, reduced differentiation rate and myotube width was observed in primary skeletal muscle cultures derived from MKO mice. Furthermore, studies of muscle performance in 2-month-old MKO mice showed reduced isometric force and power during isotonic shortening at any load as a result of the reduced cross sectional area, whereas the force developed by each myosin molecular motor was unaffected. By up- and downhill treadmill running, MKO and WT mice performed similarly. However, while the performance of WT mice was unaffected following four consecutive days of downhill running, the performance of MKO mice decreased progressively and Z-line damage was observed. Consistent with a higher susceptibility to muscle damage, progressive Z-line widening was observed in MKO skeletal muscle from about 8 months of age. RNAseq revealed downregulation of actin isoforms and other SRF-target genes in MKO muscle both at 2 and 4 weeks of age, suggesting that the smaller skeletal muscle fiber size in MKO mice is due to reduced SRF activity.

Cardiac analyses of MKO mice showed no cardiac phenotype at young age but the development of progressive cardiac dilation and decreased fractional shortening. On the other hand, in response to mechanical pressure overload induced by transaortic constriction (TAC),

MKO mice quickly developed cardiac dilation and reduced cardiac function accompanied by activation of the MAPK and AKT signaling pathways.

Ongoing investigations are focused on studying the precise mechanism by which MYPN modulates actin dynamics through the Rho-MRTF-SRF signaling pathway as well as understanding the mechanisms leading from *MYPN* mutations to cardiomyopathy.

# INTRODUCTION

## 1. INTRODUCTION TO MUSCLE TISSUE

Muscle tissue is one of the four fundamental types of tissue present in animals and is specialized in the transformation of chemical energy into movement. Movement is essential to life and takes many forms, ranging from the beating movement of cilia and intracellular transport between different compartments at the microscopic level to the explosive performance of a sprinter at the macroscopic level. Only a few families of proteins are responsible for movement in the biological world, so muscle has developed to optimize this function.

### 1.1 The origin of muscle tissue

There are three types of muscle tissue recognized in vertebrates: skeletal, cardiac, and smooth muscle [12]. The structure and organization of the contractile apparatus as well as the arrangement of muscle fibers (**myofibers**) differ between the three muscle types, reflecting the divergent cell functions (Fig 1).

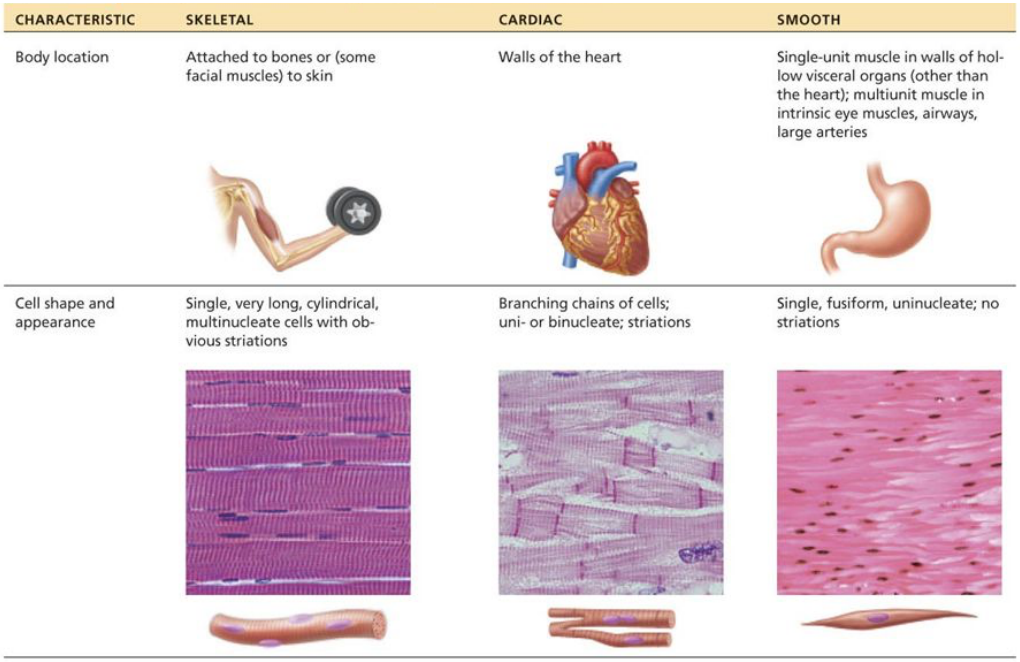



**Figure 1. The three different muscle types in vertebrates: skeletal, cardiac, and smooth muscle.** Skeletal muscle consists of multinuclear muscle fibers containing myofibrils that are responsible for the striated appearance of the cells. Cardiac muscle is also striated, but unlike skeletal muscle, cardiac muscle fibers branch and are interconnected via intercalated discs. Smooth muscle consists of splindle-shaped cells lacking cross-striations (*Copyright © 2010 Pearson Education, Inc. Three Types of Muscle Tissue 1.Skeletal muscle tissue: Attached to bones and skin Striated Voluntary - i.e., conscious control*).

During development, the three different types of muscle cells develop from the mesodermal germ layer. The formation of the mesoderm starts approximately 6.5 days post-coitum (dpc) in the mouse embryo, after which it undergoes an anatomic separation into the paraxial, intermediate, and lateral mesoderm with respect to its position from the body axis.

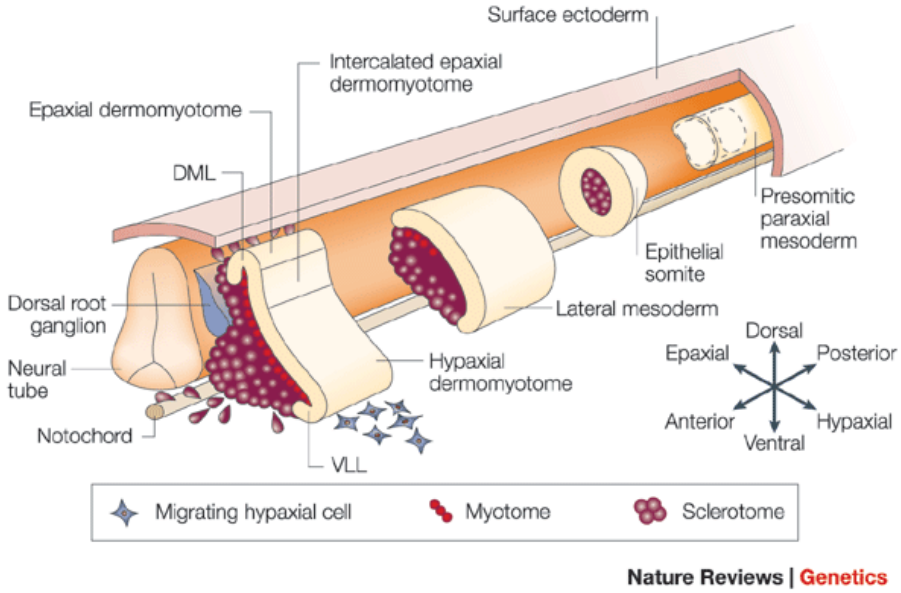



**Figure 2. The embryonic origin of limb and trunk skeletal muscle.** Segmentation of the paraxial mesoderm into somites occurs along the dorsal-ventral axis and in a rostral to caudal direction. In response to signals from the notochord and the neural tube, somites differentiate into the dermomyotome and the sclerotome. The dermomyotome is subdivided into the hypaxial and the epaxial dermomyotome, and is the source of cells for the lateral trunk musculature and deep back musculature, respectively. Cells of the dorsal medial lip (DML) migrate under the dermomyotome to form the epaxial myotome. A similar event occurs at the ventral lateral lip (VLL), which results in the formation of the hypaxial myotome. Cells of the VLL also undergo an epithelial to mesenchymal transition, delaminate and migrate to regions of presumptive intercostal, abdominal, and limb musculature [13].

All vertebrate skeletal muscles, with the exception of some head muscles, derive from the paraxial mesoderm, which runs alongside the body axis, flanking the neural tube (Fig. 2). Since embryonic day 8 (E8), blocks of the anterior paraxial mesoderm called **somites** form on both sides of the neural tube following a rostro-caudal developmental gradient, which includes Fibroblast Growth Factor (FGF), Wnt, and retinoic acid pathways [14, 15]. In the caudal part of the paraxial mesoderm, the high concentrations of FGF and Wnt retain cells in an undifferentiated state [16], but as they move rostrally, they form the somite unit, which exits the paraxial mesoderm and rapidly differentiates into the ventral **sclerotome,** which gives rise to cartilage and bone, and the dorsal **dermomyotome** (**DM**), which divides into the **dermatome** and the **myotome**. The dermatome generates the mesenchymal connective tissue of the back skin, the dermis, while the myotome forms the muscles of the back, the body wall, and the limbs [13, 17-20]. The myoblasts proliferate without differentiating until growth factors are depleted, after which the myoblasts align and finally fuse to form **myotubes** that

are multinucleated skeletal muscle cells [21]. The myotubes become organized into muscle fibers that are typically 50 μm in diameter and can be up to 50 cm long. The cell nuclei are located just under the cell membrane and the bulk of the cytoplasm is made up of parallel **myofibrils**, which are 1-2 μm in diameter and composed of repeating contractile units known as **sarcomeres**. Sarcomeres are about 2.5 μm long and 1-2 μm in diameter and are responsible for the *striated* appearance of skeletal muscle cells [22, 23].

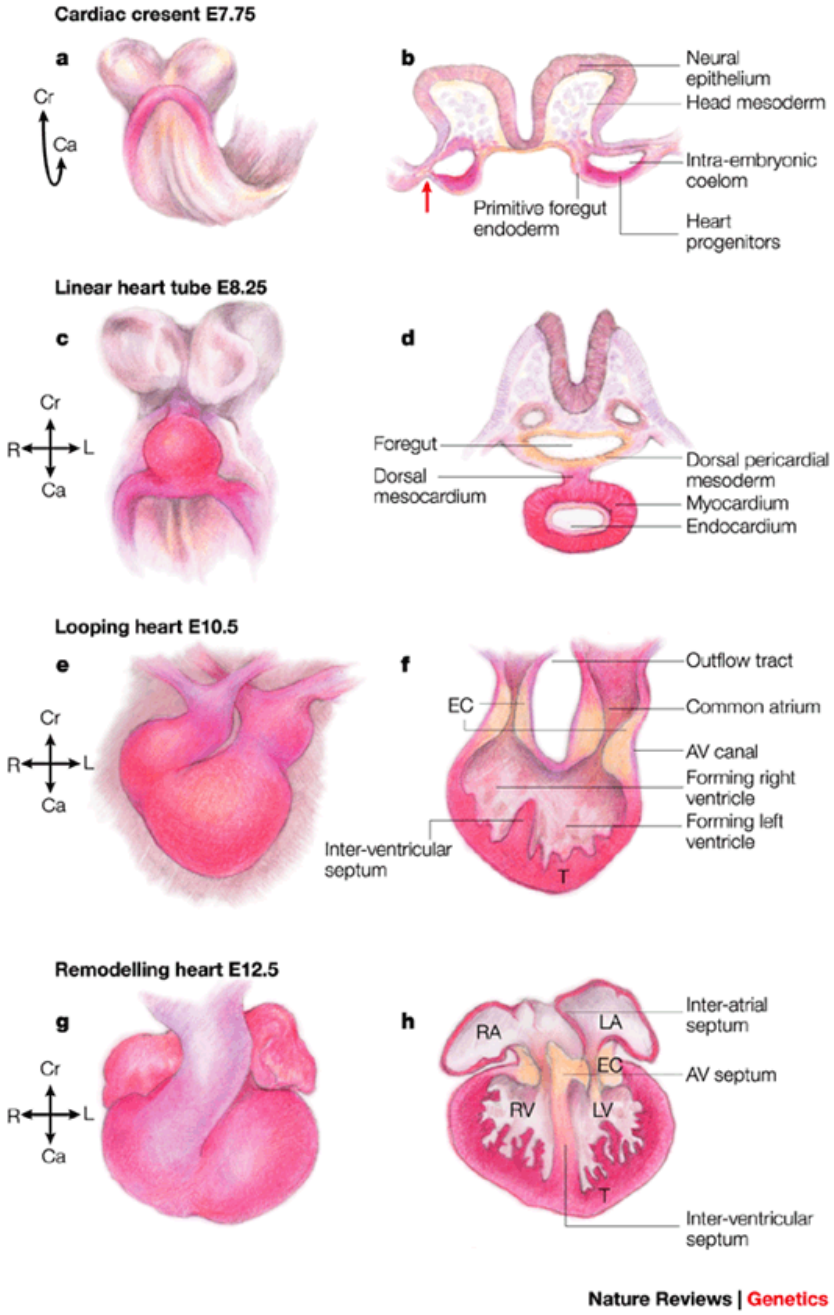



**Figure 3. Heart development.** The isolated heart is shown on the left, while on the right, a representative section (transverse in panels b and d; longitudinal in panels f and h) illustrates the main internal features. All views are ventral. Staging in days of embryonic development (E) is based on mouse development. EC, endocardial cushions; AV, atrioventricular canal; T, trabeculae; LV and RV, left and right ventricles; LA and RA, left and right atria; Ca, caudal (inferior); Cr, cranial (superior); L, left; R, right [24].

The heart originates from the anterior lateral plate mesoderm and is the first functional organ to be formed in vertebrates [21, 24-26]. Soon after gastrulation, signals from the adjacent endoderm cause progenitor cells within the anterior lateral plate mesoderm to become committed to a cardiogenic fate [27]. The cardiac precursor cells form bilaterally symmetric regions of mesordermal cells, called the **cardiogenic mesoderm**. The two cardiogenic layers migrate towards the ventral midline where they fuse in an anterior-to-posterior progression to form the primitive heart tube, consisting of an outer myocardium and an inner endocardium separated by an extracellular gelatinous matrix called the **cardiac jelly**. Before fusion is completed, the straight tubular heart initiates rhythmic contractions and then undergoes rightward looping, followed by chamber formation: two smaller atria (right, RA and left, LA) on the top, and two bigger ventricles (right, RV and left, LV) on the bottom, separated by a thick wall called the **intraventricular septum** [21, 24-26] (Fig. 3).

Cardiac muscle cells, also known as **cardiomyocytes**, make up the contractile portion of the heart wall. They are cylindrical, generally short (about 100 μm) fibers that contain one or two non-dense, slightly elongated nuclei in the center [28]. Different from skeletal muscle cells, cardiomyocytes do not fuse to form multinucleated cells but are arranged in uninucleated branched cells longitudinally connected via **intercalated discs** (ICDs). ICDs consist of highly organized and specialized cell-cell junctions that ensure the electrochemical and mechanical coupling of cardiomyocytes during contraction [29-31]. In particular, ICDs are formed by three different types of protein complexes: i) **desmosomes**, which are essential for the mechanical stabilization of cardiomyocytes, anchoring the cell membrane to the intermediate filament network [32, 33]; ii) **fascia adherens junctions**, which tightly anchor cardiomyocytes by connecting the cell membrane to the actin cytoskeleton [33, 34]; and iii) **gap junctions**, which mediate intracellular communication, allowing small molecules (<1000 Da) to shuttle between adjacent cardiomyocytes during beating [35, 36].

Smooth muscle tissue derives from the lateral mesoderm and form the contractile portion of the stomach, intestine, uterus, the arterial walls, the ducts of the secretory glands, and other tissues in which slow and sustained contractions are needed [12]. Smooth muscle is composed of a large number of uninucleated spindle-shaped cells lacking cross-striations [37]. Indeed, the contractile apparatus of smooth muscle cells is not arranged in ordered parallel myofibrils as in the striated muscle but extends alongside the major axis of cells and is attached to the plasma membrane. This contractile apparatus does not contract as rapidly as the myofibrils in striated muscle cells but allows for a greater degree of shortening [12].

The following sections will focus on the contractile machinery found in vertebrate striated muscles, since their structural unit, the sarcomere, is structurally the best characterized system.

## 1.2 From whole striated muscle to sarcomere

Myofiber arrangement and architecture within muscles are important factors determining their functional and contractile properties. The characteristic cross-striation pattern of skeletal and cardiac muscle as observed by light microscopy arises from the alternation of ordered arrays of **thick** and **thin myofilaments** [38, 39] (Fig. 4).

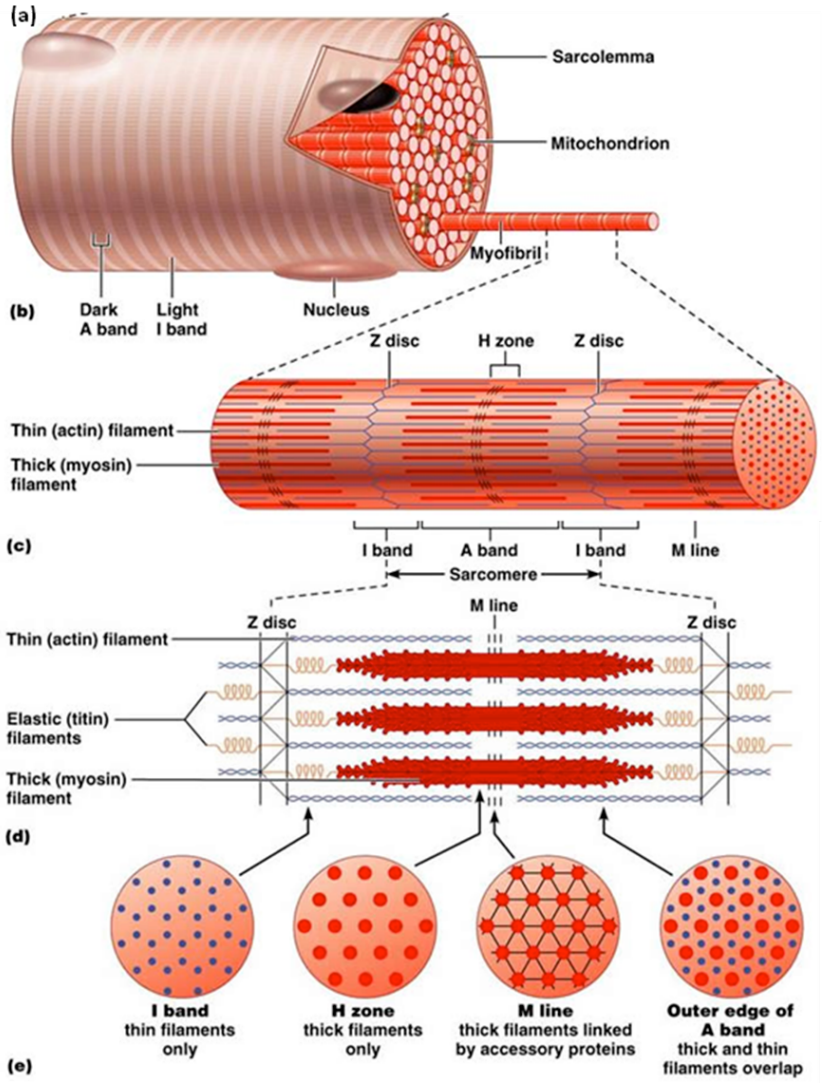



**Figure 4. Schematic diagrams of a striated muscle fiber (a), a myofibril (b), and a sarcomere (c). (e) Various cross-sectional appearances in different regions of the sarcomere**: the square array of thin filaments close to the Z-line (I-band); the hexagonal lattice of thick filaments in the nonoverlap region of the H-zone; the cross-linked hexagonal lattice of thick filaments linked by accessory proteins at the M-band, with M-bridges (lines) and M-filaments (dots); and the hexagonal lattice in the region where thick and thin filaments overlap (*Pearson Education, Inc., publishing as Benjamin Cummings 2006*).

The muscle fiber is composed of a large number of parallel myofibrils that appear in micrographs as an alternating pattern of light and dark bands. A hexagonal array of aligned bipolar thick filaments forms the dark band, while the light band is mainly composed of actin-rich thin filaments. The dark and light bands are also termed the **A-** and **I-bands**, respectively, due to their anisotropic and isotropic appearance in polarized light [39, 41, 42] (Fig. 5). The thin filaments partly overlap with thick filaments in the A-band but do not extend to the middle of A-band, called the **H-zone** (Fig. 5). In the center of the H-zone, thick filaments are cross-linked to form an electron dense region known as the **M-line** (Fig. 5). In the centre of the I-band, thin filaments of opposite polarity meet and form another electron dense structure called the **Z-line** or **Z-disc** (Fig. 5). The region between two consecutive Z-lines is the basic contractile unit of myofibrils and it is known as the **sarcomere** [43] (Fig. 5). The total number of sarcomeres within a fiber depends on muscle length and size: the larger the muscle fiber is, the greater is the proportion of contractile units.

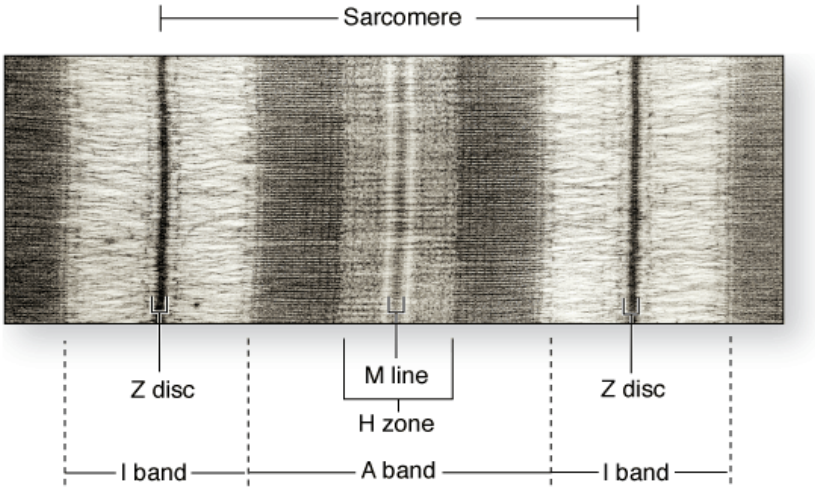



**Figure 5. Electron micrograph of striated muscle in longitudinal section, showing one sarcomere.** On each side of the Z-disc are the lightly stained I-bands, composed of actin thin filaments. The H-zone, which is made up exclusively of myosin thick filaments, is in the centre of the A-band that includes a zone of overlap between the thick and thin filaments. From [44].

## 1.3 The organization of thin and thick filaments

The proper function of striated muscle is dependent on the assembly and maintenance of a complex network of structural, contractile, and regulatory proteins, which form the highly organized sarcomere structure and are responsible for efficient contraction and synchronized force transmission, while maintaining cellular integrity.

Muscle thin filaments are ~1.0 μm long and mainly composed of filamentous actin (**F-actin**), which is formed by two chains of spherical G-actin monomers twisted around each

other to form a double helix. Each G-actin monomer has a binding site for myosin and polymerizes to create an actin filament with distinctive polarity: the **barbed end** is anchored at the Z-disc by the cross-linking protein α-actinin and capped by CapZ, whereas the **pointed end** reaches the A-band where it is capped by tropomodulin, which is essential for the preservation of the proper length of thin filaments [45] (Fig. 6). The barbed and pointed ends refer to the orientation of arrowheads generated by the myosin S1 fragment binding to actin filaments when observed under transmission electron microscopy and are the fast- and slow-growing ends of the thin filaments, respectively.

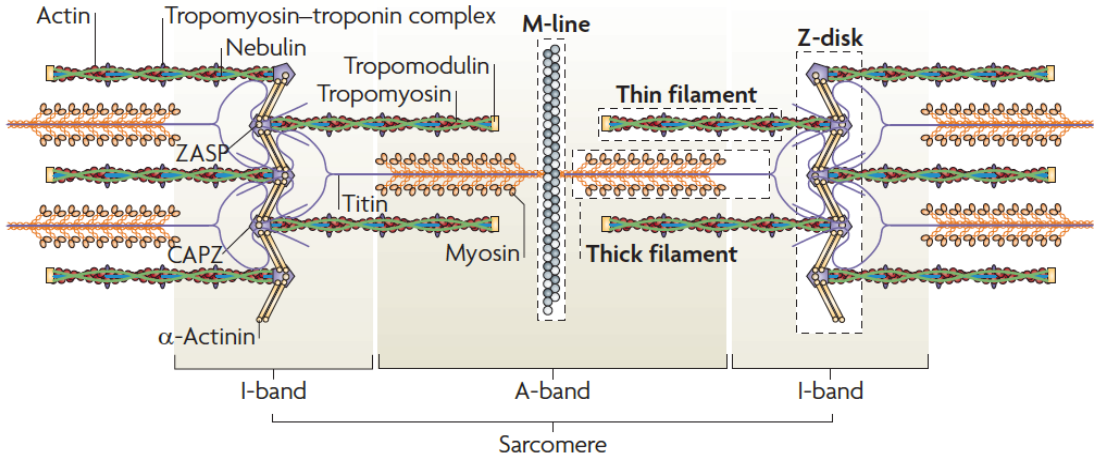



**Figure 6. Schematic structure of a skeletal muscle sarcomere.** The A-band comprises thick filaments together with interdigitating thin filaments, whereas the I-band is only composed of thin filaments. Thin filaments consist of filamentous (F)-actin and the tropomyosin–troponin complex, which is required for the proper interaction of thin filaments with myosin. Thin filaments are stabilized by the giant protein nebulin which runs along the thin filaments with its C-terminus anchored at the Z-line and the N-terminus located towards the pointed end of thin filaments [46-48]. In the Z-line thin filaments of opposite polarity are crosslinked by α-actinin and capped by CapZ, whereas thick filaments are anchored in the M-line in the middle of the sarcomere. A third filament, stretching half a sarcomere from the Z-line to the M-line, is composed of titin, which provides elastic support and anchoring of thick filaments in the middle of the sarcomere [49].

Closely associated with F-actin helices there are the so-called *regulatory proteins* **tropomyosin** and **troponin**, which are intimately involved in muscle contraction [50] (Fig. 6). Tropomyosin molecules are arranged in two-chain coiled-coil α-helices, which extend alongside F-actin filaments [51]. Each tropomyosin monomer spans 38.5 nm along the F-actin filament (which corresponds to 7 actin monomers), and is associated with one **globular troponin complex** comprising three separate polypeptides: **troponin T** (305 kDa), **I** (21 kDa), and **C** (18 kDa), named after their **T**ropomyosin binding, **I**nhibitory, and **C**$a^{2+}$-binding activities during muscle contraction [52].

Another protein closely associated with thin filaments is the *giant* phosphoprotein **nebulin** (600-900 kDa), extending from the Z-line towards the pointed end of thin filaments [46-48] (Fig. 6). This large, α-helical protein belongs to the nebulin protein family, which

includes also **nebulette**, **N-RAP** (**N**ebulin-**R**elated **A**nchoring **P**rotein), **LASP-1** (**L**IM and **S**H3 **P**rotein-**1**), and **LASP-2**, (**L**IM and **S**H3 **P**rotein-**2**/LIM-Nebulette) (reviewed in [53, 54]). Nebulin is composed of 185 repeating modules interacting with thin filament components along the length of thin filaments, whereas its N- and C-terminal regions contain unique sequences that bind to proteins at the thin filament pointed ends and the Z-line, respectively [55]. Nebulin is predominantly expressed in skeletal muscle, whereas it is barely detectable in heart, where it is replaced by its smaller homologue nebulette (107 kDa), positioned within the sarcomeric Z-line and only extending a short distance along the actin filament. Highly homologous to the nebulin C-terminus, nebulette contains 23 simple nebulin repeats, a serine-rich linker region, and a Src homology 3 (SH3) domain [56] (Fig. 7). The SH3 domains of both nebulin and nebulette bind to proline-rich regions within various proteins, including the α-actinin-associated proteins myopalladin and palladin [1, 57, 58]; the Zis1 and PEVK regions of titin [58-60]; the focal adhesion associated protein zyxin [61]; the neuronal Wiscott-Aldrich syndrome protein (N-WASP/WASL), regulating actin polymerization [62]; and the Xin actin-binding repeat-containing (XIRP) proteins Xin and XIRP2 with which nebullin and nebulette interact transiently during development and remodeling [63]. Furthermore, both the SH3 domain and the nebulin repeats bind with high affinity to α-actinin in the Z-line [64].

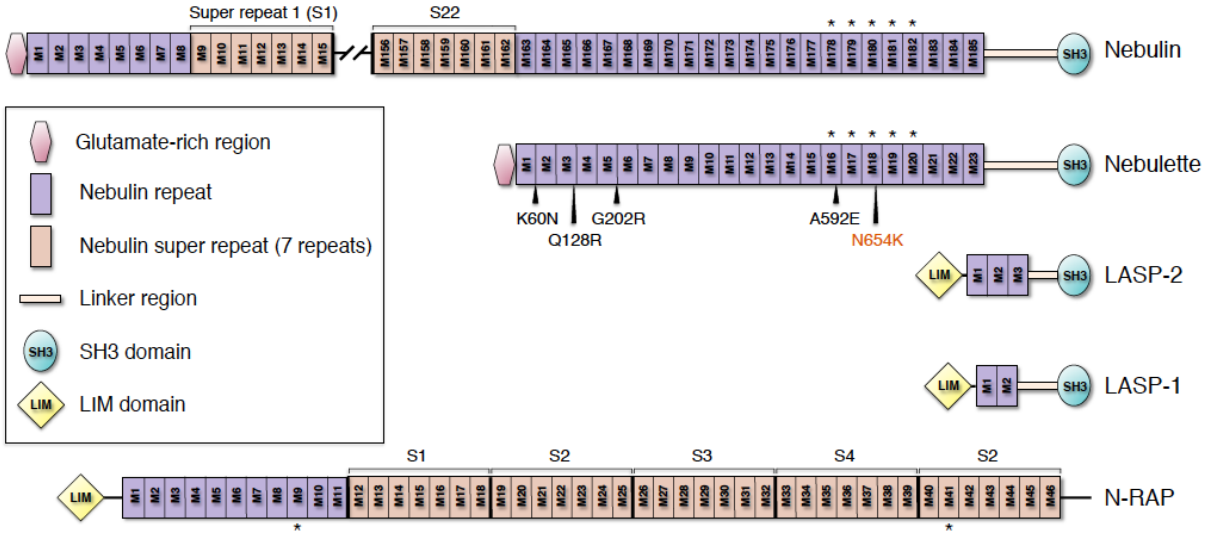



**Figure 7. Schematic structure of the nebulin family members.** The nebulin family comprises 5 actin-binding cytoskeletal proteins: nebulin, nebulette, N-RAP, LASP-1, and LASP-2, containing various numbers of 35-residue nebulin repeats. Nebulin contains 185 nebulin repeats of which 154 (repeats 9-162) are organized in 7 super-repeats [65] associated with the troponin-tropomyosin complex along the thin filament [64-69]. N-RAP contains 46 nebulin repeats of which 35 (repeats 12-46) form 5 super repeats [70, 71]. On the other hand, nebulette (109 kDa) [56, 72], LASP-1 (37 kDa) [73, 74], and LASP-2 (34 kDa) [61, 75, 76] contain only simple nebulin repeats. Except for N-RAP all nebulin family members share an SH3 domain at their C-terminus. In addition, a LIM-domain is present at the N-terminus of N-RAP, LASP-1, and LASP-2, but not in nebulin and nebulette (reviewed in [53].

Recent *in vivo* and *in vitro* studies report the implication of nebulin in various important processes, including stabilization of thin filaments [46, 60, 77-82]; promotion of actomyosin interactions [46, 83-85]; calcium handling [60, 83-86]; Z-line alignment and integrity [60, 77, 82, 87]; as well as maintenance of sarcomeric integrity during muscle contraction [55, 77]. *Nebulin* gene mutations are causative for nemaline myopathy [88, 89], while mutations in the *nebulette* gene have been identified in patients with dilated cardiomyopathy. While transgenic mice overexpressing nebulette mutants partially recapitulate the human pathology [90, 91], nebulette knockout mice show no functional phenotype, but exhibit Z-line widening [92], suggesting a similar role of nebulin and nebulette in determining Z-line width and maintaining Z-line integrity in cardiac and skeletal muscle, respectively.

Thick filaments are ~1.6 μm long and consist mostly of **myosin II** and **C-**, **H-**, and **X-myosin binding proteins**, which have structural and regulatory roles. Myosins are a family of ATP-dependent motor proteins, typically composed of one or two heavy chains and four or more light chains. **Myosin II** (420 kDa) is the major contractile protein involved in eukaryotic muscle contraction. It comprises two heavy chains (**MHC**), which exist as a dimer, and two pairs of different light chains (**MLC1** and **MLC2**) wrapped around the neck region of each heavy chain. Myosin heavy chains are thin and baculiform molecules with a length of 150 nm and a thickness of 2-3 nm and are made up of two chains twisted around each other to form the so-called *tail region*. At one end of each chain there are a *neck* and a *globular head region*, which contains the binding site for both actin and ATP as well as has enzymatic capacity to hydrolyze ATP. The two pairs of light chains are connected to the head. Several hundred myosin molecules are required to form a thick filament and the heads of the myosin molecules project to the outside of the filaments and are responsible for moving the myosin molecules along adjacent actin filaments [25].

A regulatory protein important for maintaining thick filaments centered during contraction is **titin** (Fig. 6). Also known as connectin, titin is the third most abundant protein in striated muscle and the largest protein yet discovered in humans [65, 93, 94]. Titin is composed of a single strand of 27.000-34.000 residues with a molecular weight of 3.000 to 3.700 kDa and extends over 1 μm from the Z-line at the border between sarcomeres (N-terminus) to the M-line at the center of the sarcomere (C-terminus) [65]. Titin is highly modular in structure: about 90% of titin mass is made up of globular domains of immunoglobulin (Ig) and fibronectin type III (FN3) repeats, while the remaining 10% is composed of non-repetitive sequences, including the PEVK region in the I-band region named

after the predominant amino acids in the domain as well as the serine/threonine kinase domain in the titin C-terminal region at the M-line. The I-band region of titin is composed mainly of extensible Ig domains and the PEVK region, allowing titin to function as a molecular spring responsible for the passive elasticity of muscle. The A-band region of titin is comprised of Ig and FN3 modules arranged into super-repeats, providing binding sites for thick filament proteins such as myosin-binding protein C (MyBP-C) and H (MyBP-H), myomesin-1 and -2, and the rod region of the myosin heavy chain [95-101]. Thus, titin is essential for thick filament assembly and organization during myofibrillogenesis. Within the Z-disc, titin contains a variable number of a specific 45-residue protein motif called the **Z-repeat** [102]. The number of the Z-repeats present in the central Z-disc region of titin is closely correlated with the width of the Z-disc [102, 103]. Moreover, titin interacts with thin filaments through its direct interaction with α-actinin [104-106] and titin-cap (T-cap/telethonin) [107, 108] and permits force transmission at the Z-disc. Finally, it participates in mechanosensing through binding to proteins signaling to the nucleus, and functions as a sensory and signaling mediator though its kinase domain [95-97, 99-101, 109]. Titin is extensively spliced, especially in the extensible I-band region, resulting in N2BA and N2B (cardiac muscle) and N2A (skeletal muscle) isoforms, varying in length depending on muscle developmental stage and type, determining the elastic properties of different muscle types.

## 1.4 Muscle fiber types

Mammalian skeletal muscles contain four major Myosin Heavy Chain (MHC) isoforms, the *slow* MHCIβ and the three *fast* MHCIIa, MHCIIx, and MHCIIb isoforms, and three major myosin light chain (MLC) isoforms, the *slow* MLC1s and the two *fast* MLC1f and MLC3f isoforms. The differential distribution of MHCs defines three major fiber types containing a single MHC isoform: **type I slow-twitch fibers,** which contain MHCIβ and produce low forces, and **type II fast-twitch fibers** which contain MHCIIa (**type IIA**) or MHCIIb and MHCIIx (**type IIB/X**) and produce high forces (Table 1). It has been demonstrated that muscle-unloading results in a switch from *slow* to *fast* MHC gene expression [110].

Type I fibers are *slow oxidative* fibers suited for aerobic activities, whereas type IIB/X fibers *fast glycolytic* fibers better suited for anaerobic, high intensity type of activities. Their metabolic properties (oxidative *vs*. glycolytic) depend on the expression of different metabolic gene programs, whereas speed of contraction, and hence, force development, is related to how fast the myosin ATPase hydrolyses ATP, with fast fibers having more efficient ATPases

[111]. In addition, a number of intermediate *hybrid* fiber populations exists containing both MHCIβ and MHCIIa, MHCIIa and MHCIIx, or MHCIIx and MHCIIb [112]. In mice, the gene encoding the MHCIβ isoform is located in a cluster on chromosome 14, whereas the genes encoding the type II MHC isoforms (IIa, IIx and IIb) are found in a cluster on chromosome 11, which also includes the MHC-embryonic (MHC-emb) and MHC-neonatal (MHC-neo) isoforms, expressed during muscle development and adult regeneration [113, 114]. It has been suggested that the clustered location of MHC genes is involved in their regulation [115-118]. In particular, it has been reported that MHC-emb, MHC-neo, and MHCIβ are expressed during early C2C12 murine myoblast differentiation, whereas the *fast* isoforms (MHCIIa, MHCIIx and MHCIIb) are upregulated later during differentiation. The transition between the expression of *slow* and *fast* isoforms coincides with myotube hypertrophy; thus, the different expression of MHC isoforms defines a specific phase and phenotype during muscle development [119].

In conclusion, most mammalian skeletal muscles are composed of variable proportions of different fiber types containing distinct MHC isoforms and determing the appropriate force and duration of contraction following excitatory signals. Myofiber identity is first established during embryonic development by intrinsic myogenic control mechanisms and is later modulated by neural and hormonal factors [120]. Apart from different anatomical, physiological, and biochemical features, the underlying mechanism of muscle contraction is indeed similar in all myofiber types and is the result of a *sliding mechanism* of thick myosin-rich filaments over thin actin-rich filaments after neural activation [121].

**Table 1**. **Functional and structural characteristics of skeletal muscle fiber types.** From [122].

| **Characteristic** | **Type of Fibre** | | |
|---|---|---|---|
| | **Slow Oxidative (Type I)** | **Fast Oxidative (Type IIA)** | **Fast Glycolytic (Type IIB/X)** |
| Myosin ATPase activity | Low | High | High |
| Speed of Contraction | Slow | Fast | Fast |
| Force of Contraction | Low | Moderate | High |
| Fatigue Resistance | High | Moderate | Low |
| Oxidative Capacity | High | High | Low |
| Mitochondrial Density | High | High | Low |
| Myoglobin Content | High | High | Low |
| Anaerobic Enzyme Content | Low | Moderate | High |
| Capillary Density | High | High | Low |
| Glycogen | Low | Moderate | High |
| Z-line | Intermediate | Wide | Narrow |
| Fibre Diameter | Small | Moderate | Large |

## 1.5 Muscle contraction

In the sarcomere, the thin and the thick filaments are constant in overall length, but during contraction the dark band (A-band) remains unchanged, while the light band (I-band) decreases in length. This can be explained by the *sliding filament model* [123, 124], which describes muscle contraction as the sliding of thick myosin-rich filaments over thin actin-rich filaments in an ATP-dependent manner to generate sarcomere shortening and consequently muscle contraction with no change in the length of either type of filament [121].

The globular heads of myosin II heavy chains have ATPase activity and hydrolyze ATP during their interaction with F-actin filaments. After hydrolysis of ATP to ADP and inorganic phosphate (Pi), a weak binding to actin triggers the release of Pi, which causes the myosin head to bind tightly to the actin filament. A conformational change occurs in the myosin head and it is thought to produce a "power stroke" that pulls the myosin head against the actin filament. The consequent release of ADP creates space for a new ATP molecule to bind, and consequently the myosin head detaches from the actin filament [23, 125-127].

Striated muscle contraction is initiated by a sudden increase in cytosolic $Ca^{2+}$. In skeletal muscles, contraction only takes place when a signal passes to the skeletal muscle from its motor nerve. The signal triggers an action potential (AP) in the muscle cell plasma membrane (**sarcolemma**), which spreads rapidly into the transverse tubules (**T-tubules**), the membranous folds that extend inward from the plasma membrane around each myofibril. The signal passes to the sarcoplasmic reticulum (SR) [26], which is a sheath of flattened vesicles that surround each myofibril, and causes the opening of $Ca^{2+}$ channels in the SR membrane. This allows $Ca^{2+}$ to enter the cytosol from the SR and this sudden rise in free $Ca^{2+}$ in the cytosol leads to the simultaneous contraction of all myofibrils. $Ca^{2+}$ is rapidly pumped back into the SR by a $Ca^{2+}$ ATPase in its membrane, thereby causing the myofibrils to relax [12, 128-130]. Cardiac muscle cells have the capacity to spontaneously depolarize and in the intact heart, the depolarization spreads rapidly in a specialized conduction system. Therefore, cardiac muscle does not require motor nerve activation, but contracts autonomously. Specialized peacemaker cells are responsible for determining the heart rate [131].

The $Ca^{2+}$ dependence of striated muscle contraction is explained by the *steric blocking model* in which thin filament regulation in the *off* ($Ca^{2+}$-free) and *on* ($Ca^{2+}$-bound) states is due to the actin-associated regulatory proteins tropomyosin and troponin [42, 132, 133]. Indeed, in the absence of these proteins, myosin ATPase is constitutively activated by actin. Basically, during the *off* state the actin-myosin interaction is inhibited by troponin I and

tropomyosin strands, which cover up the myosin-binding site on actin monomers. However, when troponin C binds $Ca^{2+}$ ions in the *on* state, troponin I detaches from actin, thereby causing tropomyosin to change its position on the actin filament. This causes a conformational change of actin monomers [134], which can interact with myosin heads leading to the activation of ATPase activity and the resultant muscle contraction [133-137]. At the end of the AP, $Ca^{2+}$ is removed from the cytosol by SR uptake via the SR $Ca^{2+}$ transporter (SERCA) [138] and by extrusion through the sarcolemma via the $Na^{+}/Ca^{2+}$ exchanger [139].

In smooth muscle, contraction is also triggered by a rise in cytosolic $Ca^{2+}$, but not through the troponin-tropomyosin complex. The formation of a $Ca^{2+}$-calmodulin complex activates the myosin light chain kinase (MLCK), which phosphorylates light chains in myosin heads and increases myosin ATPase activity. Consequently, active myosin crossbridges interact with and slide along actin filaments, causing muscle contraction [140].

Therefore, in striated muscle tissues, $Ca^{2+}$ directly couples excitation with contraction and is absolutely required for contraction. Conversely, in smooth muscle cells $Ca^{2+}$ functions as a second messenger and contraction can persist after $Ca^{2+}$ has been removed [131].

## 1.6 Myofibrillogenesis

Efficient muscle contraction is dependent on the precise assembly and uniform organization of contractile proteins into sarcomeric units to form **myofibrils**. The formation of myofibrils is called myofibrillogenesis. Several studies using different models have investigated myofibrils assembly and identified the sequence of events involved in myofibrillogenesis [141]. Premyofibrils consisting of minisarcomeres, composed of non muscle myosin II and thin actin filaments, are located at the edge of muscle cells. Z-bodies at the border between minisarcomeres contain α-actinin and interact with the barbed ends of actin filaments. When the premyofibrils start to align and become thicker, the presence of titin and muscle myosin II can be observed. At this stage, the Z-bodies start to align and the fibrils are classified as nascent myofibrils. In the transition from nascent to mature myofibrils, nonmuscle myosin is not present anymore but is replaced by muscle myosin II, which makes up the thick filaments. C-protein and myomesin are incorporated in the A-band, and Z-bodies transform and become aligned to form Z-lines or Z-discs [142, 143] (Fig. 8).

Overexpression of the N-terminal part of myopalladin (MYPN) leads to Z-disc disruption and sarcomere disassembly, implying a role for MYPN in the maintenance and coordination of myofibrillogenesis [1].

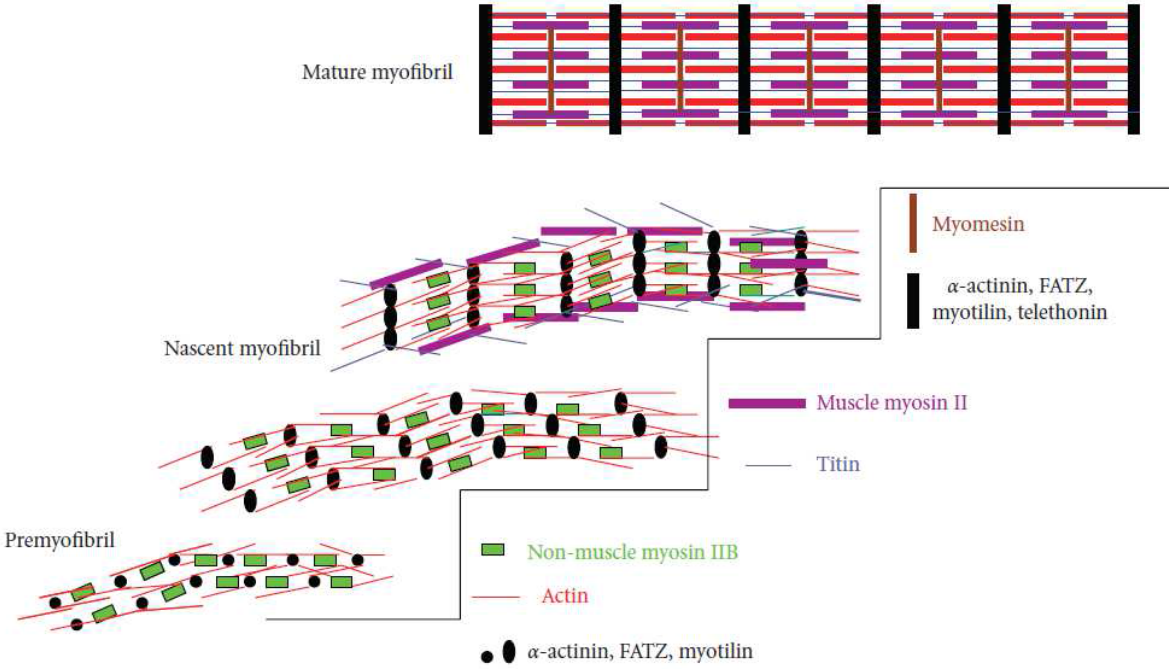



**Figure 8. Premyofibril model.** Premyofibrils are made up of minisarcomeres, nonmuscle myosin II aligned with actin filaments embedded in the Z-bodies. Nascent myofibrils contain muscle myosin II and Z-bodies become aligned in adjacent fibrils. In mature myofibrils fusion of Z-bodies to Z-discs, alignment of muscle myosin II in the A-band, and complete absence of nonmuscle myosin can be observed. From [143].

## 2. THE SARCOMERIC Z-LINE

The **Z-line** (also termed Z-band or Z-disc) is a multiprotein complex, which defines the boundaries between sarcomeres and plays an essential role in striated muscle structure and function, including the assembly and organization of the sarcomere, sarcolemmal membrane integrity, and the generation and transmission of muscle force [55, 144-146].

During muscle development, the first detectable structures of the sarcomere are the **I-Z-I bodies**, precursor structures of Z-lines within which epitopes of actin, α-actinin, titin, and nebulin co-localize [25, 147-150]. Thus, Z-line associated proteins appear to be crucial for early stages of myofibril formation.

The major component of the Z-line is the muscle-specific protein α-actinin which exists as a rod-shaped antiparallel homodimer [151], comprising two calponin homology domains followed by four spectrin-like repeats and a calmodulin-like domain. The main function of α-actinin is to act as a scaffold for the assembly of the Z-line. Indeed, in the Z-

line, the overlapping barbed ends of actin thin filaments from adjacent sarcomeres are cross-linked by α-actinin homodimers [152] as well as the N-terminal region of titin filaments [106, 107]. In addition, the C-terminal region of nebulin and its smaller homologue nebulette also extend into the Z-line of skeletal and cardiac muscle, respectively. Based on immunoelectron microscopy they were originally proposed to insert only partially into the Z-line with their N-termini projecting out of the Z-line along the I-band [153, 154]. However, the location of binding sites for the Z-line associated proteins CapZ [155] and desmin [153] within nebulin repeats M160-164 has led to an alternative model proposing the overlapping of nebulin from adiacent sarcomeres within the Z-line and the binding to CapZ at the barbed end of thin filaments from the opposing thin filament, thereby cross-linking neighboring sarcomeres [155, 156]. Based on the similarity of nebulette to nebulin, it is likely to be inserted into the Z-line in a similar way, even though no evidence of nebulette binding to desmin and CapZ has been reported [153, 154].

The thickness of Z-lines in different muscle fiber types is greatly variable, ranging from approximately 30-50 nm in fast skeletal muscle fibers [157, 158] to 100-140 nm in cardiac muscle and slow skeletal muscle fibers [159, 160], presumably to allow the mechanical strength of the Z-line to be varied. In this context, different models for the modular architecture of the Z-line have been proposed. Gautel *et al*. [102] hypothesized that the number of C-terminal titin Z-repeats correlates closely with the thickness of the Z-line in different muscle types, and that the differential expression of the Z-repeats modulates the strength of the titin/α-actinin interaction, which could be relevant for a specific response of the Z-line to mechanical stress [102, 103]. However, a more complex model for the periodicity of Z-line ultrastructure has been proposed by Luther *et al*. [161], involving either two overlapping titin molecules at the Z-disc, or "Z-repeats" within nebulin filaments [47, 65]. In transverse view, in the light and electron microscope, two different structural states of the Z-line have been revealed: a "square" and a "basketweave" pattern. The Z-line square conformation arises from the ordered crossing of bridging thin filaments, whereas the basketweave pattern emerges from the cross-linking of thin filaments with various Z-line proteins including actin, CapZ, α-actinin, the N-terminal region of titin, titin-cap (T-cap/telethonin), the C-terminal region of nebulin/nebulette, and obscurin (contains like titin, tandem Ig domains in an elastic region) (Fig. 9).

Apart from these proteins, during the last decades, the detection of multiple novel Z-line proteins and their interacting partners has led to the identification of new functions of the

Z-line. Z-discs modify their lattice network in conjunction with changes in the actin-myosin interaction, supporting their role as mechanosensors [160, 162, 163].

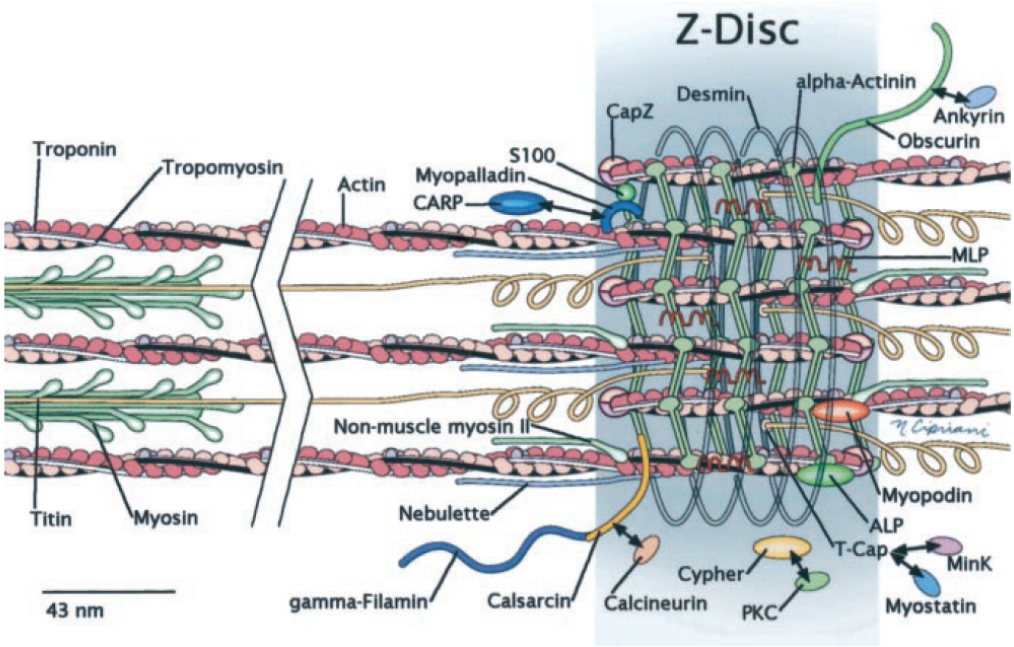



**Figure 9. Z-disc structure.** Schematic representation of the network of proteins making up the Z-disc. Stoichiometric relationships are not shown. From [164].

Traditionally, the Z-line has been considered as a passive constituent of the sarcomere important only for the transmission of force generated by the myofilaments [164, 165], but recently a pivotal role of the Z-line in signal transduction and mechanosensing in both cardiac and skeletal muscles has been proposed [166]. In fact, the newly identified proteins are not only important for the structural and mechanical stability of the sarcomere, but also serve as docking site for transcription factors, $Ca^{2+}$-signaling proteins, phosphatases, and kinases, influencing function and gene expression. Moreover, many proteins shuttle between the Z-line and other cellular compartments such as the nucleus, underlying the dynamic nature of Z-line-dependent signaling. Particularly, the potential role of the Z-line as a myocardial "stretch receptor" is being extensively discussed. This proposed structure would allow the cardiomyocyte to sense the increased mechanical load and to respond with changes in its own gene expression, ultimately resulting in cellular hypertrophy [166]. In this regard, the involvement of muscle Lim protein (MLP), calsarcin, and titin-Cap (T-cap)/telethonin in Z-line-based mechanotransduction has been reported [167, 168]. Indeed, the important role of the Z-line is illustrated by the identification of a growing number of mutations in Z-line associated proteins causing cardiomyopathies and muscular dystrophies. Among these proteins is ***myopalladin*** (MYPN), a Z-line associated protein important for both the structural

aspects of sarcomere assembly and regulation of sarcomeric gene expression [1, 169]. Recently, several *MYPN* gene mutations have been identified in patients affected by cardiac diseases, thus confirming the important role of MYPN in the organization of sarcomere architecture and maintenance of Z-line integrity.

## 2.1 The structure and expression of Myopalladin and Palladin

The Z-disc protein MYPN, encoded by the *MYPN* gene situated in the 10q22.1 locus, was first identified by Bang *et al*., in a yeast two-hybrid screening for proteins interacting with the nebulin SH3 domain in the Z-disc [1]. The name myopalladin derives from its high homology to the ubiquitously expressed protein palladin (PALLD). MYPN and PALLD, together with the small Z-disc protein myotilin (MYOT), belong to the same gene family, encoding closely related immunoglobulin C2 (IgC2)-containing proteins (Fig. 10). In particular, MYPN is a 145 kDa protein containing five IgC2 domains (two N-terminal and three C-terminal) and a proline-rich region nearly identical to one of two proline rich regions found in the major isoform of PALLD (200 kDa) (Fig. 10).

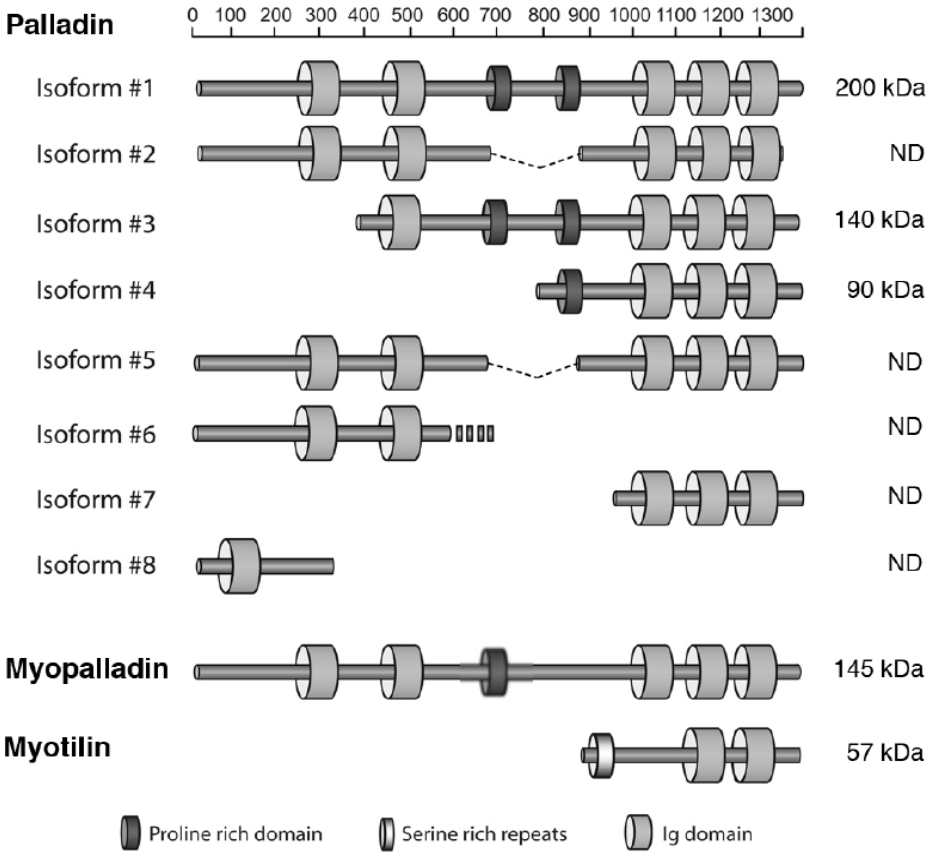



**Figure 10**. **Schematic representation of the members of the PALLD/MYPN/MYOT family and their domain organization.** ND, not determined. Adapted from [57].

While MYPN and MYOT (57 kDa) are expressed specifically in striated muscle as single isoforms, PALLD is ubiquitously expressed and exists in various isoforms (about 8), arising from at least four different promoters (for the three major isoforms of 90-92 kDa, 140 kDa, and 200 kDa) [170, 171], as well as alternative splicing and early termination [171, 172]. This high degree of isoform variability is associated with the different functions of PALLD variants expressed in a tissue-specific manner. The 90-92 kDa isoform is the major almost ubiquitously expressed isoform of PALLD with highest levels in smooth muscle-rich tissues; the 140 kDa is present in mesenchymal tissues and represents the major isoform of the brain; and the 200 kDa is expressed only in striated muscle and testis [172].

## 2.2 Interaction partners of Myopalladin and Palladin

MYPN and PALLD interact with various proteins in the sarcomere. Within the Z-line, both MYPN and PALLD bind to α-actinin, nebulin/nebulette, and PDZ-LIM proteins through different regions. Both MYPN and PALLD bind to α-actinin through a short sequence present within the unique region between Ig2 and Ig3 ([1, 173] and see below) (Fig. 11). α-Actinin was originally reported to bind to the C-terminal region of MYPN, but in our unpublished results we found that it binds to a region homologus to the α-actinin site in PALLD. The central proline-rich region present in MYPN and longer isoforms of PALLD (isoform 1 and 3 in Fig. 10) binds to the C-terminal SH3 domain of nebulin in skeletal muscle and nebulette in the heart (Fig. 11). Furthermore, ESDEL and ESEDL motifs in the extreme C-terminal end of MYPN and PALLD, respectively, bind in a phosphorylation dependent manner to class III type PDZ domains (Fig. 11), which are present within the members of the PDZ-LIM protein family, including cypher/ZASP, CLP36, ALP and RIL [2]. PDZ-LIM proteins have been found to localize to the Z-line and function as adaptor molecules involved in the regulation of actin cytoskeleton dynamics [174, 175]. Recently, cypher has been shown to be indispensable for normal muscle function and mutations in the *Cypher*/*ZASP* gene cause cardiomyopathies and skeletal myopathies. Moreover, the binding affinity of MYPN for Cypher is increased by phosphorylation, whereas its binding to CLP36 is ablated by phosphorylation, suggesting the importance of a tight regulation of the interactions [2]. C-terminal class III type PDZ binding motifs are also present in MYOT and PALLD as well as in FATZ family members (including FATZ-1/calsarcin-2/myozenin-1, FATZ-2/calsarcin-1/myozenin-2, FATZ-3/calsarcin-3/myozenin-3), which are also located in the Z-line [176]. The motif is present almost

exclusively in these protein families and is conserved between species, indicating the significance of these interactions in the Z-line.

MYPN is also present in the nucleus and the sarcomeric I-band. Within the I-band, its two N-terminal IgC2-repeats interact with the ***Cardiac Ankyrin Repeat Protein*** (CARP) (Fig. 11), a negative regulator of gene expression in the nucleus induced by various forms of stress conditions, such as cardiomyopathies, heart failure and muscular dystrophies. CARP, in turn, binds to the N2A region of titin, which is located within titin elastic I-band region [3], forming a titin/CARP/MYPN complex that may be involved in transduction of stress/strain-induced signaling from the sarcomere to the nucleus [3, 177].

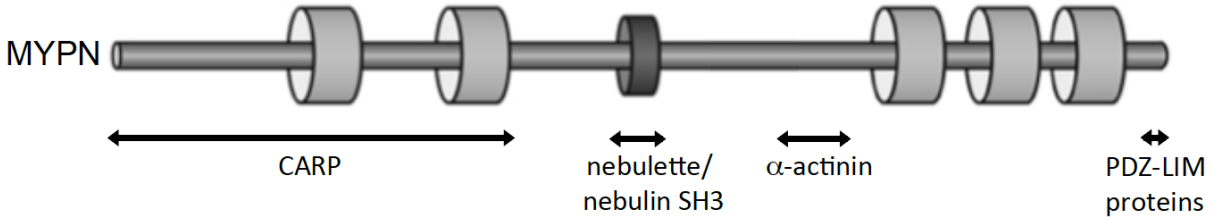



**Figure 11**. **Schematic representation of the MYPN binding sites for interaction partners.** Adapted from [57].

# 3. THE SRF-MRTF SIGNALING PATHWAY

MYPN and PALLD play a crucial role in the assembly, organization, and maintenance of the actin cytoskeleton [169]. PALLD has recently been shown to bind directly to F-actin as well as to bundle F-actin into multi-filament arrays through its immunoglobulin domain 3 (Ig3), and more strongly with a fragment containing Ig3 and Ig4 (Ig3-4), thus functioning as an actin cross-linking protein [178, 179] and promoting actin polymerization [171, 179-181]. Like PALLD, we found that also MYPN is able to bind and bundle F-actin as well as to stimulate actin polymerization (see below and unpublished data). Consistent with the interaction of PALLD with F-actin and a number of actin binding proteins, PALLD is associated with various actin-based structures, including focal adhesions, stress fibers, cell-cell junctions, and Z-lines [170]. Further evidence reveals the participation of PALLD in several actin-dependent processes, such as the epithelial to mesenchymal transition [182-186], wound healing [181, 187], and the formation of podosomes [187-189]. These processes depend on physical changes in cell appearance, shape, position, and contact with extracellular structures, including other cells, and require cellular motile functions. These are physically based on cytoskeletal scaffold structures of actin filaments, which undergo dynamic changes in polymerization from monomeric globular actin (G-actin) to F-actin, and their interaction with

specific actin-binding proteins (ABPs) after either physiological or pathological stimuli [190]. These stimuli are perceived by numerous types of plasma membrane receptors, which activate different members of the Rho GTPase family through selective Rho guanine nucleotide exchange factors (GeFs). Effectors of Rho GTPases orchestrate actin polymerization by incorporating G-actin into F-actin filaments via the Rho-associated kinase Rock-LIM kinase (LIMK)-cofilin pathway and the formin pathway [191]. In the cytoplasm, G-actin forms complexes with different ABPs, including the myocardin-related transcription factors (MRTFs). Incorporation of G-actin into F-actin filaments liberates MRTFs, which then translocates to the nucleus, where it interacts with serum response factor (SRF), causing the expression of SRF target genes (Fig. 12).

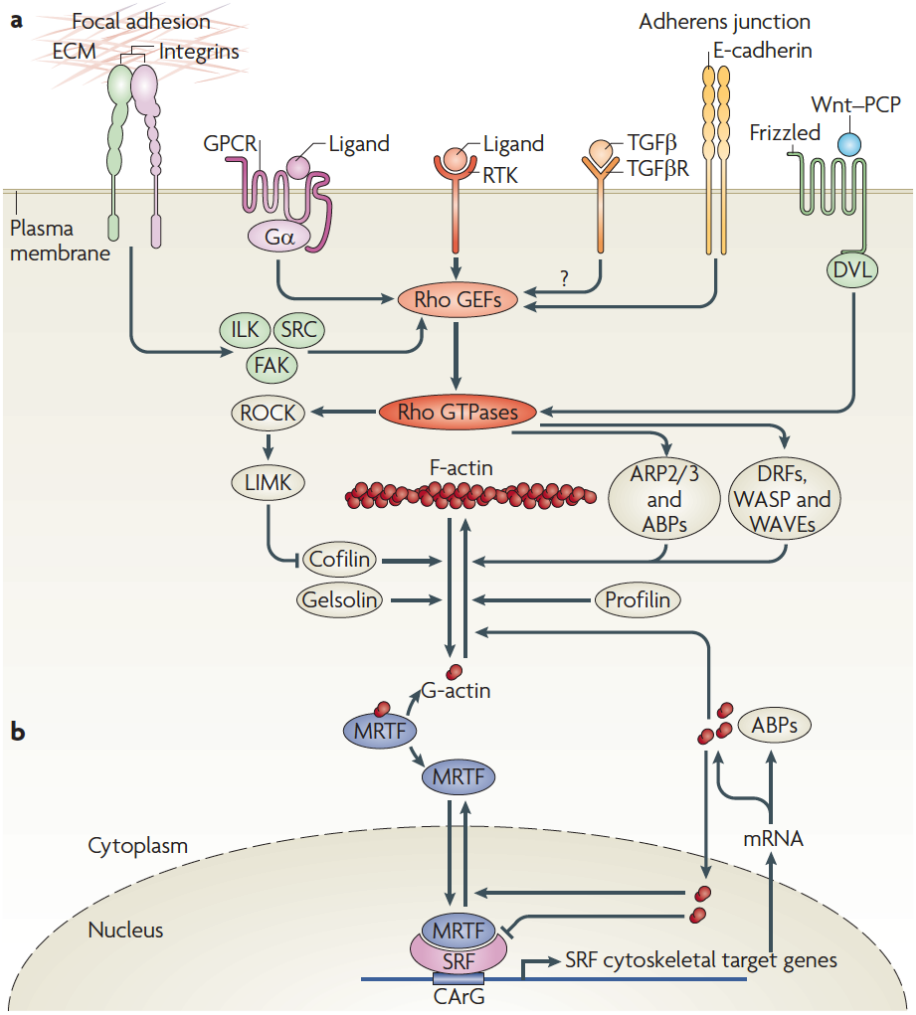



**Figure 12. MRTF-mediated regulation of SRF target genes. a)** Cytoskeletal actin dynamics are initiated by the activation of various plasma membrane receptors which modulate the activity of Rho GTPases through Rho guanine nucleotide exchange factors (GEFs). Effectors of Rho GTPases orchestrate actin polymerization by incorporating G-actin into F-actin [192]. High levels of cytoplasmic G-actin retain MRTFs in the cytoplasm. Incorporation of G-actin into the F-actin filament allows MRTFs to enter the nucleus and interact with the transcription factor SRF [193]. This triggers expression of a subset of SRF target genes. **b)** Nuclear MRTF can be complexed by nuclear G-actin, which inhibits MRTF-mediated stimulation of SRF-dependent transcription and facilitates MRTF nuclear export [194].

SRF is a ubiquitously expressed MADS-box transcription factor, which regulates the expression of several genes involved in cell growth and proliferation, cytoskeletal organization, cell migration, and muscle cell differentiation (Table 2) through its binding to a palindromic DNA motif [CC(A/T)$^6$GG] known as a **CArG box** or **Serum Response Element** (**SRE**) [193, 195]. On his own, SRF is a weak transcription factor and the differential expression of target genes depends on its combinatorial association with two families of cofactors [196, 197]: the **Ternary Complex Factors** (**TCFs**) [198-200] and the **myocardin family factors**, including **myocardin** and **MRTF-A/B** [201-204]. These two classes of SRF cofactors respond to distinct signaling inputs (**Mitogen-Activated Protein Kinase** (**MAPK**) and **RhoA-actin signaling**, respectively), and bind to SRF in a mutually exclusive manner [196] (Fig. 13).

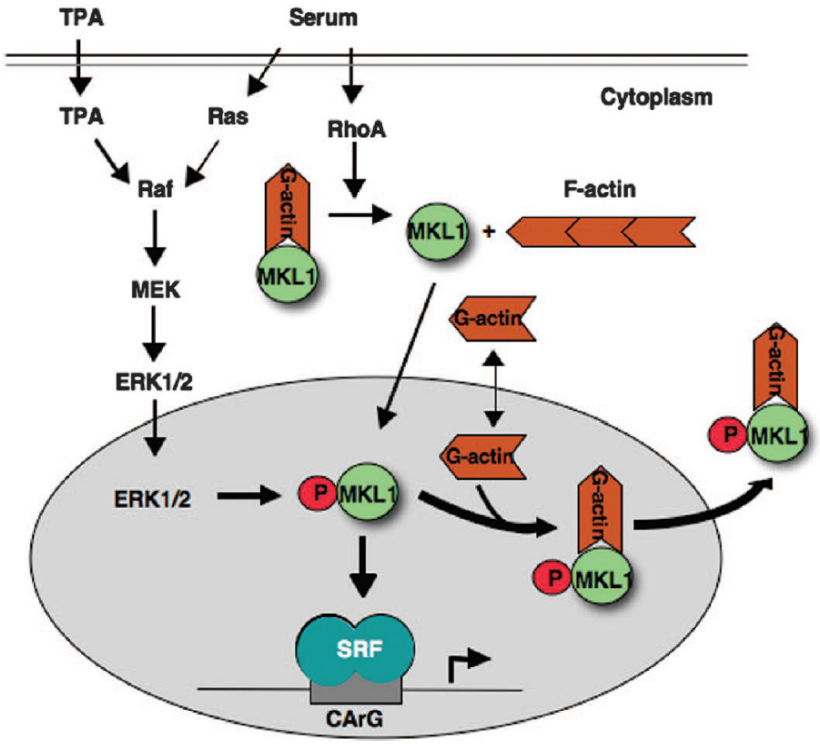



**Figure 13. Regulation of SRF activity by the MAPK and Rho-A actin signaling pathways.** Serum induction results in the activation of the RhoA- and Ras/MEK/ERK pathways. RhoA activation stimulates MRTF-A (MKL1) nuclear localization due to the formation of actin stress fibers and a decrease in G-actin levels, while nuclear export is stimulated due to ERK1/2 phosphorylation of MRTF-A and increased G-actin binding. Export of actin-bound MRTF-A reduces the amount of MRTF-A available to bind to SRF and activate transcription. From [205].

Growth promoting signals inducing the MAPK cascade activate TCFs, which displace MRTFs from SRF. In particular, serum stimulation activates MRTF-A by inducing its relocalization to the nucleus. However, serum stimulation or phorbol ester 12-*O*-tetradecanoyl-13-acetate (TPA) also causes phosphorylation of MRTF-A by Erk 1/2 at S454, which enhances its binding to actin and thus its nuclear export [205]. This phosphorylation is

likely happening after the initiation of MRTF-A-mediated transcription to terminate the induction of SRF target genes. Hence, modulation of MRTF-A binding to nuclear actin by MAPKs regulates MRTF-A-mediated transcription.

**Table 2. SRF–MRTF-regulated genes encode actin microfilament effectors**

| Gene symbol* | Gene name | Function |
|---|---|---|
| ***Structural components of microfilament function*** | | |
| *ACTA1* | Actin, alpha 1 | Microfilament building |
| *ACTA2* | Actin, alpha 2 | Microfilament building |
| *ACTB* | Actin, beta | Microfilament building |
| *ACTG1* | Actin, gamma 1 | Microfilament building |
| *ACTG2* | Actin, gamma 2 | Microfilament building |
| *CALD1* | Caldesmon 1 | Muscle cell contraction |
| *DMD* | Dystrophin | Membrane anchorage |
| *ITGB1* | Integrin, beta 1 | Focal adhesion component |
| *MYH11* | Myosin heavy chain 11 | Actomyosin structure |
| *MYH9* | Myosin heavy chain 9 | Actomyosin structure |
| *MYL9* | Myosin light chain 9 | Actomyosin structure |
| *TAGLN (SM22A)* | Transgelin | Muscle cell contraction |
| *SMTN* | Smoothelin | Muscle cell contraction |
| *TPM1* | Tropomyosin 1 | Muscle cell contraction |
| *VCL* | Vinculin | Linking integrin to microfilaments |
| ***Effectors of actin turnover*** | | |
| *ACTR3 (ARP3)* | Actin-related protein 3 | Microfilament turnover and branching |
| *CFL1* | Cofilin 1 | Microfilament turnover |
| *GSN* | Gelsolin | Microfilament turnover |
| *VIL1* | Villin 1 | Microfilament reorganization |
| *SVIL* | Supervillin | Microfilament reorganization |
| ***Regulators of actin dynamics*** | | |
| *CTGF* | Connective tissue growth factor | An ECM protein that is an integrin ligand and modulates cellular migratory activity |
| *CYR61 (CCN1)* | Cys-rich protein 61 | An ECM protein that is an integrin ligand and modulates cellular migratory activity |
| *FHL1* and *FHL2* | Four-and-half LIM domains 1 and 2 | Adherens junction signalling and transcriptional regulation (through SRF binding) |
| *FLNA* | Filamin A | Integrin signalling |
| *MMP9* | Matrix metalloprotease 9 | ECM remodelling and cell migration |
| *MYLK* | Myosin light chain kinase | Actomyosin regulation |
| *SRF* | Serum response factor | Transcriptional regulation |
| *TLN1* | Talin 1 | Integrin signalling |

SRF target genes encode proteins related to actin cytoskeletal activities. These proteins can be grouped into three categories according to their contributions to actin dynamics: structural (for example, actin), effectors of actin turnover (for example, cofilin 1) and regulators of actin dynamics (for example, talin 1) [190].

SRF target genes are mainly grouped into two classes [206]. Class I target genes, which are regulated by SRF-TCF cofactors, encode proteins with "immediate-early" cellular functions (e.g. *c-fos* and *erg-1*) [198, 207], whereas class II target genes, which are regulated by SRF in combination with myocardin or MRTFs, encode at least three types of proteins, involved in muscle-specific and contractile functions (e.g. cardiac muscle α-actin -ACTC1-, α-skeletal actin -ACTA1-, smooth muscle α-actin -α-SMA or ACTA2-, and smooth muscle 22-α -SM22α-), actin filament dynamics and cell motility (e.g. actin, cofilin 1, talin 1), and microRNA activities (e.g. miR-1 and miR-133). Since SRF target genes encode structural components of thin filaments (e.g. actin itself) and regulators of actin dynamics (e.g. gelsolin and vinculin), as well as microRNAs that provide feedback regulation in these pathways, the MRTF-SRF circuit has central importance in directing gene activities required for actin cytoskeleton organization.

SRF is an upstream regulator of genes involved in heart development and function. Indeed, loss of SRF in mouse developing heart caused defects in sarcomere organization and in stress fiber formation, leading to embryonic lethality [7, 9]. Accordingly, conditional cardiac specific deletion of SRF in adult mice resulted in downregulation of genes involved in cardiac muscle structure and contractility (force generation and transmission) [208] as well as increased expression of the fetal genes *Nppa*, *Nppb*, and *Myh7*, resulting in dilated cardiomyopathy, leading to heart failure and death [7, 11, 209].

## 3.1 The MRTFs

The myocardin-related transcription factors (MRTFs) make up a family of highly homologous proteins, including myocardin, MRTF-A (also known as MAL, MKL1, and BSAC), and MRTF-B (also known as MKL2 and MAL16). They function as powerful transcriptional coactivators of SRF and activate transcription of SRF-target genes.

Myocardin and MRTFs evolved from an ancestral gene in *Drosophila*, known as *DMRTF*, that is strictly related to MRTF-A [210]. The myocardin gene encodes two isoforms due to alternative splicing: the 935 amino acid isoform is expressed exclusively in cardiomyocytes, whereas the 856 amino acid isoform is expressed in SMCs. Both myocardin isoforms as well as MRTF-A and MRTF-B contain conserved RPEL, basic, and glutamine-rich domains (Fig. 14). Moreover, they share a conserved 35-amino acid SAP domain (so called after the associated factors SAF-A/B, acinus, and PIAS), a leucin zipper (LZ) domain, the B1 domain, situated between the basic and the glutamine-rich domains, and the B2

domain placed between RPEL motifs two and three [193] (Fig. 14). In addition, the C-terminus of the myocardin-related transcription factors contains a transcriptional activation domain (TAD) that functions with heterologous promoters. However, the TAD domain of myocardin has a low level of sequence identity with the TADs of MRTF-A and MRTF-B [204].

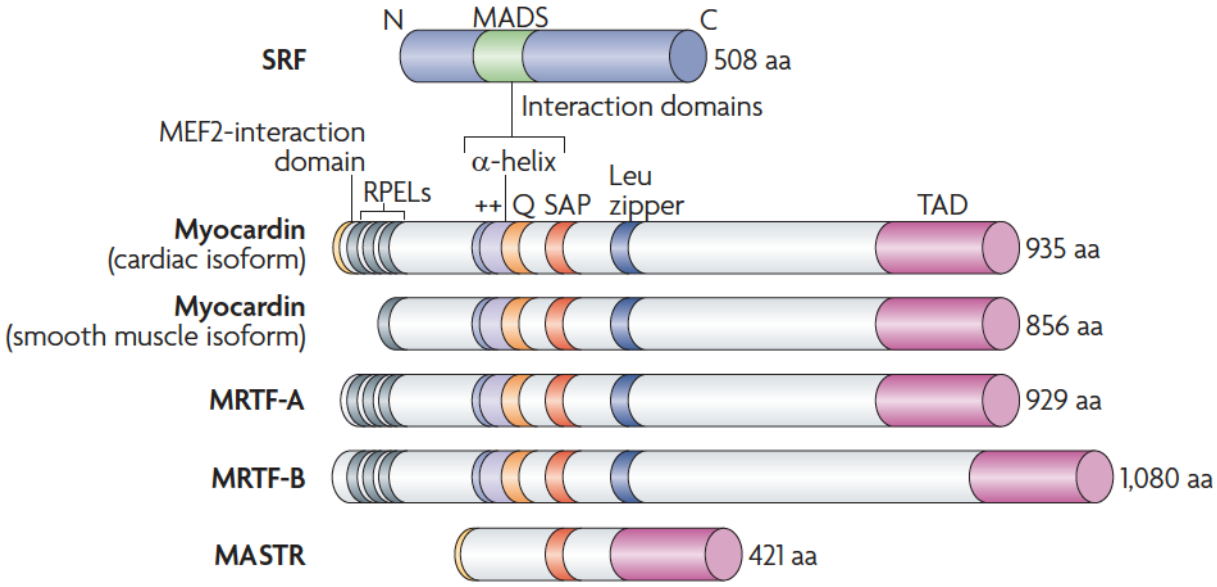



**Figure 14. Schematic representation of SRF and myocardin-related transcription factors.** Functional domains of homology among the myocardin family members are shown and the numbers of amino acids (aa) are indicated. **Top**. The SRF transcription factor contains a MADS box that regulates SRF homodimerization, cofactor-binding, and SRF-DNA binding. **Bottom**. Representation of the myocardin-related family of transcriptional coactivators. Different box colors represent the RPEL, basic (++), glutamine-rich (Q), SAP, LZ, and TAD domains. Myocardin exists as 935 aa and 865 aa isoforms generated by alternative splicing. The 935 aa isoform is expressed mostly in the heart, whereas the 865 aa isoform is mainly expressed in SMCs. The cardiac-specific splice variant of myocardin contains a unique N-terminal sequence that confers the ability to interact with the myocyte-specific enhancer factor 2 (MEF2) transcription factor, a MADS-box transcription factor related to SRF. This MEF2-interaction domain is also contained in a divergent member of the myocardin family called MEF2-activating SAP transcriptional regulator. MASTR lacks the SRF-interaction domain [190].

MRTF-A is the major ubiquitously expressed isoform of the MRTFs and, during embryonic development, it is enriched in mesenchymal, muscle, and epithelial cells [202]. MRTF-A is localized in the cytoplasm, where it is sequestered by its binding to G-actin through the RPEL motifs. In response to actin polymerization promoted by serum stimulation or other signals, it translocates into the nucleus where it binds to SRF, thereby inducing the activation of SRF target genes [211]. An important role in the nuclear import of MRTF-A is played by its B1 and the B2 domains [211] as well as by the striated muscle activator of Rho signaling (STARS), which binds to F-actin facilitating the translocation of MRTF-A to the nucleus [212].

Recent studies have reported the capability of PALLD to bind to MRTFs and both directly and indirectly activate smooth muscle cell (SMC) gene expression through the SRF pathway, thereby inducing SMC differentiation [213]. Our findings demonstrate that also MYPN can bind to MRTFs and that both MYPN and PALLD can activate MRTF-A-induced SRF signaling in myogenic cells (see below and unpublished data).

# 4. MYPN MUTATIONS IN SKELETAL AND CARDIAC DISEASES

The function of striated muscle can be compromised by various human diseases, including heart failure, cardiomyopathies, skeletal myopathies and a wide range of neuromuscular conditions [214]. Indeed, the clinical relevance of sarcomeric alterations has been recently highlighted by the discovery of mutations in a number of genes encoding sarcomeric proteins, including *MYPN* (Table 3). Many of these mutations impair muscle contraction or relaxation, or disrupt the structural integrity of the sarcomere, leading to cardiac and skeletal myopathies [214].

**Table 3. Key structural proteins of the sarcomere: genes, physiologic role, and diseases caused by mutations.**

| Protein (alternative name) | Gene | | Physiological role / Features | Disease associations | Refs |
|---|---|---|---|---|---|
| | Skeletal | Cardiac | | | |
| *Thick filament* | | | | | |
| Myosin heavy chain | • *MYH1* (fast, type 2B)<br>• *MYH2* (fast, type 2A)<br>• *MYH3* (embryonic)<br>• *MYH7* (slow, type 1)<br>• *MYH8* (fetal)<br>• *MYH13* (extraocular) | • *MYH6* (α, atrial)<br>• *MYH7* (β, ventricular) | • Principal component of the thick filament<br>• ATPase motor protein that binds actin and generates sliding force between thick and thin filaments | • *MYH2*: inclusion body myopathy<br>• *MYH3* and *MYH8*: distal arthrogryposis<br>• *MYH7*: myosin storage myopathy, HCM and DCM | 54,117 |
| Myosin essential light chain | • *MYL1* (fast)<br>• *MYL3* (slow)<br>• *MYL4* (slow) | • *MYL3* (ventricular)<br>• *MYL4* (atrial) | • Stabilizes S1 neck region of myosin heavy chain | • *MYL3*: skeletal myopathy, HCM and DCM | 155,156 |
| Myosin regulatory light chain | • *MYLF* (fast)<br>• *MYL2* (slow) | • *MYL2* (ventricular)<br>• *MYL7* (atrial) | • Stabilizes S1 neck region of myosin heavy chain | • *MYL2*: skeletal myopathy, HCM and DCM | 156 |
| Myosin-binding protein C | • *MYBPC1* (slow)<br>• *MYBPC2* (fast) | • *MYBPC3* | • Anchored to myosin LMM and titin<br>• Interacts with myosin S2<br>• Slows release rate of actin from myosin | • *MYBPC1*: distal arthrogryposis<br>• *MYBPC3*: HCM and DCM | 140, 157–160 |
| Titin | • *TTN* (isoforms 4 and 6) | • *TTN* (isoforms 3, 7 and 8) | • Giant scaffolding protein required for sarcomere assembly<br>• Numerous binding partners<br>• Determines sarcomere resting length and passive stiffness | • Hereditary myopathy with early respiratory failure, tardive tibial muscular dystrophy, limb-girdle muscular dystrophy, DCM and ARVC | 123, 161–163 |
| *Thin filament* | | | | | |
| Actin | • *ACTA1* | • *ACTC1* | • Principal component of thin filament | • *ACTA1*: nemaline myopathy<br>• *ACTC1*: HCM and DCM | 164,165 |
| Tropomyosin | • *TPM1* (α, fast)<br>• *TPM2* (β, fast, slow)<br>• *TPM3* (γ, slow)<br>• *TPM4* (δ, fast, slow) | • *TPM1* (α) | • Coiled coil that lies along thin filament and blocks myosin binding sites on actin under resting calcium concentrations | • *TPM1*: HCM and DCM<br>• *TPM2*: distal arthrogryposis and nemaline myopathy<br>• *TPM3*: nemaline myopathy | 166–170 |
| Troponin T | • *TNNT1* (slow)<br>• *TNNT3* (fast) | • *TNNT2* | • Anchors troponin complex to tropomyosin | • *TNNT1*: nemaline myopathy<br>• *TNNT2*: HCM and DCM<br>• *TNNT3*: distal arthrogryposis | 166, 171,172 |
| Troponin I | • *TNNI1* (slow)<br>• *TNNI2* (fast) | • *TNNI3* | • Inhibitory region maintains actin–tropomyosin in a blocked state preventing strong myosin binding | • *TNNI2*: distal arthrogryposis<br>• *TNNI3*: HCM and DCM | 168,173 |
| Troponin C | • *TNNC1* (slow)<br>• *TNNC2* (fast) | • *TNNC1* | • Binds the switch region of troponin I in a calcium-dependent manner to activate contraction | • *TNNC1*: HCM and DCM | 174 |
| Nebulin (nebulette only in cardiac muscle) | • *NEB* | • *NEBL* | • Giant protein that lies along the full length of thin filament in skeletal muscle<br>• Shorter homologue restricted to Z-disc in cardiac muscle | • *NEB*: nemaline myopathy<br>• *NEBL*: DCM | 119, 175–177 |
| *Z-disc* | | | | | |
| α-actinin | • *ACTN2*<br>• *ACTN3* (fast) | • *ACTN2* | • Principal Z-disc component<br>• Crosslinks actin from adjacent sarcomeres<br>• Numerous binding partners | • *ACTN2*: HCM and DCM | 178, 79 |
| Telethonin | • *TCAP* | • *TCAP* | • Crosslinks two titin N termini | • Limb-girdle muscular dystrophy, HCM and DCM | 180,181 |
| Filamin C (γ-filamin) | • *FLNC* | • *FLNC* | • Crosslinks actin<br>• Binds sarcoglycans of the dystrophin complex | • Myofibrillar myopathy | 182,183 |
| Myozenin (calsarcin, FATZ) | • *MYOZ1*<br>• *MYOZ2*<br>• *MYOZ3* | • *MYOZ2* | • Binds to α-actinin, filamin, telethonin, myotilin and ZASP | • *MYOZ2*: HCM | 184,185 |
| Myopalladin | • *MYPN* | • *MYPN* | • Binds to α-actinin, titin, nebulin and ZASP | • HCM and DCM | 186–188 |
| Myotilin | • *MYOT* | • *MYOT* | • Binds to α-actinin, filamin, actin, myozenin and ZASP | • Limb-girdle muscular dystrophy and myofibrillar myopathy | 189–191 |
| LIM-domain binding protein 3 (cypher, oracle and ZASP-3) | • *LDB3* | • *LDB3* | • Binds to C terminus of myozenin, myopalladin or myotilin<br>• Recruits PKA, PKC and calcineurin | • Myofibrillar myopathy, HCM and DCM | 192–197 |

ARVC, arrhythmogenic right ventricular cardiomyopathy; DCM, dilated cardiomyopathy; HCM, hypertrophic cardiomyopathy; LMM, light meromyosin; PKA, protein kinase A; PKC, protein kinase C; S1, myosin subfragment 1; S2, myosin subfragment 2; ZASP, Z-disc-associated, alternatively spliced, PDZ motif-containing protein [214].

Mutations in *MYPN* have been identified in patients with DCM, HCM, and RCM and include heterozygous missense and nonsense located in various conserved parts of *MYPN*, having different effects on MYPN function and protein-protein interactions and resulting in cardiomyopathies of various severity and age of disease onset (from birth to 55 years of age) [4-6, 215] (Fig. 15). The average frequency of *MYPN* mutations has been estimated to 1.86% for HCM, 1.72-3.5% for DCM, and 1.45% for RCM [4, 6]. HCM is characterized by ventricular wall thickening (hypertrophy), especially in the intraventricular septum, associated with decreased ventricular chamber volume and diastolic dysfunction [216]. DCM results in a gradual prominent ventricular dilation generated by weakness of the ventricular chamber wall caused by damage to the myocardium, thus, resulting in systolic dysfunction [217]. RCM is characterized by increased myocardial stiffness, resulting in diastolic dysfunction [217, 218].

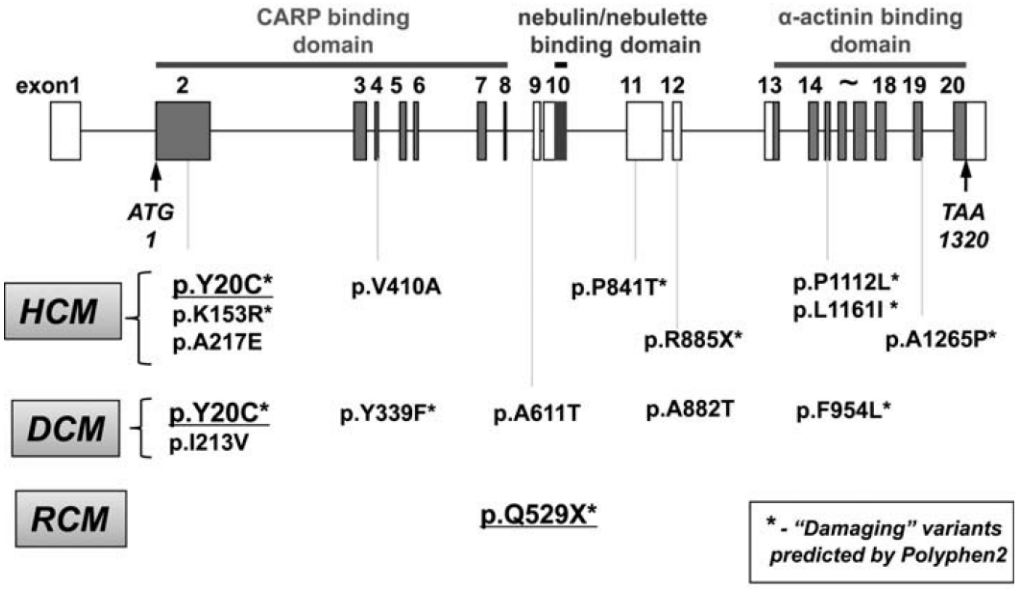



**Figure 15. Schematic representation of MYPN structure and associated mutations found in cardiac and skeletal muscle patients.** From [6].

Interestingly, the Y20C mutation in the MYPN binding region for CARP, has been identified in patients with both DCM and HCM and described in the dbSNP as a SNP with a low genotype frequency of A/G=0.001 [6]. Nevertheless, the causative effect of this mutation has been demonstrated in Y20C transgenic mice, which develop HCM, disrupted intercalated discs, and impaired nuclear translocation of MYPN, possibly due to impaired binding of MYPN to CARP and reduced CARP levels [6] (Fig. 16).

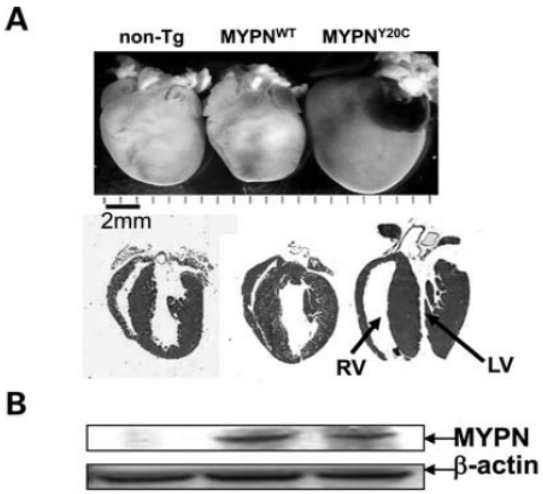



**Figure 16. Morphologic and functional assessment of MYPN Y20C transgenic (Tg) mouse hearts.** A) Morphology (upper panel) and H&E stained sections (lower panel) of non-Tg (left column), WT-Tg (middle column) and Y20C-Tg (right column) mouse hearts demonstrating concentric hypertrophy with severe thickening of the intra ventricular septum, left ventricular (LV) hypertrophy, and right ventricular (RV) dilation and thinning in MYPN-Y20C animals (arrows). B) Western blot analysis for human MYPN in non-Tg, MYPN-WT and MYPN-Y20C hearts.

In another study, a knockin mouse model for the Q529X nonsense mutation identified in a RCM family was described [219] (Fig. 15). Heterozygous knockin mice developed RCM and truncated MYPN Q526X protein was found to translocate to the nucleus, resulting in decreased levels of total and nuclear CARP, upregulation of MLP and desmin as well as reduced phosphorylation levels of Erk1/2, Smad2, and Akt and upregulation of markers of fibrosis and cardiac stress. In contrast, homozygous knockin of the Q526X mutation lead to MYPN instability with barely detectable MYPN levels in the mice, which exhibited no or only a minor cardiac phenotype [219]. Additional mutations have been studied in rat neonatal cardiomyocytes where overexpression of the V1195M and P1112L mutations were found to result in disruption of sarcomeric structure and decreased cell survival rate [4]. On the other hand, overexpression of the R1088H mutation showed no *in vitro* effects, while immunostainings of biopsies from an explanted heart revealed mislocalization of MYPN specifically in the left ventricle [4].

More insights into the role of MYPN in striated muscle and the mechanisms leading from *MYPN* mutations to the development of cardiomyopathies are essential for the development of targeted therapies for the treatment of MYPN-based cardiomyopathies.

# AIM OF THE PHD THESIS

Striated muscle is composed of a complex network of contractile, structural, and regulatory proteins, which form the highly organized sarcomere and is responsible for efficient contraction and synchronized transmission of force while maintaining cellular integrity. The sarcomere, the basic contractile unit of myofibrils, is made up of a highly ordered array of interdigitating thin (actin) and thick (myosin) filaments, which slide past each other during contraction. A third filament is formed by the giant protein titin, which stretches half a sarcomere and acts as a spring during muscle contraction and relaxation. At the Z-line, a multiprotein complex at the boundary between sarcomeres, actin and titin filaments from adjacent sarcomeres are cross-linked and connect the contractile apparatus with the cytoskeleton and extracellular matrix. The Z-line plays an essential role in efficient force generation and maintenance of striated muscle structure and function and is a focal point for mechanosensing and signal transduction [166]. This important role of the Z-line is confirmed by the identification of a growing number of mutations in Z-line associated proteins causing cardiomyopathies and muscular dystrophies, including the striated muscle specific protein MYPN.

MYPN is a 145 kDa protein belonging to a small protein family of immunoglobulin (Ig)-containing proteins, which in addition to MYPN includes PALLD and MYOT, which are all closely associated with the actin cytoskeleton [169, 220]. MYPN contains 5 IgC2 domains and is present both in the nucleus and the sarcomere where it interacts with nebulin, α-actinin, and PDZ-LIM family members in the Z-line, and CARP in the I-band [1, 2]. CARP, in turn, binds to the elastic titin N2A region, suggesting that MYPN and CARP may form a complex in the I-band involved in transduction of stretch-induced signaling from the sarcomere to the nucleus [3, 177].

In regard to the role of MYPN in actin cytoskeleton organization, we found that MYPN, like its other two family members PALLD and MYOT, can bind and bundle F-actin filaments (see below) [178, 179]. In addition, we demonstrated that MYPN, like PALLD, can bind to MRTF-A through its C-terminal region, and promote the MRTF-A-induced activation of the SRF pathway in C2C12 myogenic cells (see below). SRF is a MADS-box transcription factor, which plays an important role in regulating cardiac gene expression [11, 221] and skeletal muscle growth and maturation [8]. SRF activity is regulated by changes in actin dynamics, such as serum stimulation, leading to activation of Rho GTPase, which enhances

actin polymerization, thereby reducing the amount of free G-actin to which the transcriptional cofactor MTRF-A is bound. This releases MRTF-A from G-actin and allows it to translocate to the nucleus where it activates the transcriptional activity of SRF. Thus, proteins regulating the polymerization of actin, altering the F-actin/G-actin ratio, can influence SRF signaling.

The aim of my thesis project was to investigate the function of MYPN in skeletal and cardiac muscle structure, signaling, function, and disease based on the analysis of myopalladin knockout (MKO) mice.

The overall objective of this project is to provide new insights into the role of MYPN in striated muscle structure and function, as a better understanding of the mechanisms underlying MYPN-based cardiomyopathies is of critical importance for the future development of novel therapeutic approaches.

# MATERIAL AND METHODS

## 1. *IN VIVO* METHODS

### 1.1 Generation of Myopalladin knockout (MKO) mice

*Mypn* genomic DNA was isolated from a 129SVJ mouse genomic library (Stratagene, La Jolla, CA) and used to generate a MYPN-targeting construct for the fusion of the endogenous *Mypn* promoter with LacZ, resulting in MYPN knockout (Fig. 20A). The construct was created in the pBluescript II KS+ vector, and the 5′ arm of homology consisted of a 4,091 bp *BamH*I-*Sal*I fragment upstream of the MYPN start codon in exon 2 followed by a LacZ-neomycin cassette. The 3' arm of homology was a 4,351 *Sal*I-*Not*I fragment downstream of the *Mypn* start codon (Fig. 20A). The targeting construct was verified by sequencing and linearized with *Not*I before electroporation into R1 ES cells at the Transgenic Core Facility at the University of California, San Diego. G418-resistant ES clones were screened for homologous recombination by *Mfe*I digestion of ES cell DNA and Southern blot analysis with a 422 bp probe generated by PCR on mouse genomic DNA with *Mypn* specific primers (sense: GGAAGGCTGTAGAGCTATAAGGCATTCTAG; reverse: GCTTCAACCTTGCTATCATAGTTAAGGATG) (Fig. 20B). The WT allele is represented by the band of 8,041 kb, whereas the 9,336 kb band represents the correctly targeted mutant allele. Cells from two independent homologous recombinant ES clones were microinjected into C57BL/6 blastocysts and transferred into pseudopregnant mice. Male chimeras resulting from the microinjections were bred with female Black Swiss mice to generate germ line transmitted heterozygous MKO, which were subsequently intercrossed to generate homozygous MKO. Offspring from intercrosses were genotyped by PCR using mouse tail DNA and WT (sense: GTTCGGTATTCTCCTCGTTTTG; reverse: CTCTGGCGGGCTGTCTTTAGG), and mutant allele-specific primers (sense: GTTCGGTATTCTCCTCGTTTTG; reverse: AGATGAAACGCCGAGTTAACGC). Successful ablation of the *Mypn* gene was confirmed by Northern blot analysis using a 1000 bp probe (sense: GGCCGCAGTACAGTTCTGAAACCCAGTCCA; reverse: TCTCTGTACCACTCGACTTTCGGAGATGGG). Furthermore, Western blot analysis using a novel polyclonal antibody against MYPN (1:500, see below) confirmed the absence of MYPN from heart and skeletal muscle. Unfortunately, sequence analysis revealed that the inserted LacZ-neo cassette was out of frame with the *Mypn* start codon. The mice were

backcrossed 8 times into the C57BL/6J background. All animal studies were approved by the University of California San Diego Animal Care and Use Committee and the Italian Ministry of Health. Animal procedures were performed in full compliance with the guidelines for the Guide for the Care and Use of Laboratory Animals, eighth edition (2011) published by the US National Institutes of Health (NIH) and the Directive 2010/63/EU of the European Parliament on the protection of animals use for scientific purposes. Mice for experiments were sacrificed by cervical dislocation following anesthesia by intraperitoneal injection of a mixture of ketamine (100 mg/kg) and xylazine (5 mg/kg).

## 1.2 Mouse procedures

For surgical procedures, mice were anesthetized by intraperitoneal (IP) injection of a mixture of ketamine (100 mg/kg) and xylazine (5 mg/kg) and the depth of anesthesia was monitored by toe pinch. To study muscle regeneration following degeneration, 100 μl of 1.2% BaCl2 in 0.9% saline solution was injected into the right *Tibialis anterior* (TA) muscle under general anesthesia, while 0.9% saline solution was injected into the contralateral leg. The hindlegs were shaved before injection, allowing for better visualization of the TA. 4, 7, 14, 21, and 28 days after injection, mice were sacrificed and TA muscles were excised and frozen in isopentane cooled with liquid nitrogen. For denervation, mice were anesthetized and the sciatic nerve of the left limb was cut, while the right limb served as control. Mice were sacrificed after 14 days and muscles were excised and frozen in isopentane cooled with liquid nitrogen.

To study protein synthesis and degradation, 2- and 4-week-old MKO and WT mice were IP injected with MG262 (Apex Biotechnology Corporation, Hsinchu, Taiwan) and puromycin dihydrochloride (Merck Millipore Corporation, Billerica, MA, USA). MG262 is a reversible and cell-permeable proteasome inhibitor that inhibits chymotryptic activity in the heart, lung, skeletal muscle, and liver by 50–75%, whereas puromycin dihydrochloride is an aminonucleoside antibiotic, derived from the *Streptomyces alboniger*, that functions as a protein synthesis inhibitor that blocks translation through premature chain termination in the ribosome. MG262 injection (5 μm/Kg in 30% DMSO and 70% NaCl) was perfomed 24 h before puromycin injection (40 nmol/g in NaCl). 20 min after puromycin injection, mice were sacrified and tissues frozen in liquid nitrogen.

## 1.3 Treadmill running

To test exercise capacity, 3-month-old mice were subjected to exercise endurance tests on a 5-lane treadmill for mice (2Biological Instruments) equipped with an electric grid carrying a mild electric current forcing the animals to run. Following one day of acclimatization (0% inclination for 10 min at 15 cm/s), mice were subjected to an uphill running test at 15% inclination. One week later, mice were subjected to a downhill running test at 15% declination for 4 consecutive days. For both up- and downhill running tests, mice were warmed up for 10 min at 18 cm/s, whereafter the speed was increased by 3 cm/s every 2 min until exhaustion. The time and speed at which the mouse could not maintain sufficient speed to remain off the shock grid was recorded. Mice were sacrificed at various time points after the last downhill run and gastrocnemius and soleus muscles were processed for histological and TEM analyses. After the last run, some mice were injected with 100 µl 1% Evans blue dye in PBS (Dulbecco's Phosphate Buffered Saline, Sigma-Aldrich, St. Louis, MO, USA) at a 1% volume relative to body mass (200 ul per 20 g mouse), whereafter muscles were dissected out 24 hours later and snap frozen in isopentane cooled with liquid nitrogen. Cryosections (10 µm) were fixed in cold acetone (-20°C) for 2 min, mounted with Prolong gold antifade reagent (Life Technologies, Carlsbad, CA, USA), and visualized with the Olympus Fluoview FV1000 laser scanning confocal microscope (Olympus, Shinjuku, Tokyo) at the excitation wavelength of 568 nm.

## 1.4 *In vivo* cardiac physiology

Mice anesthetized with 1% isofluorane were subjected to transthoracic echocardiography using a Vevo 2100 System (VisualSonics) and a 30 MHz probe as previously described [222]. For surgical procedures, mice were anesthetized by intraperitoneal injection of a mixture of ketamine (100 mg/kg) and xylazine (5 mg/kg) and the depth of anesthesia was monitored by toe pinch. Transverse Aortic Constriction (TAC) was perfomed with a 27-gauge needle on 8-week-old MKO and control mice as previously described [222]. Cardiac morphology and function was assessed by echocardiography and the gradient for the arterial blood pressure between the constriction was evaluated by Echo Doppler analysis. Only mice with a pressure gradient >70 mmHg were included in the analysis. SHAM-operated mice were used as controls.

# 2. *EX VIVO* METHODS

## 2.1 Mechanical analyses

Mechanical studies were performed on fast *Extensor digitorum longus* (EDL) muscle from MKO and WT mice as well as skinned fibers isolated from the same muscles. Muscles were dissected by using scissors and forceps under a stereomicroscope (Stemi SV11, Carl Zeiss MicroImaging, Oberkochen, Germany) and mounted horizontally, between the lever of a motor/force transducer system (305C, Aurora Scientific Inc., Aurora, ON, Canada) and a lever carried by a micromanipulator, in a trough, containing physiological Krebs-Henseleit solution (119 mM NaCl, 4.7 mM KCl, 1.0 mM $MgSO_4$, 25 mM $NaHCO_3$, 1.2 mM $KH_2PO_4$ and 1.1 mM glucose) continuously saturated with carbogen (95% $O_2$ and 5% $CO_2$, pH 7.4) at room temperature (23-25°C). The muscle was straightened just above its slack length using the micromanipulator. The trough was sealed with a Perspex cover and mounted vertically on the stage with the motor/force transducer system on the top. Trains of stimuli of alternate polarity to elicit fused tetani (frequency 100-120 Hz) were delivered by means of two platinum wire electrodes running parallel to the muscle, 1 cm apart. The intensity of the stimuli was increased until the isometric plateau force reached a maximum constant value $T_0$ (indicating that all cells in the muscle were activated). The muscle length was further finely adjusted using the micromanipulator to obtain the maximum isometric force, corresponding to the plateau of the force-length relation. To compare isometric force among muscles, the isometric plateau force was normalized by the wet weight ($w$ in grams) of the muscle, measured at the end of each experiment with an electrobalance (Sartorius, Mod CP124S, Goettingen, Germany). The cross-sectional area (*CSA*) was calculated according to the relation:

$$CSA = (w \cdot \cos\theta) / (L_f \cdot \delta)\ (cm^2)$$

where $\theta$ is the pennation angle of the fibers (8° for EDL muscle, Table 1 in [223]), $L_f$ is the fiber length (cm) and $d$ is the muscle density (1.056 g/cm$^3$, [224]). $L_f$ is obtained by multiplying the muscle length by 0.51 in EDL muscle (Table 1 in [223]).

The force-velocity relation was determined by measuring the velocity of steady shortening $V$ after a drop in force from $T_0$ to a preset value $T<T_0$. The force-velocity points were fitted to the Hill hyperbolic equation [224]:

$$(T + a) \cdot (V + b) = (V_0 + b) \cdot a$$

where $a$, $b$, and $V_0$ (the unloaded shortening velocity) are the regression parameters.

To investigate the effect of absence of MYPN on force per myosin motor and calcium sensitivity of the contractile apparatus, experiments were done on glycerinated skinned fiber segments. The composition of skinning, relaxing, rigor, preactivating and activating solutions have been reported previously ([225] and references therein). Protease inhibitors (20 μg/ml leupeptin and 10 μM E-64; Sigma-Aldrich) were added to all solutions to preserve sarcomeric proteins.

Muscles were stored in skinning solution containing 50% glycerol at -20°C for up to 3-4 weeks. For mechanical testing, a muscle was transferred to a Petri dish, filled with skinning solution containing 50% glycerol, with the bottom covered by Sylgard (Dow Corning Ltd, Allesley, UK) and kept at 4-6°C. A 3-4 mm long fiber segment was cut and T-shaped aluminum clips were mounted at its extremities for attachment to transducer hooks. The fiber was mounted in a drop of relaxing solution between the lever arms of a loudspeaker motor and a capacitance force transducer and, to minimize the shortening of the fiber segment by extension of the damaged extremities and the development of inhomogeneity in sarcomere length across the fiber, the two ends of the fiber were fixed with glutaraldehyde in rigor solution (5% vol/vol) and glued to the clips with shellac dissolved in ethanol [225, 226]. The drop of solution is one of the series of drops in the system that allows rapid solution exchange [225]. The average sarcomere length (*sl*), the width (*d*) and height (*h*) of the fiber were measured in 1 to 2 points along the fiber with a x40 dry objective (NA 0.60; Carl Zeiss MicroImaging, Inc., Oberkochen, Germany) and a x25 eyepiece. The *sl* of both MKO and WT fiber was set to 2.4-2.5 μm. The *CSA* of the fiber was determined assuming elliptical geometry ($CSA = \pi/4 \cdot d \cdot h$), where $d$ is width and $h$ is height of the fiber. *CSA* was 1788 ± 133 $\mu m^2$ in WT (mean ± SD; 7 fibers) and 996 ± 84 $\mu m^2$ in MKO fibers (6 fibers). Using the rapid solution-exchange system, the fiber was transferred from relaxing solution to pre-activating solution at 2°C and, after 3 min, to activating solution at low temperature, where the isometric force developed is about 0.2 the isometric force developed at the test temperature (12-14°C). The fiber was then transferred to the activating solution at the test temperature for 6 s and subsequently transferred to relaxing solution at the same temperature. This protocol prevents the development of most of the force during calcium diffusion and thus minimizes the development of sarcomere non-uniformities. The solution exchange system allowed continuous recording of length changes of a selected population of sarcomeres (500-1200) by a striation follower [225].

The baseline force in the activating solution at the test temperature was determined by superimposing on the isometric contraction a fast shortening (rise time 3 ms, amplitude 10% of the initial bundle length $L_0$) that induces slack in the fiber. Step changes in fiber length to determine stiffness were imposed at the plateau of the isometric force.

Mechanical signals were recorded with a multifunction I/O board (PCI-6110E; National Instruments, Austin, TX, USA) at both 10 μs (experiments on skinned fibers) and 0.5 ms (experiments on muscles) sampling rates. A program written in LabVIEW (National Instruments) was used for signal recording and analysis. Data are expressed as means ± SEM except for the *CSA* (mean ± SD). Data were analysed using Origin (OriginLab Corporation) software.

## 2.2 Isolation of adult ventricular cardiomyocytes (CMCs)

For isolation of ventricular CMCs, hearts were cannulated and mounted on a Langendorff perfusion apparatus and perfused with Hank's Balanced Salt Solution (HBSS w/o $CaCl_2$ and $MgCl_2$, Gibco, Life Technologies) supplemented with 1.2 mM MgSO4, 15 mM glucose, 30 mM Taurine, and 1 mM $MgCl_2$ hexahydrate for 10 min at 37°C. Liberase blendzyme (Roche, Basel, Switzerland) (50 μg/ml) was then added to the solution and perfusion was continued for about 10 min until the heart became flaccid. Subsequently, the heart was removed and cells were dissociated and filtered through a 70 μm filter after which bovine serum albumin (BSA) (fraction V; Sigma-Aldrich) was added to a final concentration of 4% to inactivate the enzyme. The cells were then allowed to settle and resuspended in fresh solution.

## 2.3 Transmission Electron Microscopy (TEM)

Stretched EDL and soleus muscle were fixed in 3% glutaraldehyde in Ringer's solution (5 mM Sodium Phosphate buffer, 2 mM KCl, 2 mM $MgCl_2$, 100 mM NaCl, 5.6 mM glucose, pH 7.0) and subsequently stained for 1 hour in 1% osmium tetroxide, dehydrated in a series of acetone washes, and embedded in Araldite Epoxy resin (Agar Scientific, Stansted, Essex, United Kingdom) as described [227]. Ultrathin sections (90-100 nm) were cut with a Reichert Ultracut E ultramicrotome (Leica Microsystems, Wetzlar, Germany) and subsequently stained with uranyl acetate and lead citrate. For TEM, the heart was excised and fixed in 2% paraformaldehyde (PFA) and 2% glutaraldehyde in 0.15 M sodium cacodylate buffer pH 7.4 as previously described [228]. Briefly, the left ventricle was cut into small pieces (~1 mm

cubes) and stained overnight in 1% osmium tetroxide, 0.8% potassium ferrocyanide. The following day, tissue was stained for 2 hours in 2% uranyl acetate and subsequently dehydrated in a series of ethanol and acetone washes. The tissue was embedded in Durcupan resin (EMD, Gibbstown, NJ, USA) and ultra thin sections (60-70 nm) were stained with lead citrate. Electron micrographs were recorded by using a JEOL 1200EX electron microscope (Jeol, Akishima, Tokyo, Japan) operated at 80-100 kV. Z-line width was measured using ImageJ 2.0.0 software based on the analysis of >100 Z-lines per heart from 2-3 mice per genotype and time point. Z-line values were binned in 10 nm binds and plotted in histograms fitted with the Gaussian distribution using PRISM 6 software (Graphpad).

## 2.4 Histology and immunofluorescence

10 μm transverse cryosections of mouse hind limb muscles (TA, EDL, soleus) were subjected to Hematoxylin and Eosin and Picro Sirius red staining. Furthermore, ATPase staining was performed using an acidic pH of 4.3 to label type 1 fibers and a basic pH of 10.2 to label type 2 fibers [229]. The fiber type distribution in TA, EDL and soleus muscle was determined by measuring myosin heavy chain isoform levels as previously described [229].

To measure fiber cross sectional area of fibers of different fiber type, cross-sections were stained with laminin antibody (1:50, #L9393, Sigma-Aldrich) and the following myosin isoform specific antibodies (MHC2A 1:10, MHC2B 1:1, MHC2X 1:10 + MHC1 1:20; Developmental Studies Hybridoma Bank, DSHB, Iowa City, IA, Stati Uniti). Briefly, cross-sections were incubated with primary antibodies diluted in PBS for 3 days at 4°C, and subsequently with Alexa Fluor 488-conjugated or 568-conjugated Alexa Fluor IgG secondary antibodies (Invitrogen, Waltham, MA, USA) diluted at 1:100. The long incubation time was necessary because the myosin isoform specific antibodies gave only a weak signal. Confocal microscopy was performed using an Olympus Fluoview FV1000 laser scanning confocal microscope with a 60X oil immersion lens (N. A. 1.3; Olympus). Individual images (1024 x 1024) were converted to tiff format and merged as pseudocolor RGB images using ImageJ.
For histology, mouse hearts were harvested, relaxed in 50 mM KCl in PBS and fixed overnight in 4% PFA in PBS. Subsequently, hearts were dehydrated, embedded in paraffin, and cut in 10 μm sections. The heart sections were stained with hematoxylin and eosin, or Picro Sirius Red and imaged using a DotSlide Digital Virtual Microscopy System (Olympus).

# 3. *IN VITRO* METHODS

## 3.1 Cell culture

### *3.1.1 Primary skeletal muscle cells*

Primary myoblasts were isolated from the limbs of 3-day-old neonatal WT and MKO mice using a protocol modified from [230]. Briefly, skinned mouse limbs were collected from neonatal pups, minced, and subjected to serial trypsinization (successive 25 min periods until all tissue was digested) in 0.05% trypsin solution B (Biological Industries, Kibbutz Beit Haemek, Israel) in PBS by continuous stirring at 37°C. Cells were collected by centrifugation at 1000g for 5 min and resuspended in proliferation medium [DMEM with 4.5 g/L glucose (Sigma-Aldrich), 20% heat inactivated FBS (Sigma-Aldrich), 2 mM Ultraglutamine (Lonza, Verviers, Belgium), 10 mM Hepes (Lonza), and 10 U/ml penicillin and 100 U/mL streptomycin (Lonza)]. Following filtration of the homogenate in sequence through 100, 70, and 40 μm nylon mesh cell strainers, the cells were preplated for 15 min on a tissue culture dish coated with 0.1% porcine skin gelatin in bidistilled water (Sigma-Aldrich), and subsequently for 1 hour on an uncoated dish to remove fibroblasts. To further enrich the myoblast population, unwanted cells were removed using Feeder Removal Micro-Beads (Miltenyi Biotec, Bergisch Gladbach, Germany), and subsequently the Satellite Cell Isolation Kit (Miltenyi Biotec) using LS separation columns and a gentleMACS dissociator following the manufacturer's instructions. The cells were plated on a gelatin-coated plate in proliferation medium supplemented with 50 ng/ml human basic fibroblast growth factor (bFGF) (GenScript, Piscataway Township, NJ, USA). 24 hours later the cells were washed in PBS and incubated with proliferation medium supplemented with 50 ng/ml bFGF and 25 μM forskolin (Cayman Chemical, Ann Harbor, MI, USA). The addition of bFGF and forskolin allowed the cells to stay unproliferated and to be passaged, whereby the remaining few fibroblasts were eliminated through delicate detachment of myoblasts from the plate using 0.5 mM EDTA in PBS and additional preplating. The highly purified myoblasts were plated on gelatin-coated 6-well plates (1.2 x $10^6$ cells/well) in proliferation medium containing 50 ng/ml bFGF and induced to differentiate at 95% confluence by reduction of serum levels to 2% horse serum (Gibco, Life Technologies).

To study proliferation rate of MKO and WT skeletal muscle primary cells, the Click-iT® EdU Assay (Invitrogen) was used. It is a novel alternative to the BrdU assay based on the use of EdU (5-ethynyl-2´-deoxyuridine), a nucleoside analog of thymidine, which is

incorporated into DNA during active DNA synthesis [231]. Detection is based on a click copper-catalyzed covalent reaction between an azide contained in the EdU and an alkyne present in the Alexa Fluor® dye [232-235]. Briefly, MKO and WT skeletal muscle primary cells were plated on coverslips the day before treatment. EdU was added to cells to a final concentration of 10 μM and incubated for 2 hours. Subsequently, cells were washed with PBS, fixed with PFA 4% for 10 min, washed twice with 3% BSA in PBS, and permeabilized with 0.5% Triton X-100 in PBS for 20 min at room temperature. After two washes with 3% BSA in PBS, cells were incubated with Click-iT® reaction cocktail for 30 min at room temperature, protected from light. Then cells were washed once again with 3% BSA in PBS, and incubated with Hoechst 33342 solution (5 μg/ml) for 30 min at room temperature. Imaging was performed as previously above.

### *3.1.2 C2C12 cells*

The myogenic C2C12 mouse cell line was maintained at subconfluence in Dulbecco's modified Eagle's medium (DMEM) containing 4.5 g/L glucose (Sigma-Aldrich) supplemented with 20% heat inactivated Fetal Bovine Serum (FBS) (Sigma-Aldrich), 2 mM Ultraglutamine (Lonza), and 10 U/ml penicillin and 100 U/mL streptomycin (Lonza). The cells were grown at 37°C in a humidified atmosphere with 5% of CO2 in air. C2C12 cells were differentiated when they were at 95% confluence by reducing serum levels to 2% horse serum (Gibco, Life Technologies).

### *3.1.3 HEK293 cells*

Human Embryonic Kidney (HEK) cells were maintained at subconfluence in Dulbecco's modified Eagle's medium (DMEM) containing 4.5 g/L glucose (Sigma-Aldrich) supplemented with 10% heat inactivated Fetal Bovine Serum (FBS) (Sigma-Aldrich), 2 mM Ultraglutamine (Lonza), and 10 U/ml penicillin and 100 U/mL streptomycin (Lonza). The cells were grown at 37°C in a humidified atmosphere with 5% of $CO_2$ in air.

## 3.2 SRF-luciferase reporter assay

C2C12 cells were plated on 12-well dishes coated with 0.1% gelatin from porcine skin and transiently transfected using Lipofectamine LTX (Life Technologies) according to the manufacturer’s instructions, resulting in a transfection efficiency of approximately 70%. The expression vectors encoding MYPN Full Length (Pxj40-HA-MYPN FL) and/or MRTF-A

(Pxj40-FLAG-MRTF-A) (quantity as indicated in Fig. 19C) were used with a luciferase reporter gene controlled by the smooth muscle 22 (SM22) promoter (5 ng), activated by SRF. The transfection efficiency was normalized by cotransfecting cells with Renilla standardization reporter plasmid (5 ng) in which Renilla luciferase is under the control of the thymidine kinase promoter (pRLTK). 1 μg of total plasmid DNA was used and the total amount of each plasmid DNA was kept constant by adding empty expression vector. 24 hours after transfection, C2C12 myoblasts were induced to differentiate and after 48 hours of differentiation cells were lysed. Luciferase and Renilla activities were measured on a SinergyH4 (Biotek, Winooski, VT, USA) system using the Dual-Luciferase Reporter Assay System (Promega, Fitchburg, Wisconsin, USA) according to the manufacturer's instructions. Luciferase activity was normalized to Renilla activity to account for variations in transfection efficiency. All experiments were performed in triplicates and repeated at least three times.

## 3.3 Co-Immunoprecipitation (Co-IP)

HEK293 cells were plated on 60 mm dishes and transiently transfected using Lipofectamine LTX (Life Technologies) according to the manufacturer's instructions, resulting in a transfection efficiency of approximately 70%. Expression vectors encoding MYPN Full Length (Pxj40-HA-MYPN FL) and/or MRTF-A (Pxj40-FLAG-MRTF-A) were used. 48 hours after transfection cells were harvested and pellet was resuspended in 200 μl IP buffer (20 mM Tri-HCl pH 7.5, 150 mM NaCl, 1 mM EDTA, 1 mM EGTA, 1% Triton X-100) supplemented with protease inhibitors (1 mM PMSF and Complete Protease Inhibitor Cocktail Tablets; Roche). After 20 min of incubation on ice, the lysate was centrifuged at 14.000 x *g* for 10 min at 4°C and 15% of the supernatant was added with 4X SDS protein sample buffer [100 mM Tris-HCl pH 6.8, 40% (v/v) glycerol, 312 mM SDS, 174 mM DTT, 0.04% (w/v) bromophenol blue] and submitted to Western blot analysis with FLAG-antibody (Clone M2, #F3165, Sigma-Aldrich), whereas the remaining supernatant was immunoprecipitated with 10 μg HA-antibody (#H6908, Sigma-Aldrich) overnight at 4°C with agitation. 30 μl of Protein G Dynabeads (Novex, Life Technologies) are used per IP. After washing in IP buffer supplemented with protease inhibitors, the beads were mixed with lysate and first incubated for 5-10 min at room temperature, and subsequently for 1 hour at 4°C with agitation. At the end of the incubation, the mixed beads-lysate was washed 5 times with IP buffer and added with 4X SDS protein sample buffer for Western blot analysis using FLAG-antibody.

# 4. BIOCHEMISTRY AND MOLECULAR BIOLOGY

## 4.1 Plasmid constructs

MYPN and MRTF-A cDNA were isolated by PCR from mouse or human cDNA as a template and cloned into Pxj40-HA, Pxj40-FLAG, pGADT7, pGBKT7 vectors using the In-Fusion HD cloning kit (Clontech Laboratories Inc, Mountain View, CA, USA) according to the manufacturer's instructions. Primer sequences and plasmid construct designs are described in Table 4. All constructs were confirmed by sequencing. The plasmid constructs PxJ40-Flag mouse MRTF-A and pGADT7 human MRTF-B were kindly provided by Dr. Carol Otey (University of North Carolina, USA) and Dr. Maria K. Vartiainen (University of Helsinki, Finland), respectively.

**Table 4. List of plasmid constructs and primers used for cloning.**

| **Construct** | |
|---|---|
| **Pxj40-HA mouse MYPN FL** | **Sense Primer**<br>atccaagcttctcgag/ATGCAAGAAGACAGCATAGAGGCATCCA<br>**Reverse Primer**<br>agatctggtaccctgcagcc/TTAAAGTTCATCGCTCTCCACTACACTCC |
| **Pxj40-HA mouse MYPN Ig3-Ig4** | **Sense Primer**<br>atccaagcttctcgag/TGCATCGCGCCCATCTTTGACAAAAGGCTCAAG<br>**Reverse Primer**<br>agatctggtaccctgcagcc/CTTCTTTACCTCTTTGGCTACCACAGTGAGCTCC |
| **pGBKT7 human MYPN FL** | **Sense Primer**<br>tttcatatg/ATGCAAGACGACAGCATAGAAGCTTCTACT<br>**Reverse Primer**<br>tttggatcc/TTAAAGTTCATCACTCTCCACTACACTCCG |
| **pGBKT7 human MYPN C-term** | **Sense Primer**<br>tttcatatg/CCCACGGGCAAGTGTATTGCTCCCATCTTT<br>**Reverse Primer**<br>tttggatcc/TTAAAGTTCATCACTCTCCACTACACTCCG |
| **pGADT7 human MRTFA** | **Sense Primer**<br>ggaggccagtgaattc/ATGCCGCCTTTGAAAAGTCCAGC<br>**Reverse Primer**<br>cgagctcgatggatcc/CTACAAGCAGGAATCCCAGTGCAG |

## 4.2 Yeast techniques

### *4.2.1 Yeast two-hybrid screening*

*Principle*

The yeast two-hybrid system can be used to identify novel protein interactions by screening cDNA libraries, confirm putative interactions, and define interacting domains. In the yeast two-hybrid system, a bait gene is expressed as a fusion to the GAL4 DNA-binding domain (DNA-BD), while another gene or cDNA is expressed as a fusion to the GAL4 activation domain (AD) [236, 237]. The recombinant hybrid proteins are coexpressed in yeast and are targeted to the yeast nucleus. When bait and library fusion proteins interact, the DNA-BD and AD are brough into proximity. As a result of a yeast two-hybrid interaction, the transcriptional activator will be functionally reconstituted and will activate the transcription of reporter genes (Fig. 17).

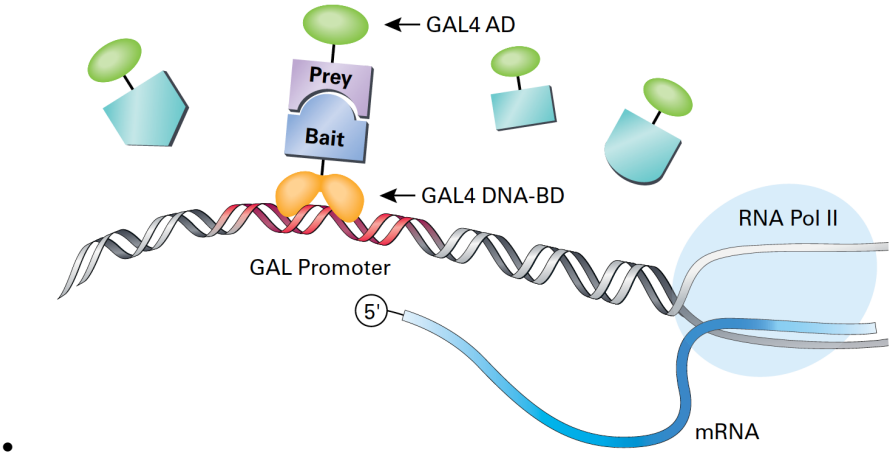



**Figure 17. The two-hybrid principle.** Two proteins are expressed separately, one (a bait protein) fused to the Gal4 DNA-binding domain (BD) and the other (a prey protein) fused to the Gal4 transciptional activation domain (AD). When bait and library (prey) fusion proteins interact, the DNA-BD and AD are brought into proximity to activate the transcription of reporter genes. In the Y2H system, activation of the reporters (AUR1-C, ADE2, HIS3, and MEL1) only occurs in a cell that contains proteins, which interact and bind to the Gal4-responsive promoter (Modified from Matchmaker™ Gold Yeast Two-Hybrid System User Manual).

We took advantage of the Yeast two hybrid gold system from Clontech Laboratories in which the following reporter genes are used:

- **AUR1-C**, a dominant mutant version of the AUR1 gene that encodes the enzyme inositol phosphoryl ceramide synthase, which confers strong resistance to the highly toxic drug Aureobasidin A;
- **HIS3**, which permits cells to biosynthesize histidine and grow on -histidin (-His) minimal medium.
- **ADE2**, which allows cells to grow on -adenin (-Ade) minimal medium.

- **MEL1**, which encodes α-galactosidase, an enzyme occurring naturally in many yeast strains. As a result of two-hybrid interactions, α-galactosidase (MEL1) is expressed and secreted by the yeast cells and yeast colonies that express Mel1 turn blue in the presence of the chromagenic substrate X-α-Gal.

*Procedure*

pGBKT7-BD and pGADT7-AD vectors (Clontech Laboratories Inc.) containg cDNA encoding the proteins of interest were cloned using the In-Fusion HD cloning kit as described above (Clontech Laboratories Inc.). pGBKT7-BD is a yeast two-hybrid bait expression vector that is designed to express a fusion protein of the GAL4 DNA-binding domain (DNA-BD; amino acids 1-147) and a bait protein, whereas pGADT7-AD is a yeast expression vector that is designed to express a fusion protein between the GAL4 activation domain (AD; amino acids 768-881) and a protein of interest. Bait and prey vectors were transformed together into the Y2H Gold yeast strain (Clontech Laboratories Inc.) using the Frozen-EZ Yeast Transformation II$^{TM}$ kit (Zymo Research, Irvine, CA, USA) following the manufacturer's instructions. Briefly, yeast cells were grown overnight at 30°C in yeast-extract peptone-dextrose (YPD) medium (Clontech Laboratories Inc.) with maximal shaking. The following morning, $OD_{600}$ was measured and yeast cells were diluted to a concentration of $5*10^6$ cells/ml (corresponding to $OD_{600} = 3*10^7$ cells/ml) and grown for 3-4 hours until the cell titer reached 2 x $10^7$ cells/ml ($OD_{600}$ = 0.6-0.8). The cells were harvested by centrifugation at 500 x *g* for 4 min and washed with EZ 1 solution. After a second centrifugation, EZ2 solution was added to the pellet. At this point, the competent cells can be used for transformations or stored at –80°C for future. For transformation, 10 ul competent cells were mixed with 1.5 ug DNA (0.75 ug of each construct) and 100 ul EZ3 solution, and incubated at 30°C (heat block shaker) for 90 min. 1 mL of YPD was then added to the reaction mix and yeast cells were incubated for other 2 h at 30°C. Subsequently, cells were spun down and washed with 1 mL of water. After resuspension in 30 ul water, yeast cells were spotted (5 µl) on selective plates of synthetically defined (SD) medium lacking the amino acids tryptophan (Trp), leucin (Leu), histidin (His), and adenine (Ade) containing 120 ng/mL aureobasidin A and incubated at 30°C for 3-4 days to verify the interaction. The succesful transformation of the two plasmids was confirmed by spotting on SD/-Trp/-Leu plates. Possible autoactivation of the bait and the prey constructs was tested by cotransformation of the bait or prey vector with empty prey or bait vector, respectively.

## 4.3 Actin assays

### *4.3.1 Protein expression and purification*

The coding sequence of MYPN Ig3 was subcloned into the pTBSG vector with N-terminal $His_6$-tag and a tobacco etch virus (TEV) protease cleavage site. The plasmids were transformed into BL21-DE3 cells and proteins were expressed using auto-induction media [239], starting the growth at 37°C until $A_{600}$ = 0.6-0.8, then lowering to 18°C for 20-24 hours. Cells were harvested by centrifugation for 20 min at 2,000 x *g*. Cells were resuspended in lysis buffer (50 mM Tris-Cl, 300 mM NaCl, 5 mM imidazole, pH 8.0, Complete Protease Inhibitor Cocktail Tablets; Roche) and lysed by sonication for 20 min. The lysate was centrifuged at 48,000 x *g* for 45 min to pellet cell debris. Supernatant was loaded on a pre-equilibrated Ni-NTA column (Thermo Fisher Scientific, Waltham, MA). The column was washed twice with 50 mL wash buffer (50 mM Tris-Cl, 300 mM NaCl, 25 mM imidazole, pH 8.0) and the fusion protein was eluted with 50 mL elution buffer (50 mM Tris-Cl, 300 mM NaCl, 500 mM imidazole, pH 8.0). The N-terminal $His_6$-tag was cleaved overnight at 4 °C in the elution buffer using TEV protease and protein was further purified as previously reported [240].

### *4.3.2 Actin co-sedimentation assays*

Actin was purified from rabbit muscle acetone powder as described previously and snap-frozen [241]. Frozen stocks of G-actin were allowed to polymerize by adding an equal volume of 2X F-buffer (20 mM Tris-Cl, 200 mM KCl, 4 mM $MgCl_2$, 4 mM DTT, pH 8.0) and incubating for 30 min at room temperature. The purified MYPN Ig3 domain was centrifuged at 150,000 x *g* for 30 min to pellet any insoluble protein before use. The final concentration of polymerized actin (5 or 10 μM) was incubated with various concentrations of MYPN Ig3 domain (1-50 μM) for 1 hour with the final volume of each sample made up to 100 μL with 1X F-buffer, then centrifuged at 150k x *g* in an Beckman Airfuge® Air-Driven ultracentrifuge for 30 min for binding assays. Supernatants were separated and the pellets were resuspended in 100 μL 2X SDS running buffer. Finally, 35 μL of 4X loading dye was added to each of the samples, which were boiled for 4 min and loaded on 15% SDS-PAGE gels. The gel bands were visualized by Coomassie stain and the relative amount of MYPN in the supernatants and pellets was measured by densitometry of SDS-PAGE bands using ImageJ [242].

To monitor actin bundling or crosslinking, a differential sedimentation assay was carried out as above with one modification. After the polymerized actin was incubated with

various concentrations of protein for 1 hour at room temperature, the mixture was centrifuged at 5,000 x *g* for 10 min in a Sorvall™ microcentrifuge. The supernatant was then transferred to another tube for further centrifugation at 150,000 x *g* for 30 min. The slow speed pellet, or bundled actin, was dissolved in 100 μL 2X SDS buffer. The high-speed supernatant and the pellet was resuspended in 100 μL 2X SDS running buffer. Loading dye was added to each of the samples, boiled for 4 min, and loaded on 15% SDS-PAGE gels. The gel bands were visualized by Coomassie stain and the ratio of actin that appeared in bundles, supernatants, and pellets was measured by densitometry of SDS-PAGE bands using ImageJ [242].

#### *4.3.3. Fluorescence microscopy of actin filament bundles*

10 μM polymerized F-actin in 1x F-actin buffer was mixed with various concentrations of MYPN Ig3 domain (0, 5, 10 μM) and allowed to incubate for 30 min before dilution with 1.5 μM Alexa Fluor-488 phalloidin (Life Technologies), first to 1 μM F-actin and subsequently to 100 μM. 5 μL of each sample was placed between a coverslip and glass slide and visualized by confocal microscopy using a Nikon TE200-U microscope with 60x objective lens, an optional 1.5x tube lens, and a Hamamatsu Orca-ER camera.

#### *4.3.4 Pyrene fluorescence assay*

Gel-filtered G-actin was labeled with pyrene as reported earlier [243]. Pyrenyl actin and unlabeled G-actin were mixed together to make 10 μM 5% pyrene-labeled G-actin stock. Ca-G-actin (100 μL) was incubated with 10 μL of 10X priming solution (10 mM EGTA and 1 mM $MgCl_2$) for 2 min, and then polymerization was induced by adding various concentrations of MYPN with 25 mM KCl (polymerizing condition) or without KCl (G-buffer condition). Pyrene fluorescence was measured immediately with excitation at 365 nm and emission at 385 nm.

## 4.4 RNA analyses

#### *4.4.1 RNA Extraction, RNA Reverse Transcription, and Quantitative Real-Time Polymerase Chain Reaction (qRT-PCR)*

Total RNA was isolated using PureZol™ RNA Isolation Reagent (BioRad Laboratories, Hercules, CA, USA) according to the manufacturer's instructions. RNA purity and

concentration were evaluated using a NanoDrop 1000 spectrophotometer (Thermo Fisher Scientific).

1 μg of total RNA from each sample was reverse transcribed using the High Capacity cDNA Reverse Transcription kit (Applied Biosystems, Foster City, CA, USA) according to the manufacturer's instructions. The cDNA was stored at -20°C or analyzed by qRT-PCR.

qRT-PCR reaction was conducted using the ViiA$^{TM}$ 7 Real-Time PCR System (Applied Byosystems) with the following thermal cycler conditions: 95°C for 20 s, 40 cycles of 95°C for 1 s, and 60°C for 20 s. qRT-PCR was performed in triplicate with custom designed oligos (Table 5) using the SYBR Select Master Mix (Life Technologies). The cDNA levels were normalized to those of the *housekeeping GAPDH* or *β-actin* gene and calculated relatively to controls by the $2^{-\Delta\Delta Ct}$ method [244].

**Table 5. Mouse specific qRT-PCR primers.**

| GENE | SENSE PRIMER | REVERSE PRIMER |
|---|---|---|
| ***Mypn*** | CATGCTTTGCTTCCAACATT | GGCTTCTGGATTCGATTCAT |
| ***Gapdh*** | ACCCAGAAGACTGTGGATGG | CACATTGGGGGTAGGAACAC |
| ***β-Actin*** | TGTTACCAACTGGGACGACA | GGGGTGTTGAAGGTCTCAAA |

### *4.4.2 RNA sequencing*

Indexed sequencing libraries were generated from 1 ug RNA, using the TruSeq Stranded Total RNA Sample Prep Kit with Ribo-Zero ribosomal RNA reduction chemistry (Illumina, San Diego, CA). Electrophoresis of the libraries on a Bioanalyzer 2100 instrument (Agilent) showed highest peaks at 230-270 bp. Paired-end multiplexed sequencing of libraries (four per flow cell lane) to generate reads of 100 bp was performed on a HiSeq 1000 instrument with TruSeq SBS and PE Cluster v3 Kits (Illumina). 70-100 million reads for all samples were obtained.

### *4.4.3 RNA sequencing analysis*

Differential expression analysis of read counts was performed using the Generalized Linear Model approach for multiple groups implemented in the Bioconductor package "edgeR" [245, 246]. For analyses of RNA-sequencing data, *p* values were corrected for multiplicity according to the Benjamini-Hochberg procedure (false discovery rate (FDR)) [247]. The threshold used for the FDR was 0.05. The differentially expressed genes were further filtered by change magnitude (fold change ≥ 1.5). Hierarchical clustering was performed using Cluster 3.0 software [248], including the significantly modulated genes. The normalized

expression value (RPKM, Reads Per Kilobase per Million mapped reads) was adjusted to log transform data and "median" was selected to center genes. Clustering was performed using the *Pearson* correlation function. The heatmap images were exported with Java TreeView software [248]. In addition, Ingenuity Pathway Analysis (IPA) was performed to determine significantly affected pathways and molecular networks.

## 4.5 Protein assays

### *4.5.1 Protein extraction*

For protein extraction, muscle tissue was homogenized in RIPA buffer [50 mM Tris-HCl pH 7.5, 150 mM NaCl, 0.5 mM DTT, 1 mM EDTA, 1% (v/v) SDS, 1% (v/v) Triton X-100] supplemented with protease inhibitors (1 mM PMSF and Complete Protease Inhibitor Cocktail Tablets; Roche), and phosphatase inhibitors (Pierce™ Phosphatase Inhibitor Mini Tablets; Thermo Fisher Scientific) using TissueLyser II (Qiagen, Valencia, CA, USA). Cells were lysed in standard RIPA buffer containing 0.1% SDS. Lysates were incubated on ice for at least 30 min and then centrifuged at 12.000 x *g* for 20 min at 4°C. The supernatant containing the protein extracts was transferred into a new eppendorf tube and stored at -20°C or submitted to Bradford protein assay using the BioRad DC™ Protein Assay Kit (BioRad Laboratories) according to the manufacturer's instructions.

### *4.5.2 Determination of protein concentration*

The Bradford protein assay (BioRad Laboratories) was used to determine protein concentration. It is a colorimetric assay based on the proportional binding of Coomassie Brilliant Blue G-250 dye to proteins [249]. Coomassie absorbs at 465 nm, but this value shifts to 595 nm when it binds to proteins. The absorbance increase at 595 nm is proportional to the amount of bound dye and, thus, to the concentration of proteins present in the sample. The protein concentration was determined using a standard curve in which the increasing concentration values of the BSA standard protein solutions were reported in the x axis and the corresponding absorbance values in the y axis. The sample protein concentration was determined based on the BSA absorbance in concentration known solutions.

### *4.5.3 SDS-Polyacrylamide Gel Electrophoresis (SDS-PAGE)*

Protein separation was performed on polyacrylamide gels, using the BioRad Mini Protean 3 Cell Electrophoresis System (Bio-Rad Laboratories) following the instructions of the

manufacturer. The polyacrylamide gels were made up of an upper stacking gel containing 4% acrylamide/bis-acrylamide, and a lower running separation gel of different acrylamide/bis-acrylamide concentrations (e.g. 8-15%), according to the molecular weight (MW) of the analyzed proteins (Table 6).

**Table 6. Components of upper stacking and lower separation/running gel for SDS-PAGE.**

| COMPONENTS OF STACKING GEL (Vf = 4 ml) | 4% |
|---|---|
| $H_2O$ | 2.87 ml |
| 0.5 M Tris-HCl pH 6.8 | 0.48 ml |
| 30% (w/v) Acrylamide/Bis-Acrylamide | 0.53 ml |
| 10% (w/v) SDS (Sodium Dodecyl Sulfate) | 0.04 ml |
| 10% (w/v) APS (Ammonium Persulfate) | 0.04 ml |
| TEMED (N,N,N′,N′-Tetramethylethylenediamine) stock | 0.004 ml |

| COMPONENTS OF SEPARATION/RUNNING GEL (Vf = 8 ml) | 8% | 10% | 12% | 15% |
|---|---|---|---|---|
| $H_2O$ | 3.70 ml | 3.10 ml | 2.60 ml | 1.80 ml |
| 1.5 M Tris-HCl pH 8.8 | 2.08 ml | 2.08 ml | 2.08 ml | 2.08 ml |
| 30% (w/v) Acrylamide/Bis-Acrylamide | 2.10 ml | 2.70 ml | 3.20 ml | 4.00 ml |
| 10% (w/v) SDS (Sodium Dodecyl Sulfate) | 0.08 ml | 0.08 ml | 0.08 ml | 0.08 ml |
| 10% (w/v) APS (Ammonium Persulfate) | 0.08 ml | 0.08 ml | 0.08 ml | 0.08 ml |
| TEMED (N,N,N′,N′-Tetramethylethylenediamine) stock | 0.008 ml | 0.008 ml | 0.008 ml | 0.008 ml |

In order to promote protein denaturation, protein extracts were added with 4X SDS protein sample buffer [100 mM Tris-HCl pH 6.8, 40% (v/v) glycerol, 312 mM SDS, 174 mM DTT, 0.04% (w/v) bromophenol blue], and boiled for 5 min at 95°C. Equal amounts of protein extracts (50 µg) for each sample were loaded onto the gel together with molecular weight standards (Precision Plus Protein™ Dual Color Standards, Bio-Rad Laboratories), and separated at 120V in *running buffer* [25 mM Tris, 192 mM glycine, 0.1% (w/v) SDS pH 8.3, BioRad Laboratories]. At the end of the run, proteins were transferred onto a PVDF membrane (Bio-Rad Laboratories) as described by *Towbin et al.* [250]. The electrotransfer was perfomed in *Towbin buffer* composed of *transfer buffer* [25 mM Tris, 192 mM glycine pH 8.3 (BioRad Laboratories)] supplemented with 20% (v/v) methanol at 100 for 1h at room temperature, using the Bio-Rad Transblot System (BioRad Laboratories). The protein transfer from the polyacrylamide gel to the PVDF membrane was confirmed by reversibly staining with *Ponceau S Red* (Sigma-Aldrich), which was subsequently washed away with PBS (Sigma-Aldrich) with 0.1% Tween 20 (PBST).

### *4.5.4 Western Blot analysis*

To block non-specific binding sites, the PVDF membrane was incubated with 5% non-fat powdered dry milk in PBST for 1h at room temperature. The membrane was then incubated with primary antibody diluted in 5% non-fat powdered dry milk (Sigma-Aldrich) or BSA in PBST overnight at 4°C (Table 7). It was then washed three times for 10 min in PBST and incubated with secondary antibody (Goat Anti-Rabbit IgG Horseradish Peroxidase (HRP) #31460, Thermo Fisher Scientific; Goat Anti-Mouse IgG-HRP #31430 Thermo Fisher Scientific; Donkey Anti-Goat IgG-HRP sc2020, Santa Cruz Biotechnology, Dallas, Texas, USA) diluted in 5% non-fat powdered dry milk in PBST for 1h at room temperature. After three wash in PBST, the membrane was incubated with the Immobilion$^{TM}$ Western Chemiluminescent HRP Substrate (Merck Millipore Corporation), whose chemiluminescence allowed for the detection of proteins bound by the antibody on a Chemidoc$^{TM}$ MP System (BioRad Laboratories).

**Table 7. Primary antibodies used for Western blot analysis.**

| Protein | Corporation | Concentration |
|---|---|---|
| **MYPN** | From [55] | 1:1.000 |
| **CARP** | Proteintech Europe 11427-AP | 1:1.000 |
| **IGF-1BR** | Cell Signaling 3027 | 1:500 |
| **PDK1-S241** | Cell Signaling 3438 | 1:500 |
| **PDK1** | Calbiochem St-1036 | 1:2.000 |
| **AKT-T308** | Cell Signaling 2965 | 1:1.000 |
| **AKT-S473** | Cell Signaling 4060 | 1:1.000 |
| **AKT** | Cell Signaling 9272 | 1:1.000 |
| **GSK3β-S9** | Cell Signaling 5558 | 1:500 |
| **GSK3β** | Cell Signaling 9315 | 1:1.000 |
| **p70S6K-T421/S424** | Cell Signaling 9204 | 1:500 |
| **p70S6K** | Cell Signaling 2708 | 1:500 |
| **ERK 1/2-T202/Y204** | Cell Signaling 4376 | 1:1.000 |
| **ERK 1/2** | Cell Signaling 4695 | 1:1.000 |
| **PAK1/2-S144/S141** | Cell Signaling 2606 | 1:500 |
| **PAK1** | Cell Signaling 2602 | 1:1000 |
| **P21** | Santa Cruz 6246 | 1:500 |
| **α-ACTININ** | Sigma-Aldrich, clone EA-53, A7811 | 1:50.000 |
| **Anti-Ubiquitinylated proteins** | Millipore, clone FK2, 04-263 | 1:1.000 |
| **Anti-PUROMYCIN** | Millipore, clone 12D10, MABE343 | 1:25.000 |
| **β-ACTIN** | Santa Cruz 1615 | 1:1.000 |
| **α-TUBULIN** | Abcam 176560 | 1:4.000 |
| **GAPDH** | Proteintech Europe 10494-1-AP | 1:15.000 |

# 5. STATISTICAL ANALYSIS

Data are presented as mean ± standard deviation (SD) or standard error of the mean (SEM) as indicated. Statistical comparisons between MKO and WT were done using the unpaired Student's t-test [251]. Simultaneous effects of genotype and another experimental variable were determined using two-way analysis of variance (ANOVA) post-hoc Fisher's protected least-significant difference (PLSD) analysis. $P < 0.05$ was considered significant. Statistical analysis was performed using Origin (OriginLab Corporation) software (muscle mechanics) or Prism 6 software (GraphPad).

# RESULTS

## 1. THE ROLE OF MYPN IN THE ORGANIZATION OF THE ACTIN CYTOSKELETON

### 1.1 MYPN binds and bundles F-actin and promotes actin polymerization

PALLD has previously been shown to bind and bundle filamentous actin (F-actin) through its immunoglobulin domain 3 (Ig3) and more strongly with a fragment containing Ig3 and Ig4 (Ig3-4) [179]. Due to the high homology of MYPN to PALLD, we tested whether MYPN Ig3 may also bind to F-actin in collaboration with Dr. Moriah Beck (Wichita State University, Wichita, Kansas, USA). MYPN Ig3 was cloned into the pTBSG vector (NEB) for expression of $His_6$-tagged protein with a TEV protein cleavage site, allowing for removing of the $His_6$-tag after purification. Using purified MYPN Ig3 domain, actin-cosedimentation assays were performed by ultracentrifugation (150,000 x *g*) of polymerized actin with various concentrations of MYPN Ig3 domain, which demonstrated the ability of the MYPN Ig3 domain to bind to F-actin (Fig. 18A, B). To determine whether MYPN can also bundle F-actin, the assay was repeated with an additional low speed spin (5,000 x *g*) to pellet actin bundles. This caused actin filaments to pellet in the presence of MYPN Ig3, demonstrating the ability of MYPN to bundle F-actin (Fig. 18C, D). This was further confirmed by visualization of actin bundling with fluorescent phalloidin on a confocal microscope (Fig. 18E). To determine the effect of MYPN on actin polymerization, an actin polymerization assay was performed using pyrene-labeled actin, which revealed an increased actin polymerization rate in the presence of the MYPN Ig3 domain (Fig. 18F). Thus, myopalladin may reduce the time necessary for the initial phase of actin polymerization.

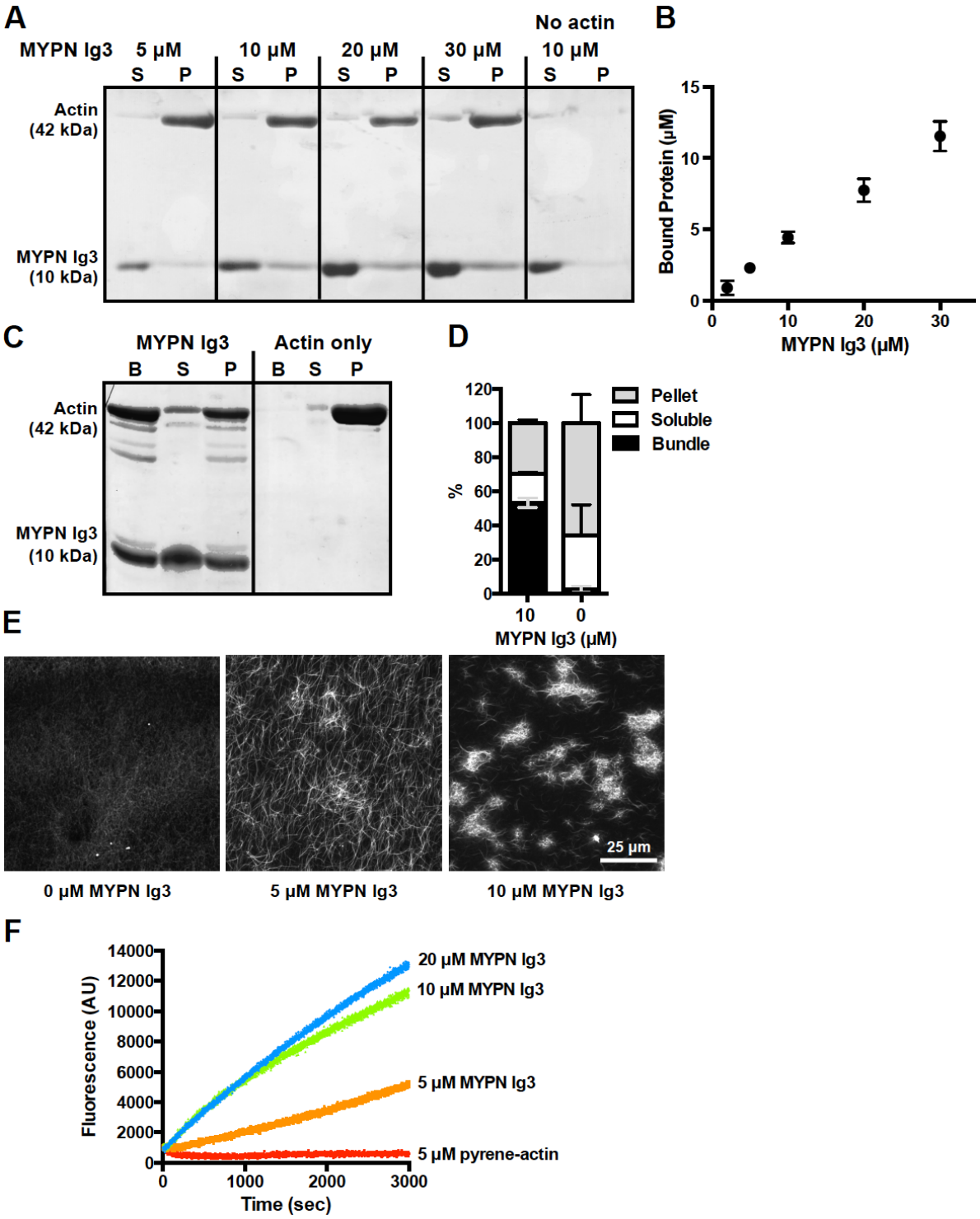



**Figure 18. MYPN binds and crosslinks F-actin and promotes actin polymerization. A)** The MYPN Ig3 domain was assayed for actin binding by co-sedimentation with F-actin with increasing concentrations of the MYPN Ig3 domain and 10 µM F-actin, followed by SDS-PAGE of supernatants (S) and pellets (P). **B)** The fraction of MYPN Ig3 domain that co-sediments with F-actin was determined by densitometry of the SDS-PAGE gel. **C)** The MYPN Ig3 domain is capable of bundling F-actin as shown by low speed centrifugation, allowing only bundled F-actin to sediment. The pellet containing actin bundles (B) was collected before sedimenting the remaining F-actin by ultracentrifugation whereafter SDS-PAGE was performed. B, low speed pellet containing bundled F-actin; S, supernatant; P, pellet. **D)** Quantification of actin bundling by densitometry of actin bands showed that 53.3% of F-actin is bundled in the presence of the MYPN Ig3 domain *vs*. 3.2% with actin only. **E)** Polymerized actin was visualized with fluorescent phalloidin, using confocal microscopy. Actin bundles were generated in greater amounts with increasing concentrations of MYPN (0 µM; 5 µM; 10 µM MYPN). **F)** *In vitro* actin polymerization assays reveal that the Ig3 domain of MYPN accelerates polymerization. Pyrene fluorescence was used to monitor the polymerization rate of G-actin in the presence of increasing concentrations of the MYPN Ig3 domain.

## 1.2 MYPN binds to MRTFs and promotes MRTF-induced SRF signaling in C2C12 myogenic cells

The C-terminal region of PALLD was recently shown to target to the nucleus in podocytes [252] and smooth muscle cells (SMCs) [213], where it binds to MRTFs through its C-terminal regional and both directly and indirectly activates SMC promoter activity via the SRF pathway, thereby inducing SMC differentiation. To determine whether the corresponding region of MYPN may also bind to MRTF-A and -B, we used the yeast two-hybrid (Y2H) system. As shown in Fig. 19A, the C-terminal region of MYPN bound strongly to MRTF-A and weakly to MRTF-B, while full-length (FL) MYPN did not bind. This was confirmed by co-immunoprecipitation (co-IP) with anti-HA antibody and protein G beads after cotransfection of HEK293 cells with HA-tagged MYPN and FLAG-tagged MRTF-A, where both MYPN FL and MYPN Ig3-4 were found to bind to MRTF-A (Fig. 19B).

To assess whether MYPN, like PALLD, can activate the SRF signaling pathway, we performed SRF-luciferase reporter assays by cotransfecting myogenic C2C12 cells with increasing amounts of HA-MYPN in the presence and absence of FLAG-MRTF-A as well as SM22 luciferase reporter and *Renilla* standardization reporter plasmid. After transfection, C2C12 myoblasts were induced to differentiate and the reporter assay was performed after 2 days of differentiation. As shown in Fig. 19C, MYPN promotes SRF-activity and increases MRTF-A-mediated activation of SRF activity in a dose dependent manner (Fig. 19C).

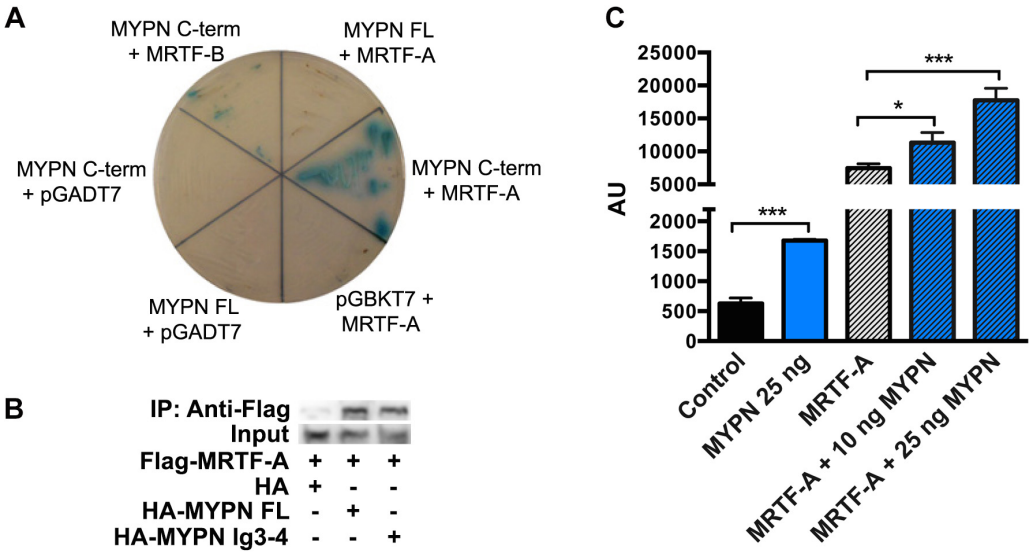



**Figure 19. MYPN binds to MRTFs and activates MRTF-A-induced SRF signaling. A)** Yeast-two hybrid assay showing binding of the MYPN C-terminal region to MRTF-A and weakly to MRTF-B. **B)** Co-IP with anti-HA antibody after transfection of HEK293 cells with HA-tagged MYPN constructs and FLAG-tagged MRTF-A. This reveals that the MYPN Ig3-4 domain is sufficient for binding to MRTF-A. **C)** The SRF-luciferase reporter assay in myogenic C2C12 cells showed that MYPN activates SRF and increases MRTF-A activation of SRF activity in a dose dependent manner ($n$ = 3 in three independent experiments).

# 2. GENERATION OF MYPN KNOCKOUT (MKO) MICE

To study the role of MYPN *in vivo*, constitutive MYPN knockout (MKO) mice were generated by knocking in a *LacZ-Neo* cassette downstream of the endogenous *Mypn* promoter, thereby simultaneously disrupting the *Mypn* gene (Fig. 20A). Targeted ES cells clones were identified by Southern blot analysis (Fig. 20B) and the successful ablation of MYPN was confirmed by Northern and Western blot analyses (Fig. 20C and D).

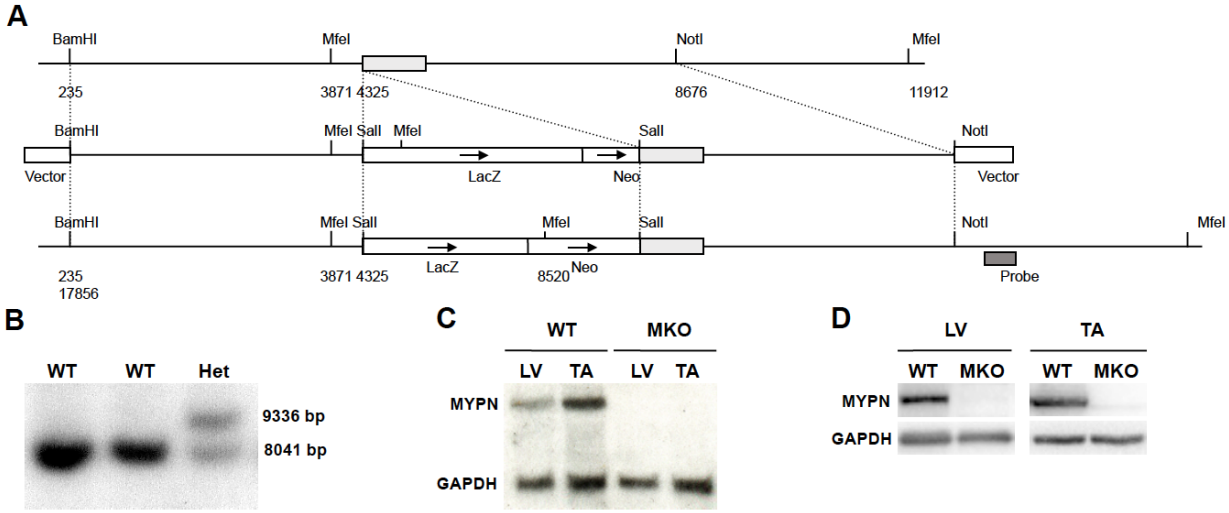



**Figure 20. Targeting of the *Mypn* gene. A)** Targeting strategy for generation of MYPN knockout (MKO) mice. A restriction map of the relevant genomic region of *Mypn* is shown on top, the targeting construct is shown int eh middle, and the mutated locus after recombination is shown at the bottom. The grey box indicates exon 1. Neo, neomycin resistance gene. **B)** Detection of WT and targeted alleles by Southern blot analysis after digestion with MfeI using the probe shown in A. **C)** Northern blot analysis showing the successful ablation of MYPN in the left ventricle (LV) and *Tibialis anterior* (TA) muscle from MKO and WT mice. **D)** Detection of MYPN protein by Western blot analysis. GAPDH antibody was used as loading control.

## 2.1 Skeletal muscle MKO phenotype

### *2.1.1 MKO mice are smaller compared to WT littermates and have reduced skeletal muscle fiber cross sectional area (CSA)*

MKO mice were born at Mendelian ratios, were fertile, and had normal life spans. However, MKO mice had a significantly smaller body weight compared to WT littermate controls (~22% smaller 3 days after birth, ~17% at 4 weeks of age, and ~9% at 8 weeks of age) (Fig. 21A). Histological analysis by hematoxylin and eosin (H&E) staining of fast EDL muscle from MKO and WT controls up to 1 year of age showed no centralized nuclei or necrosis in MKO muscle (Fig. 21B). However, analysis of laminin-stained sections revealed a significantly reduced fiber cross-sectional area (CSA) in EDL, TA, and soleus muscle (~48% in all muscles at 8 weeks of age) at all stages up to 1 year of age (Fig. 21B, C and data not

shown). Quantification of the CSA of different fiber types (1, 2A, 2B, 2X) revealed that all fiber types were affected (Fig. 21D, E, F) The reduction in CSA was associated with a significant increase in fiber number in MKO TA muscle compared to WT as well as a tendency towards a higher fiber number also in EDL and soleus muscle (Fig. 21G). ATPase stainings and SDS-PAGE for myosin heavy chain composition revealed no significant differences in fiber type distribution between MKO and WT mice (data not shown).

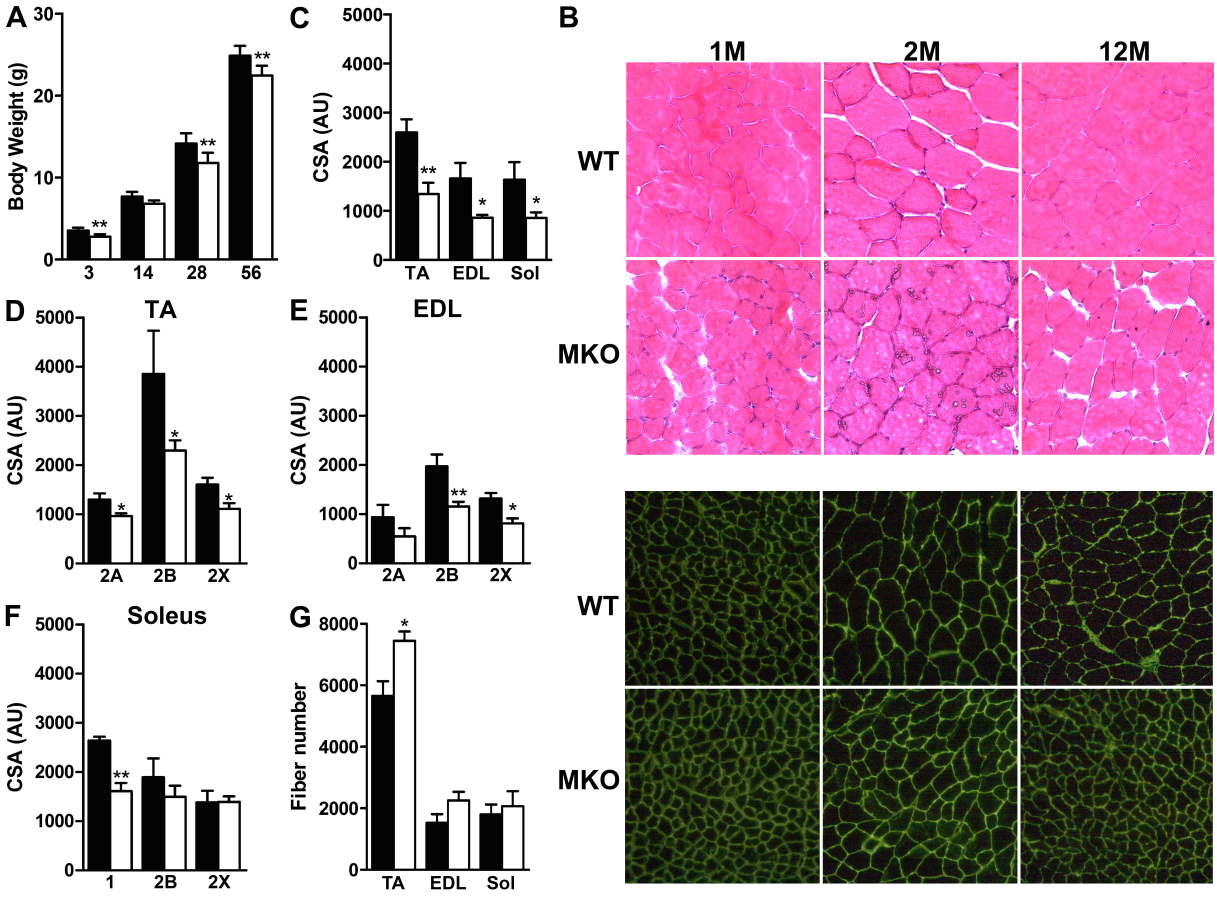



**Figure 21. Smaller body weight and reduced skeletal muscle CSA in MKO mice compared to WT. A)** Body weight of MKO and WT littermates 3, 14, 28, 56 days after birth ($n$ = 6). **B)** H&E and laminin stainings of cross-sections of EDL muscle from MKO and WT littermate controls of different ages (1 month, 1M; 2 months, 2M; 12 months, 12M). **C)** CSA of TA, EDL, and soleus muscle from 8-week-old MKO and WT mice ($n$ = 3). **D), E), F)** CSA of different fiber types (1, 2A, 2B, 2X) in TA, EDL, and soleus muscle from 8-week-old MKO and WT mice ($n$ = 3). **G)** Fiber numbers in TA, EDL, and soleus muscles from 8-week-old MKO and WT mice ($n$ = 3). Error bars represent standard deviation (SD). *P < 0.05; **P < 0.01.

### *2.1.2 Progressive Z-line widening in MKO skeletal muscle*

Transmission electron microscopy (TEM) analysis on EDL muscle from 3, 8, and 24 month-old MKO and WT mice revealed progressive Z-line widening in MKO muscle starting from 8 months of age (Fig. 22). No abnormalities in mitochondria or other organelles were observed, but M-line abnormalities were observed at 2 years of age (data not shown).

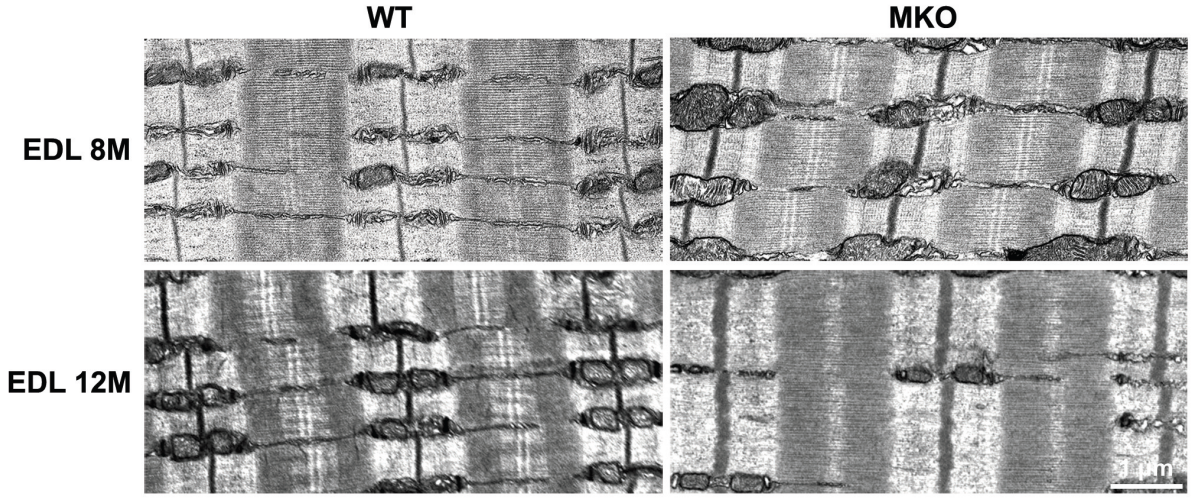



**Figure 22. Transmission electron microscopy analysis of EDL from MKO mice compared to WT.** Progressive Z-line widening was found in MKO EDL muscle compared to WT from about 8 months of age.

### *2.1.3 MKO mice are more susceptible to exercise-induced injury*

To test the exercise capacity of MKO mice, endurance tests were performed by uphill (15% incline; concentric exercise) and downhill (15% decline; eccentric exercise) running on a 5-lane treadmill. Eccentric contraction, which results in muscle injury in untrained individuals, primarily recruits fast-twitch glycolytic fibers, as opposed to the recruitment of slower, smaller, oxidative fibers during concentric contractions. Both for up and downhill runs, the speed was increased by 3 cm/s every 2 min and the time and speed at which the mouse could not maintain sufficient speed to remain off the shock grid was recorded. No differences between MKO and WT mice were observed by uphill and downhill running on the first day of running (Fig. 23A). On the other hand, when mice were run downhill for 4 consecutive days, the performance was significantly reduced from the second day of running (Fig. 23B), suggesting that MKO are more susceptible to eccentric induced injury. This was further supported by histological analyses of soleus and gastrocnemius from MKO and control mice 48 h after the end of running training, which revealed the presence of fibers with centralized nuclei, a sign of muscle regeneration, in MKO mice (Fig. 23C). In addition, Z-line irregularities were observed by electron microscopy analyses of soleus muscle from MKO mice, while WT controls had normal Z-lines (Fig. 23C).

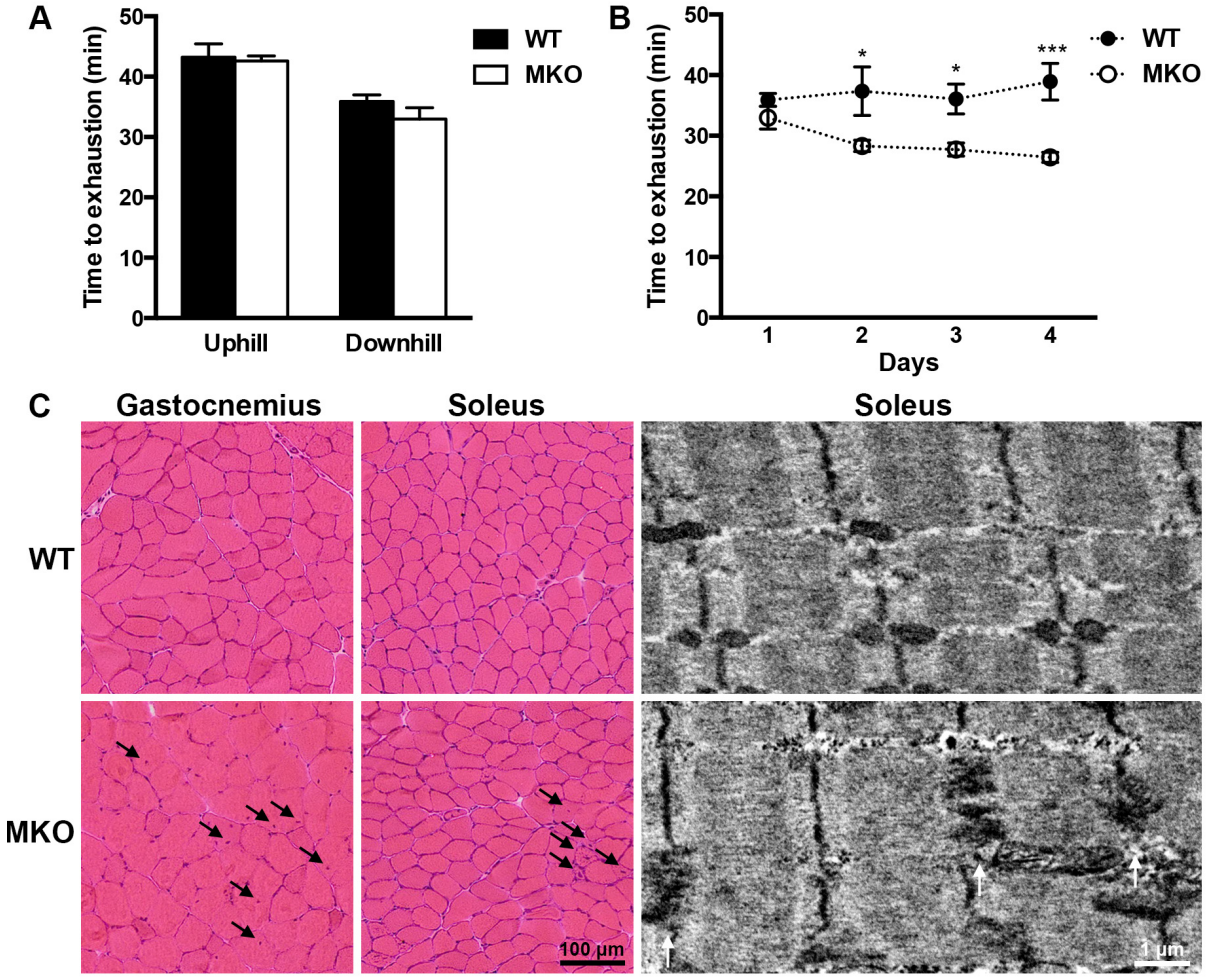



**Figure 23. MKO mice are more susceptible to eccentric contraction induced injury. A)** Time to exhaustion after uphill and downhill running. **B)** Downhill running to exhaustion for 4 consecutive days ($n$ = 10). All values are represented as mean ± standard error of the mean (SEM). *P < 0.05; ***P < 0.001. **C)** H&E staining of gastrocnemius and soleus showing centralized nuclei (black arrowheads) in MKO mice. Electron microscopy analysis of soleus revealed the severe disorganization of Z-line in MKO mice after 4 days of consecutive downhill running.

### *2.1.4 Recovery following $BaCl_2$-induced skeletal muscle injury*

To determine the ability of MKO muscle to regenerate following injury, $BaCl_2$ was injected into the TA muscle of one leg, while PBS was injected into the contralateral leg. Muscles were collected 7, 14, and 21 days after injection and characterized by histological analyses. As shown in Fig. 24A, the regenerating rate was similar between MKO and WT muscle fibers after $BaCl_2$-induced injury (Fig. 24A), although the CSA of the newly forming muscles 21 days after $BaCl_2$ injection were smaller in MKO mice compared to WT controls (Fig. 24B). The number of nuclei in regenerating fibers was similar in MKO and WT $BaCl_2$-injected muscle (Fig 24C).

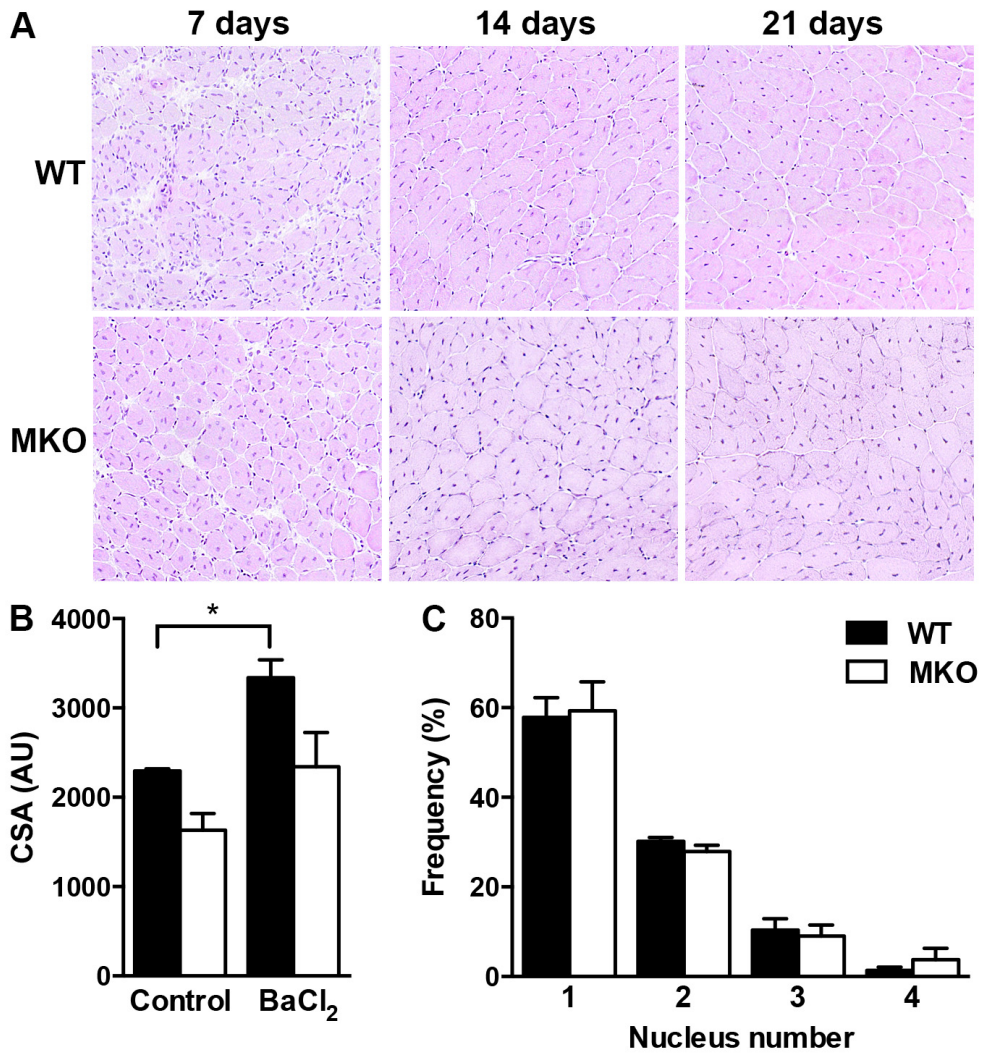



**Figure 24. MKO muscle regenerate normally after injury, but have smaller fiber CSA. A)** H&E staining revealed a normal regeneration rate after $BaCl_2$-induced injury in MKO mice compared to WT controls. **B)** The fiber CSA is reduced in MKO muscle 21 days after $BaCl_2$-injection, but the relative reduction in fiber size is similar between after $BaCl_2$-injected MKO and control muscle. **C)** The number of nuclei in newly forming fibers was similar between $BaCl_2$-injected MKO and WT muscle. Error bars represent standard deviation (SD). *P < 0.05.

### *2.1.5 Muscle denervation-induced atrophy*

To determine whether MYPN may play a role in muscle atrophy, MKO and control mice were subjected to denervation by cutting the sciatic nerve of the left limb. The right limb was used as control. 21 days after denervation, the CSA of different fiber types of the TA muscle was determined by immunostaining with antibodies against laminin and myosin heavy chain (MHC) 2A, 2B, and 2X. The CSA of all fiber types was reduced in denervated TA muscle from MKO mice compared to WT (Fig. 25A). However, although the CSA was smaller in denervated MYPN muscle compared to WT, the relative reduction in CSA in denervated muscle compared to control muscle was similar between MKO and WT mice (Fig. 25B), suggesting that MYPN is not involved in muscle atrophy.

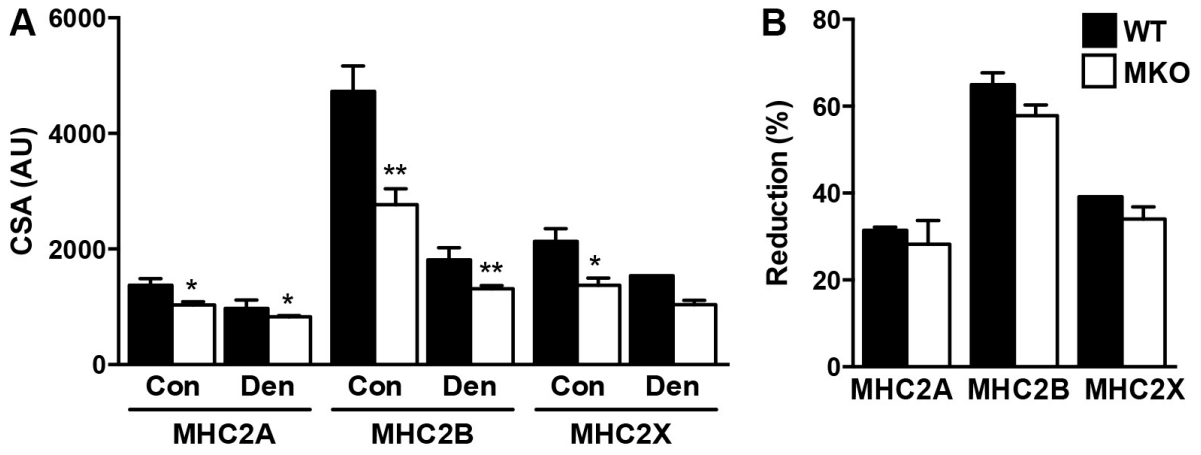



**Figure 25. Similar reduction in fiber CSA in response to denervation in MKO and WT mice. A)** The CSA of all fiber types was reduced in denervated TA muscle compared to control muscle in both MKO and WT muscle ($n$ = 3). **B)** The relative reduction in fiber CSA in denervated TA muscle compared to control muscle was similar between MKO and WT mice. Den: denervated muscle; Con: control muscle.

### *2.1.6 The absence of MYPN affects specific force and power output in EDL muscle (Collaboration with Prof. Marco Linari, University of Florence, Florence, Italy)*

To investigate the functional consequence of MYPN deletion on skeletal muscle mechanical properties, measurements of isometric force production and power output in limb muscles from MKO and WT mice was performed in collaboration with Prof. Linari. In particular, the maximum steady force elicited by the isometric tetanus $T_0$ and the force-velocity relation were determined in EDL muscle from 10-week-old MKO and WT control mice. In MKO EDL muscle, $T_0$ was about one-half the control value with a significant reduction in CSA (20%), calculated by wet muscle weight as well as in specific isometric force ($T_0$/CSA) (38%) (Table 8 and Fig. 26). The force-velocity relation was determined by measuring the shortening velocity $V$ at constant loads ($T<T_0$) (Fig. 26B and C), which revealed a signficant reduction in power output ($T^*V$) in EDL muscle from MKO mice compared to WT at each load (Fig. 26D), and at the load for maximum power ($W_{max}$), about $0.3^*T_0$, the power was reduced by about 40% of the control value (Table 8 and Fig. 26D).

| ***Genotype* (*n*)** | **WT (7)** | **MKO (5)** | ***P*** |
|---|---|---|---|
| ***Isometric contraction*** | | | |
| $T_0$ **(mN)** | 337 ± 18 | 175 ± 31 | < 0.05 * |
| $L_0$ **(mm)** | 10.9 ± 0.3 | 10.6 ± 0.4 | > 0.5 |
| ***w*** **(mg)** | 11.1 ± 0.3 | 8.8 ± 0.6 | < 0.05 * |
| ***CSA*** **($cm^2$)** | 0.019 ± 0.001 | 0.015 ± 0.001 | < 0.05 * |
| $T_0$ **(N/g)** | 30.4 ± 1.5 | 19.7 ± 3.4 | < 0.05 * |
| $T_0$ **($kN/m^2$)** | 180 ± 6 | 112 ± 20 | < 0.05 * |

| ***Genotype* (*n*)** | **WT (4)** | **MKO (4)** | ***P*** |
|---|---|---|---|
| ***Isotonic shortening*** | | | |
| $T_0$ **($kN/m^2$)** | 179 ± 4 | 109 ± 10 | < 0.05 * |
| $V_0$ **($L_0$/s)** | 4.94 ± 0.17 | 4.97 ± 0.42 | > 0.5 |
| ***a*** **(mN)** | 98.1 ± 12.9 | 42.2 ± 13.6 | < 0.05 * |
| $a/T_0$ | 0.291 ± 0.035 | 0.241 ± 0.065 | > 0.5 |
| ***b*** **($L_0$/s)** | 1.35 ± 0.17 | 1.11 ± 0.33 | > 0.5 |
| $W_{max}$ **(mW/g)** | 91.7 ± 2.9 | 57.1 ± 3.3 | < 0.05 * |

**Table 8. Mechanical parameters during isometric contraction and isotonic shortening of EDL muscle from MKO and WT mice.** Isometric contraction parameters: $T_0$, isometric force; $L_0$, muscle length at the plateau of the force-length relation; *w*, muscle wet weight; *CSA*, cross-sectional area. Isotonic shortening parameters: $V_0$, *a* and *b* are parameters of the Hill hyperbolic equation interpolated to the pooled data; $W_{max}$, maximum power, obtained with a load ~ 1/3 $T_0$; *n*, number of samples used. Values are means ± standard deviation (SD). *P < 0.05.

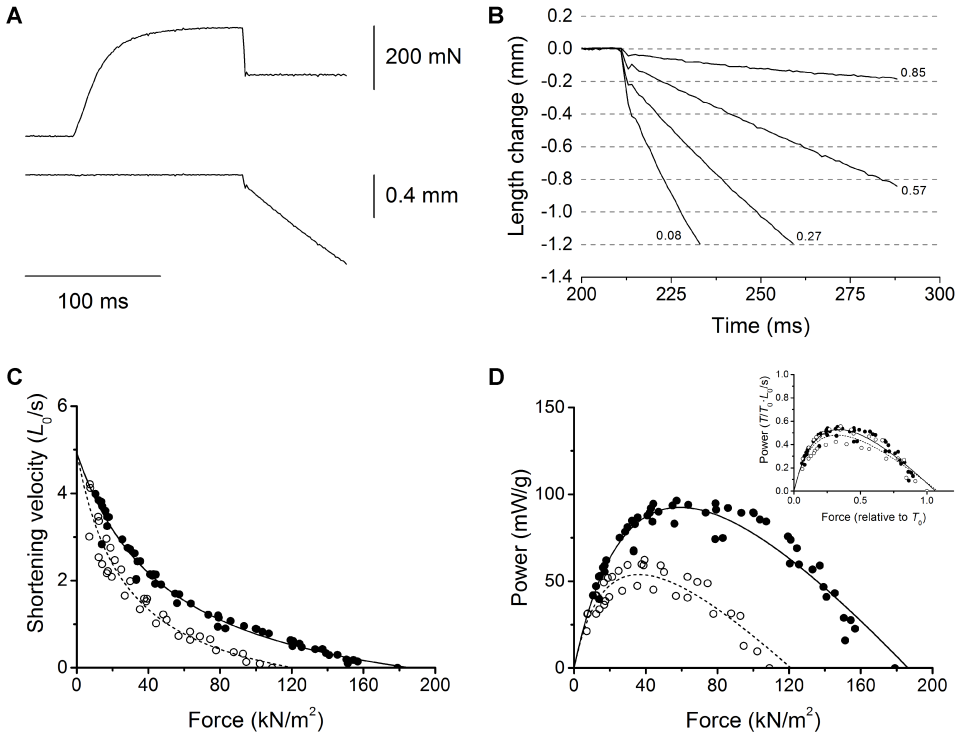



**Figure 26. Mechanical measurements on EDL muscle from MKO and WT mice. A)** Sample record of length (lower trace) after a drop of force from $T_0$ to 0.5 $T_0$ (upper trace). **B)** Length changes following a drop of force of different amplitude (indicated by the figures close to the traces). **C)** Force-velocity (T-V) relation in WT (filled circles) and MKO mice (non filled circles). Lines are the Hill hyperbolic equation interpolated on the pooled data for WT (continuous line) and KO (dashed line) mice. **D)** Power-force relations obtained from the same data as in C. Inset, power-force relation relative to its own specific isometric force (*n* = 7).

All together, these results showed a reduction in specific force and power output in EDL muscle from MKO mice compared to WT, which was not proportional to the reduction in CSA of MKO muscle. However, it should be noted that the CSA was not directly measured but was calculated from the wet weight of the EDL muscle, assuming that the absence of MYPN does not affect the fiber density. To determine whether the reduction in isometric force could be related to the reduced CSA at the single fiber level, the isometric force per unit area was measured in fully activated (pCa, 4.5) single skinned fibers from MKO and WT EDL muscle. As shown in Table 9, $T_0$ was reduced by 52% in MKO mice compared to WT controls, while no significant reduction in $T_0/CSA$ were observed in MKO mice. Therefore, the lower isometric force observed in EDL muscle in the absence of MYPN can be completely explained by the reduction in CSA of the single fibers, not accompanied by a proportional reduction of the wet weight of muscle.

| ***Genotype* (n)** | **WT (7)** | **MKO (6)** | ***P*** |
|---|---|---|---|
| **$T_0$ (mN)** | 0.23 ± 0.02 | 0.11 ± 0.01 | < 0.01** |
| ***CSA* (µm$^2$)** | 1788 ± 133 | 996 ± 84 | < 0.01** |
| **$T_0/CSA$ (kPa)** | 131 ± 11 | 111 ± 2 | > 0.1 |

**Table 9. Mechanical parameters during isometric contraction in fibers from MKO and WT EDL muscle.** $T_0$, isometric force; CSA, cross-sectional area. *n*, number of analysed fibers. ** P < 0.01.

### *2.1.6.1 Effect of the absence of myopalladin on force per myosin motor*

To investigate whether the absence of MYPN affects the number of actin-myosin motors and/or the force per motor, the average strain in the myosin motors was estimated by determining the strain-force relation ($Y_0$-$T_0$) at different [$Ca^{2+}$] as previously described [83]. [$Ca^{2+}$] modulates the number of myosin motors attached in the half-sarcomere, and thus the isometric force, without affecting the force per motor [225]. The ordinate intercept of the $Y_0$-$T_0$ relation is an estimate of the average strain (and thus force) per attached motor, while the slope of the relation is an estimate of the compliance of the filaments (actin and myosin) in series to the motors. This analysis was performed by determining the fiber stiffness at different [$Ca^{2+}$] by imposing small steps in sarcomere length on the isometrically contracting fiber. Fiber stiffness was estimated by the slope of the relation between the peak force at the end of the step ($T_1$) and the step size ($T_1$ relation) [225, 253] (Fig. 27Aa). The fiber stiffness (slope of the $T_1$ relations) at any [$Ca^{2+}$] decreased with less than in proportion to the reduction in $T_0$ in both MKO and WT mice (Fig. 26Aa). The abscissa intercept of the line fitted to the

$T_1$ relation ($Y_0$) is a measure of the extension in fiber elasticity at the isometric condition before the step [253]. As shown in Figure 27Ab, both the slope and the ordinate intercept of the $Y_0$-$T_0$ relation were similar in MKO and WT fibers (Table 10), indicating that the absence of MYPN does not affect the compliance of actin and myosin filaments nor the average strain, and thus the average force per attached motor.

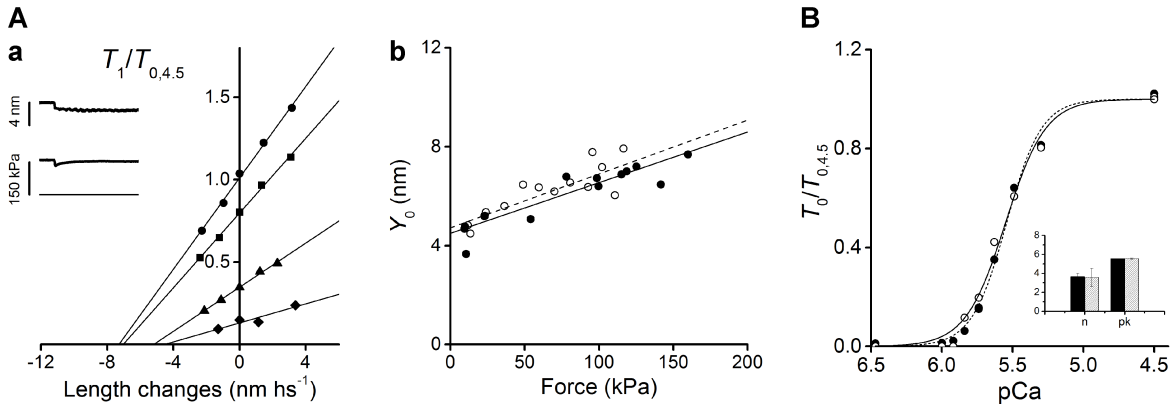



**Figure 27. Aa) $T_1$ relations for four pCas.** The relations are obtained by plotting the extreme force obtained at the end of the length step, $T_1$ (relative to $T_0$ at pCa=4.5), versus the step amplitude. Different symbols refer to different pCas values: circles, 4.50; squares, 5.30; triangles, 5.63; diamonds, 5.74. The lines are linear regressions fitted to the experimental points for each pCa. Inset, force response (lower trace) to a length step (upper trace) in a fiber from WT mouse activated at pCa 4.50 (horizontal line below force response, force baseline). Fiber length, 1.97 mm; sarcomere length, 2.54 µm; *CSA*, 1850 µm$^2$; $T_0$, 153 kPa; temperature, 12.1°C. **Ab)** Relation between strain and isometric force in fibers from MKO (open circles, 3 fibers) and WT (filled circles, 3 fibers) EDL muscles. **B)** Force-pCa relations in skinned fibers from EDL muscle of MKO (open circles) and WT (filled circles) mice. Solid (WT) and dashed (MKO) lines are Hill sigmoidal equations (see text) fitted to data. Inset: mean ± SEM values of the parameters.WT: same fiber as in Aa). MKO: fiber length, 1.51 mm; sarcomere length, 2.51 µm; *CSA*, 1060 µm$^2$; $T_0$, 113 kPa; temperature, 12.0°C.

| ***Genotype* (n)** | **WT (3)** | **MKO (3)** | ***P*** |
|---|---|---|---|
| **$T_0$ (kPa)** | 131 ± 15 | 109 ± 7 | > 0.15 |
| **$s_0$ (nm)** | 4.50 ± 0.14 | 4.72 ± 0.27 | > 0.4 |
| **$C_f$ (nm/kPa)** | 0.021 ± 0.003 | 0.020 ± 0.001 | > 0.7 |

**Table 10. Slope ($C_f$) and ordinate intercept ($s_0$) estimated by linear regression fitted to the data plotted in Fig. 27Ab.** Values are expressed as mean ± SEM. *n* indicates the number of fibers.

### *2.1.6.2 Force-pCa relation*

The effect of MYPN on the $Ca^{2+}$ sensitivity of the contractile system was tested by determining the force-pCa relationship [129]. As shown in Fig. 27B, the MKO relation superimposes on the WT relation. Thus, MYPN doesn't affect either the degree of cooperativity of $Ca^{2+}$ activation ($n_H$) or the $Ca^{2+}$ sensitivity of the myofilaments (*pK*) (Table 11).

| *Genotype* (n) | WT (3) | MKO (3) | *P* |
|---|---|---|---|
| $n_H$ | 3.66 ± 0.21 | 3.57 ± 0.57 | > 0.9 |
| *pK* | 5.53 ± 0.01 | 5.57 ± 0.04 | > 0.6 |

**Table 11. Coefficients of the sigmoid Hill equation fitted to the data plotted in Fig. 27B.** Values are mean ± SEM. *n* indicates the number of fibers.

### *2.1.7 MYPN is expressed during myoblast differentiation*

To determine the RNA and protein expression levels of MYPN during myoblast proliferation and differentiation, qRT-PCR and Western blot analyses for MYPN were performed during proliferation and differentiation of the myogenic C2C12 cell line. As shown in Fig. 28, MYPN is not expressed during proliferation, while its expression is dramatically increased during differentiation.

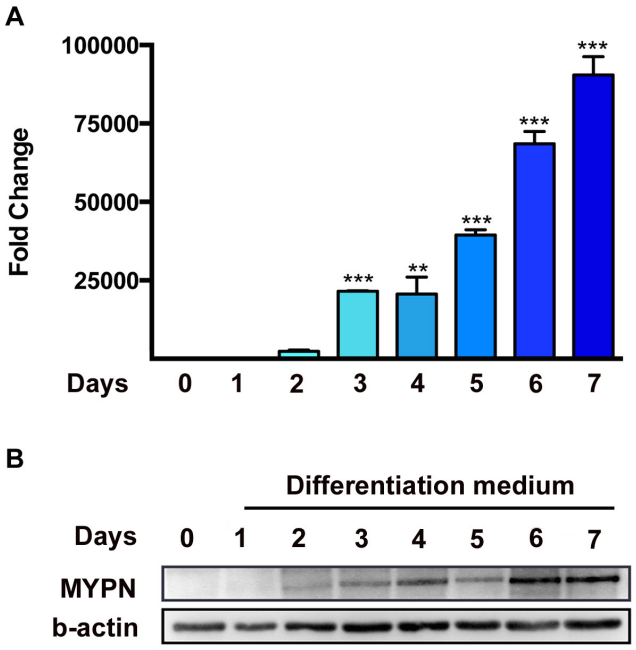



**Figure 28. MYPN is espressed during myoblast differentiation. A)** qRT-PCR and **B)** Western blot analyses for MYPN on C2C12 cells during prolifereation and at different stages following induction of differentiation.

### *2.1.8 Reduced myoblast differentiation rate in MKO mice compared to WT*

To investigate the reason for the reduced CSA in MKO muscle, skeletal muscle primary myoblasts were isolated from neonatal MKO and WT mice. Myoblast proliferation rate was measured after 24 hours of culture using the Click-iT EdU Cell Proliferation Assay (Invitrogen). Consistent with the absent MYPN expression during proliferation, the myoblast proliferation rate was similar in MKO and WT cells (Fig. 29A). On the other hand, following induction of differentiation, thinner myotubes were observed in MKO cultures compared to WT, while the fusion index was similar betweem WT and MKO cultures (Fig. 29A, C, D).

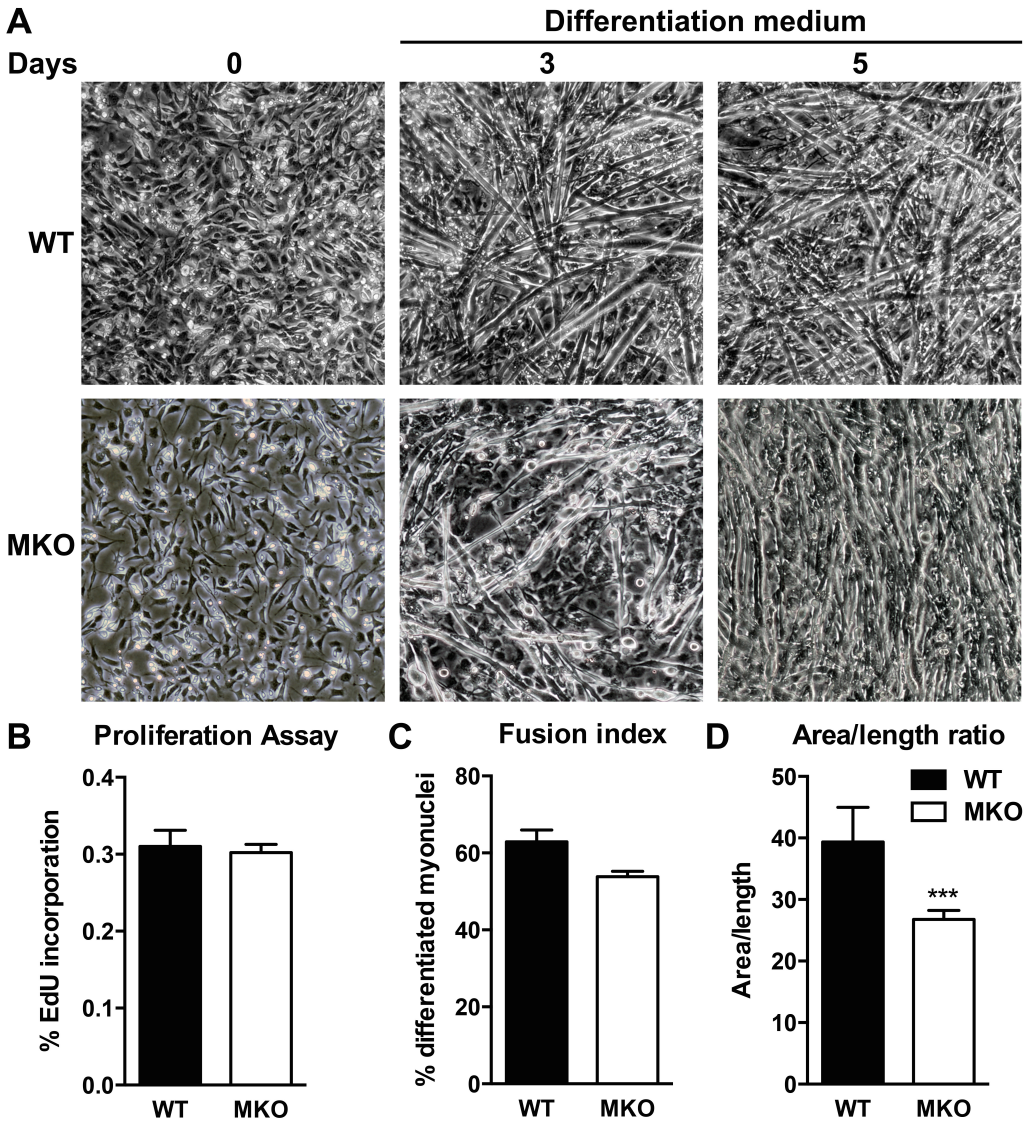



**Figure 29. Primary skeletal muscle culture studies. A)** Isolated skeletal muscle cultures derived from MKO and WT mice during proliferation and 3 and 6 days after induction of differentiation. **B)** Fusion index and Area to lenght ratio of arbitrarily selected myotubes at the fully differentiated stage (5 days after induction of differentiation) measured using Image J show thinner myotubes in MKO cultures compared to WT. *** $P < 0.001$.

### *2.1.9 RNA-Sequencing (RNA-Seq) reveals abnormal SRF signaling in MKO mice*

To dissect the molecular mechanism responsible for the reduced fiber CSA in the skeletal muscle of MKO mice, RNA-Seq analyses were perfomed on TA muscle from 2- and 4-week-old MKO and WT control mice. These time points were chosen to determine changes in gene expression during postnatal growth. Hierarchical clustering of significantly modulated genes revealed a dataset of commonly downregulated genes in 2- and 4-week-old MKO mice involved in actin cytoskeleton organization and skeletal myofibril assembly (Fig. 30A, B, and C). In particular, the actin isoforms (*Actc1*, *Acta1*, *Acta2*) and various other SRF target genes, including *Pdlim7*, *Ctfg*, *Myl9*, *Fhl2*, and *Ankrd1*, were found to be downregulated in MKO

muscle compared to WT controls. Consistently, Ingenuity Pathway Analysis showed SRF as the upstream regulator of these downregulated genes, suggesting that the smaller skeletal muscle fiber size in MKO mice could be related to reduced SRF signaling.

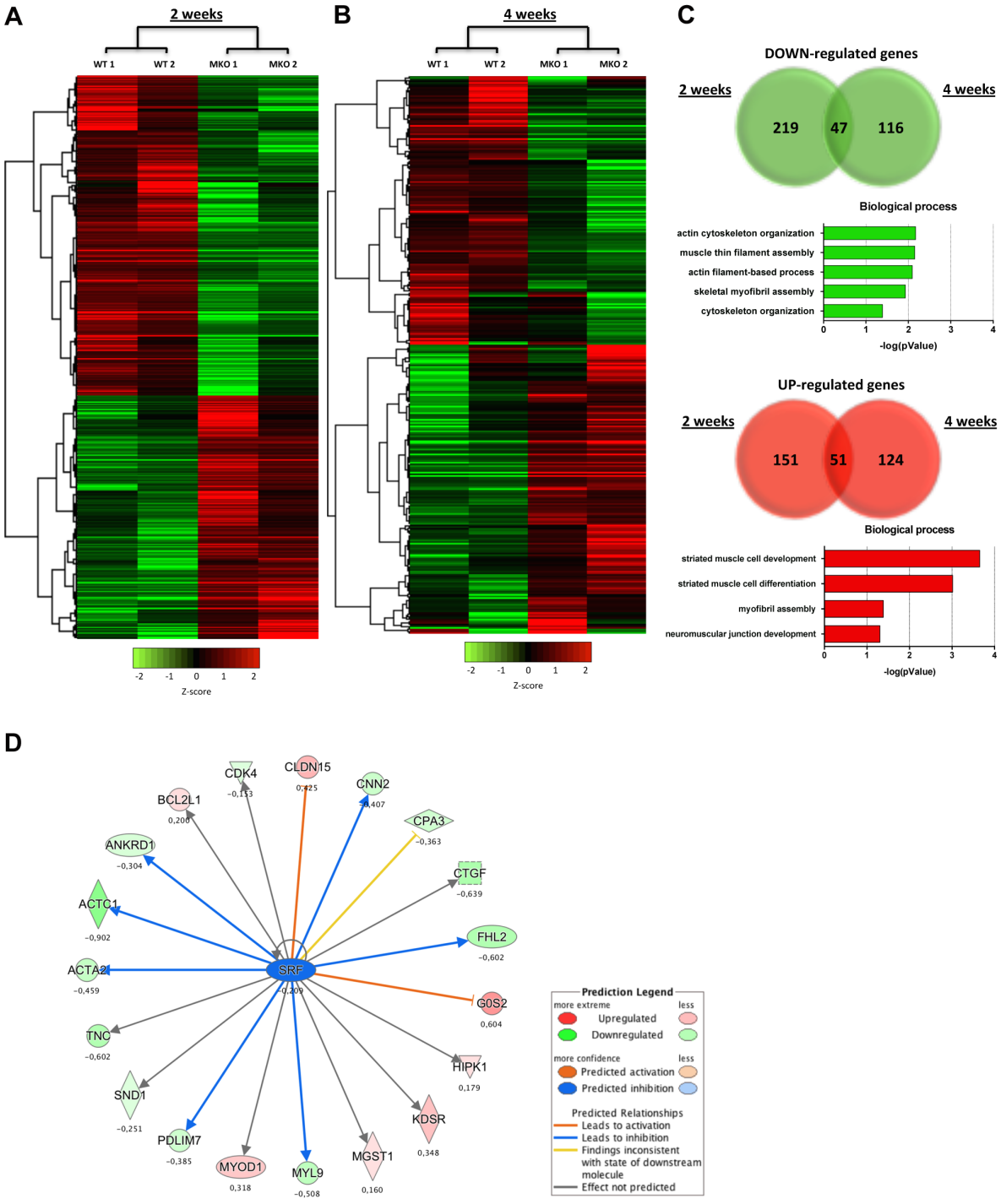



**Figure 30. RNA-Seq analyses on TA muscle from 2- and 4-week-old MKO and WT mice. A)** and **B)** Heat maps of genes modulated in TA muscle from 2- and 4-week-old MKO and WT mice, respectively. **C)** Gene ontology analysis showing the number of commonly downregulated (top) and upregulated (bottom) genes between MKO and WT control mice at 2 and 4 weeks of age, and the main biological processes in which these genes are involved. **D)** Ingenuity Pathway Analysis (IPA) revealed SRF as the upstream regulator of various dysregulated genes involved in actin cytoskeleton organization, including *Actc1*, *Acta1*, *Acta2*, *Pdlim7*, *Ctfg*, *Myl9*, *Fhl2*, *Ankrd1*. $P < 0.01$.

### *2.1.10 No changes in protein synthesis and degradation in MKO muscle*

To determine whether protein synthesis and degradation may be affected in MKO muscle, 4- and 8-week-old MKO and WT mice were intraperitoneally injected with the reversible and cell-permeable proteasome inhibitor MG262 and 24 hours after with puromycin dihydrochloride, a protein synthesis inhibitor that blocks translation through premature chain termination in the ribosome. No significant differences in the levels of ubiquitinylated and puromycilated proteins were found in MKO and WT mice (Fig. 31A and B), indicating protein synthesis and degradation is not affected at these time points.

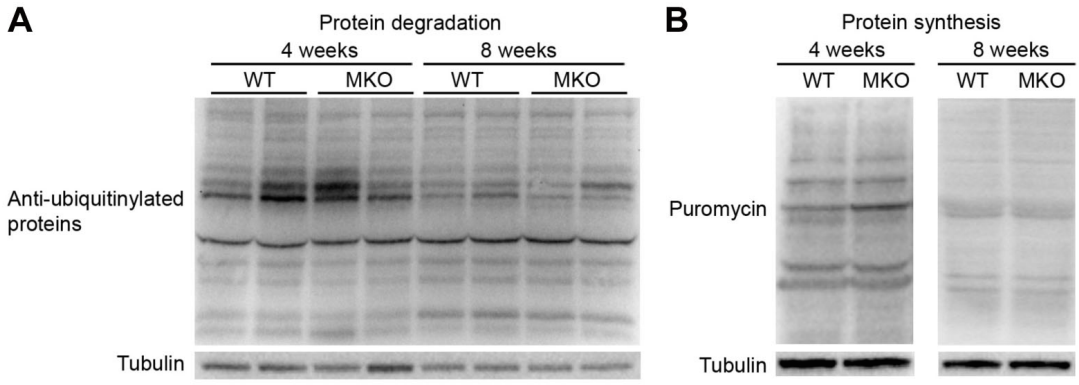



**Figure 31. Protein synthesis and degradation analyses in 4- and 8-week-old MKO and WT mice. A)** Western blot analysis on *Tibialis anterior* lysate from MKO and WT mice showed no differences in the levels of ubiquitinanylated proteins prompted to lysosomial degradation. **B)** No changes in the puromycilated protein levels were observed in MKO compared to control mice at 4- and 8-weeks of age. α-Tubulin was used as loading control. The blots are representative of at least three different experiments.

### *2.1.11 Upregulation of PAK1 in MKO skeletal muscle*

To determine the signaling pathways affected by the ablation of MYPN, Western blot analysis was performed on TA muscle lysate from 2 month-old MKO and WT mice (Fig. 32). In particular, p21-activated kinase 1 (PAK1) was found to be strongly upregulated in MKO mice, while no changes in its phosphorylation level or the expression of its upstream regulator p21 were observed (Fig. 32). This is consistent with the RNA-Seq data where PAK1 was found to be 1.5 and 2.1 fold upregualted at 2 and 4 weeks of age. PAK1 is a critical effector that links the Rho family of GTPases (Rho GTPases) to cytoskeleton reorganization and nuclear signaling. In particular, it serves as target for the small GTP binding proteins Cdc42 and Rac and regulates actin-based cellular morphology and motility [254]. Thus, its upregulation in MKO mice may be related to the skeletal muscle phenotype of MKO mice. A slight activation of AKT signaling was also observed in MKO muscle, while the levels of total and phospho p70S6 kinase, a marker of protein synthesis, were similar between MKO and WT muscle.

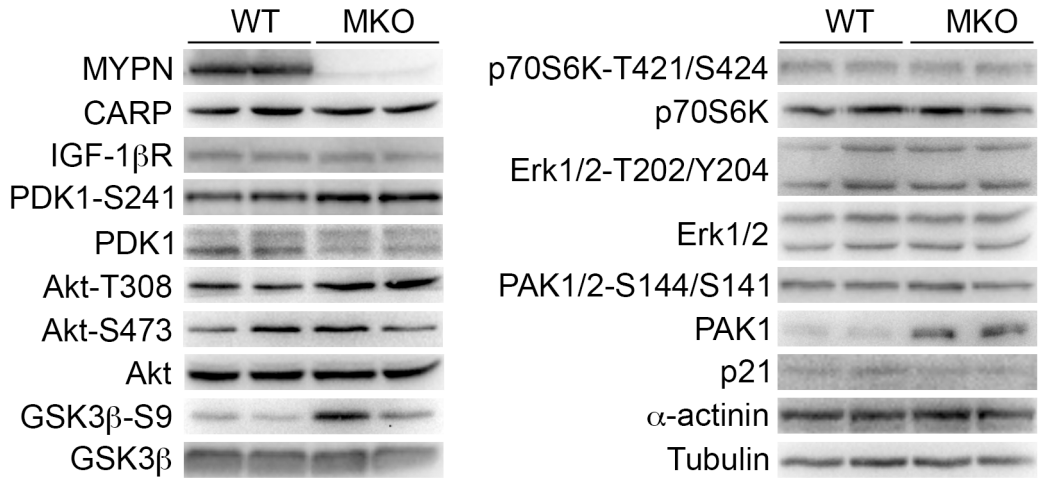



**Figure 32. Western blot analysis on *Tibialis anterior* lysate from 2-month-old MKO and WT mice.** α-Tubulin was used as loading control. The blots are representative of at least three different experiments.

## 2.2 Cardiac Phenotype of MKO Mice

### *2.2.1 Histological and ultrastructural analyses of MKO mouse hearts*

Histological analyses by H&E staining of hearts from MKO and WT mice revealed no histological abnormalities up to 6 months of age and Picro Serius Red stainings showed no evidence of fibrosis in MKO mice compared to WT (Fig. 33). In addition, no changes in cardiomyocyte (CMC) size were observed in MKO mice compared to WT (data not shown), and no apoptosis was observed by TUNEL staining (data not shown).

Electron microscopy analyses on papillary muscle from 8-month-old MKO and control mice revealed no ultrastructural alterations of sarcomere organization and no evidence of Z-line widening (Fig. 33).

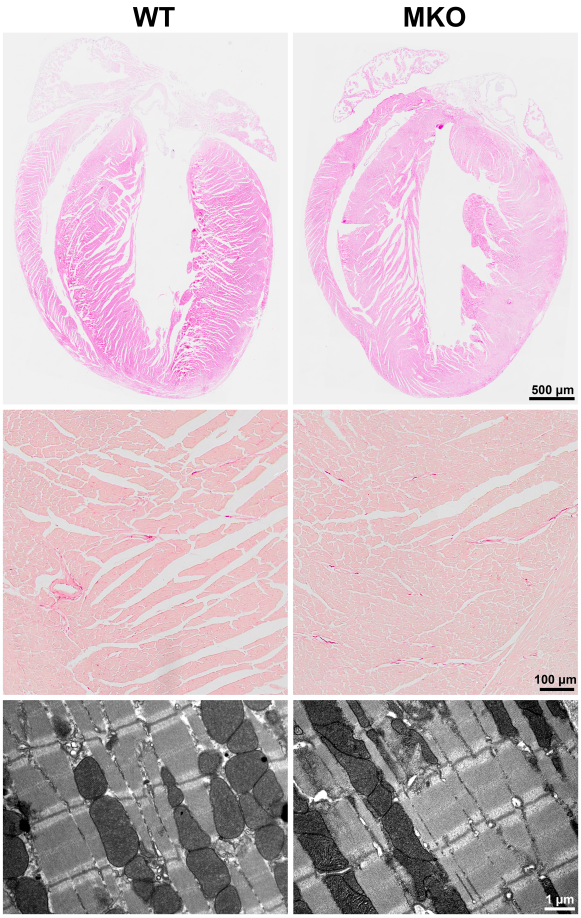



**Figure 33. Histological and electron microscopy analyses of hearts from MKO male mice compared to WT mice.** H&E (top) and Picro Sirius Red (middle) stainings showed no morphological abnormalities and fibrosis in the heart of 6-month-old MKO mice compared to WT. Transmission electron microscopy analyses of papillary muscle from 8-month-old MKO and WT male mice revealed normal sarcomere and Z-line organization (bottom).

### *2.2.2 Echocardiographic analysis reveals progressive cardiac dilation and systolic dysfunction in MKO mice*

To evaluate the effect of MYPN ablation on cardiac morphology and function, echocardiography was performed on MKO and WT control male mice at 10 weeks, 4 months, and 6 months of age. Echocardiographic analyses of 10-week-old MKO mice showed no cardiac abnormalities (Fig. 34), while MKO mice exhibited mild progressive left ventricular dilation and reduced cardiac systolic function starting from 4 months of age (Fig. 34).

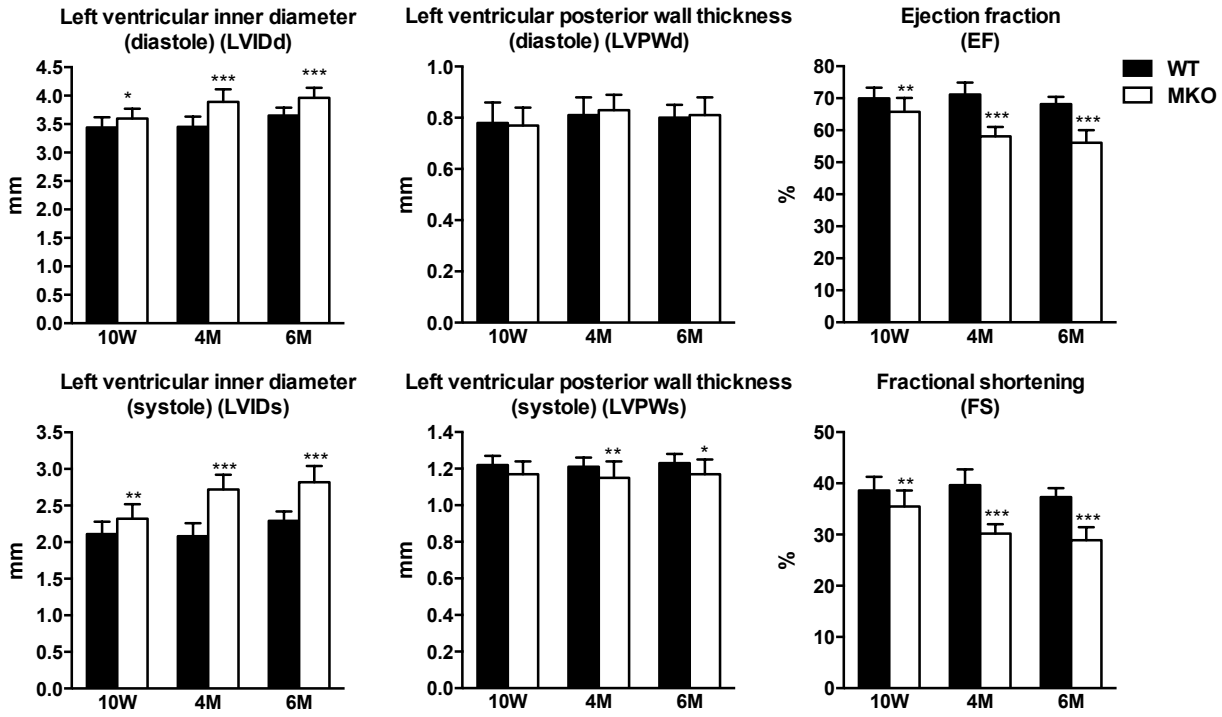



**Figure 34. Echocardiographic analyses of MKO male mice compared to control mice at 10 weeks, 4 months, and 6 months of age.** MKO mice develop progressive cardiac dilation and systolic dysfunction from 4 months of age. All values are represented as mean ± SD. *P < 0.05; **P < 0.01; ***P < 0.001.

### *2.2.3 MKO mouse hearts develop chamber dilation and significantly reduced cardiac function following transaortic constriction (TAC)*

To determine the response to mechanical pressure overload, 8-week-old MKO and WT mice were subjected to transaortic constriction (TAC). Pressure gradients were measured by Doppler echocardiography and cardiac morphology and function was evaluated by echocardiography 1, 2, and 4 weeks after the procedure (Fig. 35A). As shown in Fig. 35B, MKO mice exhibited a normal hypertrophic response to TAC, but developed chamber dilation and reduced fractional shortening compared to WT controls already from 1 week after TAC (Fig. 35B). No significant alterations in heart weight to body weight ratio were observed (Fig.

35B). Histological analyses 1 month after TAC showed severe dilation of the left ventricle of MKO mice, often associated with an enlarged left atria (Fig. 35C), whereas electron microscopy analyses of papillary muscle revealed no ultrastructural abnormalities in MKO mice compared to WT controls (Fig. 35C). Thus, MKO mice exhibit progressive moderate cardiac dilation under basal conditions, but quickly develop a dilated cardiomyopathy (DCM) phenotype followed mechanical pressure overload.

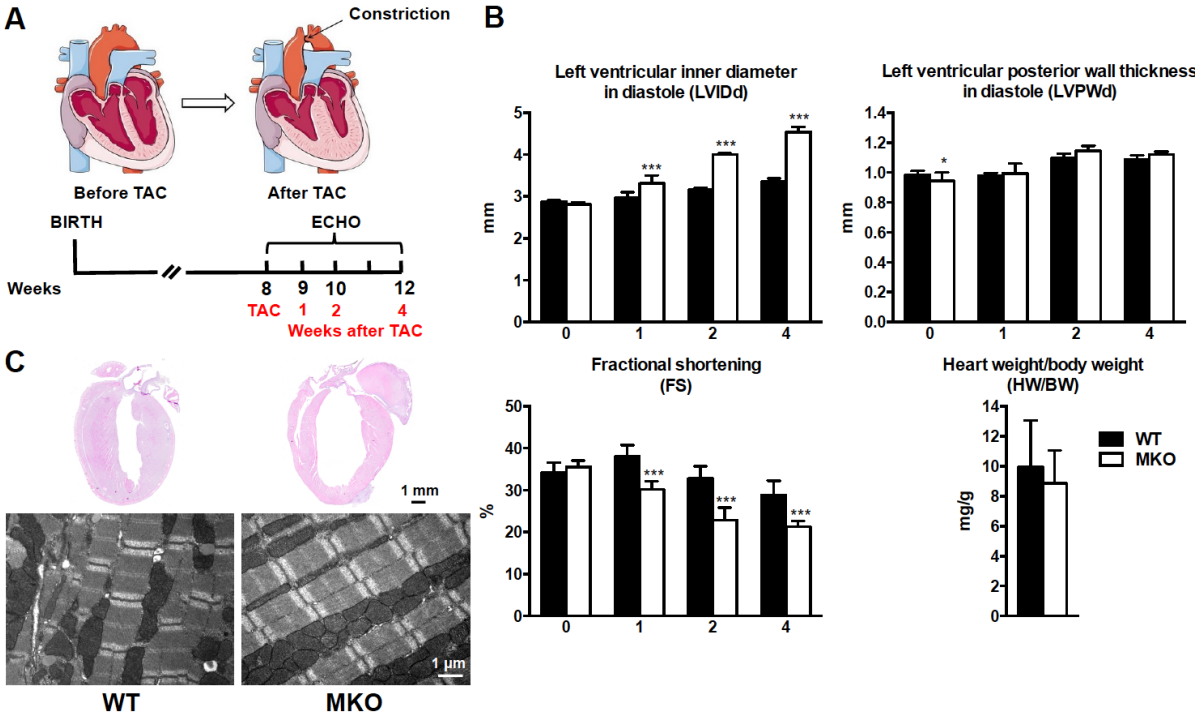



**Figure 35. Functional, histological, and electron microscopy analyses of hearts from MKO and control mice under basal conditions and following transaortic constriction (TAC). A)** Schematic representation of the TAC procedure (top) and the experimental setup for echocardiographic analyses after TAC (bottom). **B)** Echocardiography analyses of MKO and WT controls at basal conditions and 1, 2, and 4 weeks after TAC. Pressure gradient > 50 mmHg. All values are represented as mean ± standard deviation (SD). *P < 0.05; **P < 0.01; ***P < 0.001. **C)** H&E staining and electron microscopy of papillary muscle from MKO and WT mice 1 month after TAC.

### *2.2.4 Activation of AKT and ERK in MKO mice following TAC*

To determine the pathways affected by the ablation of MYPN, Western blot analyses were performed on left ventricular lysate from MKO and WT mice under basal conditions and following TAC (Fig. 36). Western blot analyses for the activation of various cardiac signaling pathways revealed the activation of AKT and extracellular signal-regulated protein kinase 1/2 (ERK1/2) in MKO mice, suggesting a potential role of MYPN in the AKT and MAPK pathways (Fig. 36). In addition, CARP was found to be upregulated in MKO mice 1 month after TAC, consistent with a possible role of the titin/CARP/MYPN complex in mechanosensing [3, 177].

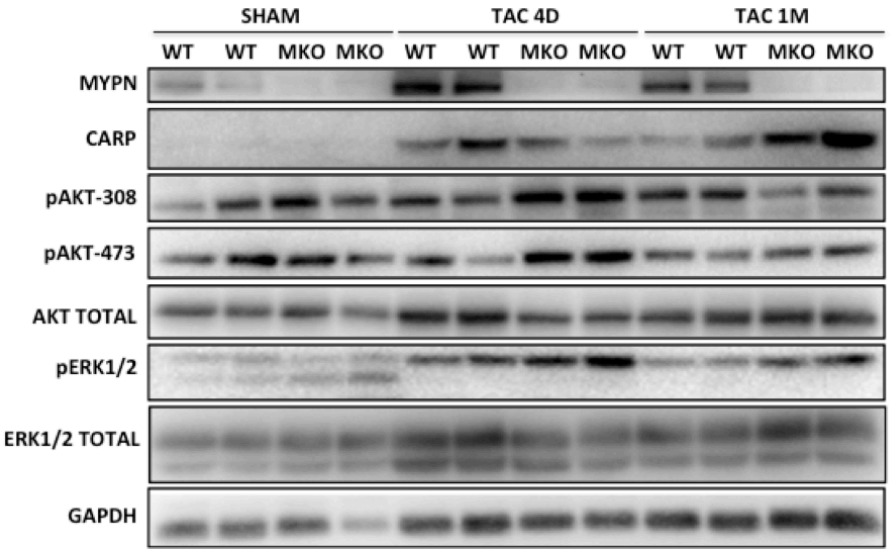



**Figure 36. Western blot analysis on left ventricular lysate from MKO and WT mice 4 days and 1 month after TAC compared to sham mice.** GAPDH was used as loading control. The blots are representative of at least three different experiments.

# DISCUSSION

The sarcomere represents the basic contractile unit of skeletal and cardiac muscle, composed of interdigitating actin-rich thin and myosin-rich thick filaments, which slide over each other during contraction. A multiprotein complex comprising various actin and myosin-associated proteins, known as Z-line, is located at the lateral borders of sarcomere. Besides its involvement in sarcomere architecture, the Z-line plays a key role for efficient force transmission, mechanosensing, and generation of intracellular signaling. This crucial implication of the Z-line in skeletal and cardiac muscle structure and function is sustained by the recent identification of several mutations in human genes encoding Z-line proteins, among which is the actin associated protein MYPN.

MYPN is an immunoglobulin-C2-containing protein specifically expressed in striated muscle and involved in actin cytoskeleton organization [169]. Its ubiquitously expressed homologue PALLD has been shown to promote actin polymerization through direct binding of its Ig3 domain to F-actin [171, 179, 180, 255] and binds to several proteins involved in the regulation of actin dynamics [169]. Here, we found that also the Ig3 domain of MYPN is able to bind and bundle F-actin and to promote actin polymerization, thus playing a crucial role in actin-based processes. PALLD was also recently shown to bind to MRTFs and activate the SRF target genes SMA and SM22 [188]. SRF is a MADS-box transcription factor that regulates genes involved in cell growth and differentiation by binding to a DNA motif known as a CArG box or serum response element [8]. SRF activity depends on changes in actin dynamics, resulting in alterations in the intracellular G-actin/F-actin ratio. Basically, when in response to various stimuli, such as serum deprivation, the Rho GTPase cascade is activated, actin polymerization increases, thereby reducing the amount of free G-actin to which the transcriptional cofactor MTRF-A is bound. This releases MRTF-A from G-actin and allows it to translocate to the nucleus where it binds and activates SRF. Thus, proteins regulating actin polymerization and altering the balance of polymerized F-actin and unpolymerized G-actin can influence SRF signaling. Similarly to PALLD, we found that also MYPN can bind to MRTF-A through its C-terminus and activate the MRTF-A/SRF pathway in muscle cells. In particular, we demonstrated that MYPN promotes SRF activity and increases MRTF-A activation of SRF in a dose dependent manner. However, further investigation is needed to determine whether MYPN activates SRF through its effect on actin polymerization or whether

it may also directly affect the shuttling of MRTF-A between the cytoplasm and the nucleus through its direct binding to MRTF-A.

To determine the functional role of MYPN *in vivo* both in skeletal and cardiac muscle, we generated and studied constitutive MYPN knockout mice. MKO mice had a normal life span, even though their body weight was significantly smaller compared to WT controls. Consistent with this, a reduction in skeletal muscle fiber size was observed in MKO mice at all stages. Consequently, isometric force generation and power output during isotonic shortening was found to be reduced in MKO muscle compared to WT as a result of the reduced fiber CSA in MKO muscle. On the other hand, the force developed by each myosin molecular motor was unaffected in the absence of MYPN, which was therefore not associated with alterations in the actomyosin interaction. Ultrastructural analyses of EDL muscle revealed progressive Z-line widening starting from around 8 months of age, demonstrating an important role of MYPN for the maintenance of Z-line assembly and integrity. Consistently, MKO mice were found to be more susceptible to eccentric exercise induced damage following downhill running as evidenced by the presence of Z-line damage and myofibers with centralized fibers in MKO muscle, whereas no damage or signs of regeneration was observed in muscles of WT mice subjected to the same exercise protocol.

To further investigate the effect of MYPN absence on skeletal muscle fiber size, we isolated skeletal muscle primary myoblasts from MKO and WT mice. Consistent with the absent expression of MYPN during proliferation, the myoblast proliferation rate was similar between MKO and WT cells. On the other hand, although no evidence of fusion defects were observed, differentiation of MKO cells resulted in significantly thinner myotubes compared to WT, thus capitulating the phenotype of MKO mouse muscle. At the molecular level, the reduced CSA in MKO muscle was associated with the downregulation of various genes involved in actin cytoskeleton organization and sarcomere assembly, including the actin isoforms and other SRF-target genes. Skeletal muscle specific deletion of SRF was previously shown to result in postnatal lethality due to a failure of muscle fibers to grow without affecting myoblast fusion [8]. Thus, reduced SRF activity due to the absence of MYPN may provide the molecular mechanism responsible for the reduced fiber size in MKO muscle compared to WT.

Interestingly, PAK1 expression was strongly increased in MKO muscle both at the RNA and protein level, while the PAK1 phosphorylation level was unchanged. In the literature, PAK1 is reported as an important regulator of actin dynamics through its

phosphorylation of LIM-kinase 1 (LIMK-1), which phosphorylates the actin-regulatory protein cofilin, preventing its interaction with actin and thereby stabilizing F-actin filaments [256]. This phosphorylation cascade results in cellular F-actin accumulation and G-actin reduction, which in turn stimulates SRF activity [257]. More studies are required to determine whether MYPN ablation directly or indirectly affects PAK1 expression and whether the upregulation of PAK1 may be a compensatory response to the reduced SRF signaling in MKO muscle.

In contrast to the MKO skeletal muscle phenotype, no alterations in cardiomyocyte size or Z-line width was found in the heart of MKO mice at any stage. In addition, no cardiac morphological or functional phenotype was evident at young age, while MKO mice developed progressive cardiac dilation and decreased fractional shortening starting from around 4 months of age. Conversely, in response to mechanical pressure overload induced by TAC in 10-week-old mice, although MKO mice exhibited a normal hypertrophic response, they quickly developed cardiac dilation and systolic dysfunction, associated with the activation of ERK1/2 and AKT as well as upregulation of CARP. The MAPK and AKT signaling pathways are known to play important roles in the regulation of heart function, and in particular stretch sensing [258]. In addition, CARP is strongly upregulated in response to various forms of stress and MYPN and CARP are thought to form a complex in the I-band involved in the transmission of stretch-induced signals from the sarcomere to the nucleus, affecting gene expression [3]. The relative weak basal phenotype of MKO mice compared to the severe effects of human mutations in the *MYPN* gene, leading to DCM, HCM, and RCM, suggests that the human mutations have dominant negative effects and that compensatory mechanisms may partially protect heart function in the complete absence of MYPN. A likely candidate is the major isoform of PALLD, which is highly similar in structure to MYPN, although this remains to be determined.

All together, these data demonstrate an important role of MYPN for normal heart function and its ablation results in the development of progressive DCM. Further investigation is required to determine the precise molecular mechanisms leading to the DCM phenotype as well as the potential involvement of SRF signaling in this process.

A better understanding of the role of MYPN in striated muscle structure and function, and the mechanisms underlying MYPN-based cardiomyopathies is the prerequisite for the future development of novel more targeted therapies.

# REFERENCES


1. Bang, M.L., et al., *Myopalladin, a novel 145-kilodalton sarcomeric protein with multiple roles in Z-disc and I-band protein assemblies.* J Cell Biol, 2001. **153**(2): p. 413-27.
2. von Nandelstadh, P., et al., *A class III PDZ binding motif in the myotilin and FATZ families binds enigma family proteins: a common link for Z-disc myopathies.* Molecular and cellular biology, 2009. **29**(3): p. 822-834.
3. Miller, M.K., et al., *The muscle ankyrin repeat proteins: CARP, ankrd2/Arpp and DARP as a family of titin filament-based stress response molecules.* J Mol Biol, 2003. **333**(5): p. 951-64.
4. Duboscq-Bidot, L., et al., *Mutations in the Z-band protein myopalladin gene and idiopathic dilated cardiomyopathy.* Cardiovascular research, 2008. **77**(1): p. 118-125.
5. Meyer, T., et al., *Novel mutations in the sarcomeric protein myopalladin in patients with dilated cardiomyopathy.* Eur J Hum Genet, 2013. **21**(3): p. 294-300.
6. Purevjav, E., et al., *Molecular Basis for Clinical Heterogeneity in Inherited Cardiomyopathies Due to Myopalladin Mutations.* Hum Mol Genet, 2012. **21**(9): p. 2039-53.
7. Balza, R.O. and R.P. Misra, *Role of the serum response factor in regulating contractile apparatus gene expression and sarcomeric integrity in cardiomyocytes.* Journal of Biological Chemistry, 2006. **281**(10): p. 6498-6510.
8. Li, S., et al., *Requirement for serum response factor for skeletal muscle growth and maturation revealed by tissue-specific gene deletion in mice.* Proc Natl Acad Sci U S A, 2005. **102**(4): p. 1082-7.
9. Miano, J.M., et al., *Restricted inactivation of serum response factor to the cardiovascular system.* Proceedings of the National Academy of Sciences of the United States of America, 2004. **101**(49): p. 17132-17137.
10. Niu, Z., et al., *Conditional mutagenesis of the murine serum response factor gene blocks cardiogenesis and the transcription of downstream gene targets.* Journal of Biological Chemistry, 2005. **280**(37): p. 32531-32538.
11. Parlakian, A., et al., *Temporally controlled onset of dilated cardiomyopathy through disruption of the SRF gene in adult heart.* Circulation, 2005. **112**(19): p. 2930-2939.
12. Alberts, B., et al., *Molecular Biology of the Cell (Garland, New York, 1994).* There is no corresponding record for this reference.
13. Parker, M.H., P. Seale, and M.A. Rudnicki, *Looking back to the embryo: defining transcriptional networks in adult myogenesis.* Nature Reviews Genetics, 2003. **4**(7): p. 497-507.
14. Aulehla, A. and O. Pourquié, *On periodicity and directionality of somitogenesis.* Anatomy and embryology, 2006. **211**(1): p. 3-8.
15. Biressi, S., M. Molinaro, and G. Cossu, *Cellular heterogeneity during vertebrate skeletal muscle development.* Developmental biology, 2007. **308**(2): p. 281-293.
16. Aulehla, A. and O. Pourquié, *Signaling gradients during paraxial mesoderm development.* Cold Spring Harbor perspectives in biology, 2010. **2**(2): p. a000869.
17. Cossu, G., S. Tajbakhsh, and M. Buckingham, *How is myogenesis initiated in the embryo?* Trends in Genetics, 1996. **12**(6): p. 218-223.
18. Miller, J.B., L. Schaefer, and J.A. Dominov, *Seeking muscle stem cells.* Current topics in developmental biology, 1998. **43**: p. 191-219.

19. Pirskanen, A., J.C. Kiefer, and S.D. Hauschka, *IGFs, insulin, Shh, bFGF, and TGF-β1 interact synergistically to promote somite myogenesis in vitro.* Developmental biology, 2000. **224**(2): p. 189-203.
20. Takahashi, Y., *Somitogenesis in vertebrate development.* eLS, 2001.
21. Gilbert, S.F., *Developmental Biology. Sunderland, MA*, 2000, Sinauer Associates, Inc.
22. Peachey, L. and B. Eisenberg, *Helicoids in the T system and striations of frog skeletal muscle fibers seen by high voltage electron microscopy.* Biophysical journal, 1978. **22**(2): p. 145.
23. Squire, J.M., *Architecture and function in the muscle sarcomere.* Current opinion in structural biology, 1997. **7**(2): p. 247-257.
24. Harvey, R.P., *Patterning the vertebrate heart.* Nature Reviews Genetics, 2002. **3**(7): p. 544-556.
25. Gregorio, C.C. and P.B. Antin, *To the heart of myofibril assembly.* Trends in cell biology, 2000. **10**(9): p. 355-362.
26. Olson, E.N. and D. Srivastava, *Molecular pathways controlling heart development.* Science, 1996. **272**(5262): p. 671.
27. Lough, J. and Y. Sugi, *Endoderm and heart development.* Developmental Dynamics, 2000. **217**(4): p. 327-342.
28. Marian, A. and R. Roberts, *The molecular genetic basis for hypertrophic cardiomyopathy.* Journal of molecular and cellular cardiology, 2001. **33**(4): p. 655-670.
29. Perriard, J.-C., A. Hirschy, and E. Ehler, *Dilated cardiomyopathy: a disease of the intercalated disc?* Trends in cardiovascular medicine, 2003. **13**(1): p. 30-38.
30. Sheikh, F., R.S. Ross, and J. Chen, *Cell-cell connection to cardiac disease.* Trends in cardiovascular medicine, 2009. **19**(6): p. 182-190.
31. Woodcock, E.A. and S.J. Matkovich, *Cardiomyocytes structure, function and associated pathologies.* The international journal of biochemistry & cell biology, 2005. **37**(9): p. 1746-1751.
32. Capetanaki, Y., *Desmin cytoskeleton in healthy and failing heart.* Heart failure reviews, 2000. **5**(3): p. 203-220.
33. Jamora, C. and E. Fuchs, *Intercellular adhesion, signalling and the cytoskeleton.* Nature cell biology, 2002. **4**(4): p. E101-E108.
34. Yamada, S., et al., *Deconstructing the cadherin-catenin-actin complex.* Cell, 2005. **123**(5): p. 889-901.
35. Norman, C., et al., *Isolation and properties of cDNA clones encoding SRF, a transcription factor that binds to the c-fos serum response element.* Cell, 1988. **55**(6): p. 989-1003.
36. Severs, N.J., et al., *Remodelling of gap junctions and connexin expression in diseased myocardium.* Cardiovascular research, 2008. **80**(1): p. 9-19.
37. Campbell, N., J. Reece, and L. Mitchell, *Biology, Edition*, 1999, Benjamin/Cummings, Menlo Park.
38. Cooke, R., *The actomyosin engine.* The FASEB journal, 1995. **9**(8): p. 636-642.
39. Squire, J., *The structural basis of muscular contraction Plenum Press.* New York, 1981: p. 168-171.
40. Dishmon, D.A., et al., *Hypovitaminosis D and valvular calcification in patients with dilated cardiomyopathy.* Am J Med Sci, 2009. **337**(5): p. 312-6.
41. Cooke, P., *A periodic cytoskeletal lattice in striated muscle*, in *Cell and muscle motility*. 1985, Springer. p. 287-313.

42. Huxley, H. *Structural changes in the actin-and myosin-eontaining filaments during contraction*. in *Cold Spring Harbor Symposia on Quantitative Biology*. 1973. Cold Spring Harbor Laboratory Press.
43. Gregorio, C.C., et al., *Muscle assembly: a titanic achievement?* Current opinion in cell biology, 1999. **11**(1): p. 18-25.
44. McElhinny, A.S., et al., *Nebulin: the nebulous, multifunctional giant of striated muscle.* Trends in cardiovascular medicine, 2003. **13**(5): p. 195-201.
45. Ono, S., *Dynamic regulation of sarcomeric actin filaments in striated muscle.* Cytoskeleton, 2010. **67**(11): p. 677-692.
46. Castillo, A., et al., *A nebulin ruler does not dictate thin filament lengths.* Biophys J, 2009. **96**(5): p. 1856-65.
47. Millevoi, S., et al., *Characterization of nebulette and nebulin and emerging concepts of their roles for vertebrate Z-discs.* J Mol Biol, 1998. **282**(1): p. 111-23.
48. Wang, K. and J. Wright, *Architecture of the sarcomere matrix of skeletal muscle: immunoelectron microscopic evidence that suggests a set of parallel inextensible nebulin filaments anchored at the Z line.* The Journal of cell biology, 1988. **107**(6): p. 2199-2212.
49. Sparrow, J.C. and F. Schöck, *The initial steps of myofibril assembly: integrins pave the way.* Nature Reviews Molecular Cell Biology, 2009. **10**(4): p. 293-298.
50. Tobacman, L.S., *Thin filament-mediated regulation of cardiac contraction.* Annual Review of Physiology, 1996. **58**(1): p. 447-481.
51. Phillips, G.N. and S. Chacko, *Mechanical properties of tropomyosin and implications for muscle regulation.* Biopolymers, 1996. **38**(1): p. 89-95.
52. Ohtsuki, I., K. Maruyama, and S. Ebashi, *Regulatory and cytoskeletal proteins of vertebrate skeletal muscle.* Adv Protein Chem, 1986. **38**: p. 1-67.
53. Bang, M.-L. and J. Chen, *Roles of Nebulin Family Members in the Heart.* Circulation Journal, 2015(0).
54. Pappas, C.T., et al., *The Nebulin family: an actin support group.* Trends in cell biology, 2011. **21**(1): p. 29-37.
55. Yamamoto, D.L., et al., *The nebulin SH3 domain is dispensable for normal skeletal muscle structure but is required for effective active load bearing in mouse.* Journal of cell science, 2013. **126**(23): p. 5477-5489.
56. Millevoi, S., et al., *Characterization of nebulette and nebulin and emerging concepts of their roles for vertebrate Z-discs.* Journal of molecular biology, 1998. **282**(1): p. 111-123.
57. Goicoechea, S.M., D. Arneman, and C.A. Otey, *The role of palladin in actin organization and cell motility.* Eur J Cell Biol, 2008. **87**(8-9): p. 517-25.
58. Ma, K. and K. Wang, *Interaction of nebulin SH3 domain with titin PEVK and myopalladin: implications for the signaling and assembly role of titin and nebulin.* FEBS Lett, 2002. **532**(3): p. 273-8.
59. Ma, K., et al., *Titin as a giant scaffold for integrating stress and Src homology domain 3-mediated signaling pathways: the clustering of novel overlap ligand motifs in the elastic PEVK segment.* J Biol Chem, 2006. **281**(37): p. 27539-56.
60. Witt, C.C., et al., *Nebulin regulates thin filament length, contractility, and Z-disk structure in vivo.* Embo J, 2006. **25**(16): p. 3843-55.
61. Li, B., L. Zhuang, and B. Trueb, *Zyxin interacts with the SH3 domains of the cytoskeletal proteins LIM-nebulette and Lasp-1.* J Biol Chem, 2004. **279**(19): p. 20401-10.

62. Takano, K., et al., *Nebulin and N-WASP cooperate to cause IGF-1-induced sarcomeric actin filament formation.* Science, 2010. **330**(6010): p. 1536-40.
63. Eulitz, S., et al., *Identification of Xin-repeat proteins as novel ligands of the SH3 domains of nebulin and nebulette and analysis of their interaction during myofibril formation and remodeling.* Mol Biol Cell, 2013. **24**(20): p. 3215-26.
64. Moncman, C.L. and K. Wang, *Functional dissection of nebulette demonstrates actin binding of nebulin-like repeats and Z-line targeting of SH3 and linker domains.* Cell Motil Cytoskeleton, 1999. **44**(1): p. 1-22.
65. Labeit, S. and B. Kolmerer, *The complete primary structure of human nebulin and its correlation to muscle structure.* J Mol Biol, 1995. **248**(2): p. 308-15.
66. Bonzo, J.R., et al., *The nebulette repeat domain is necessary for proper maintenance of tropomyosin with the cardiac sarcomere.* Exp Cell Res, 2008. **314**(19): p. 3519-30.
67. Holmes, W.B. and C.L. Moncman, *Nebulette interacts with filamin C.* Cell Motil Cytoskeleton, 2008. **65**(2): p. 130-42.
68. Marttila, M., et al., *Nebulin interactions with actin and tropomyosin are altered by disease-causing mutations.* Skelet Muscle, 2014. **4**: p. 15.
69. Ogut, O., M.M. Hossain, and J.P. Jin, *Interactions between nebulin-like motifs and thin filament regulatory proteins.* J Biol Chem, 2003. **278**(5): p. 3089-97.
70. Luo, G., et al., *Complete cDNA sequence and tissue localization of N-RAP, a novel nebulin-related protein of striated muscle.* Cell Motil Cytoskeleton, 1997. **38**(1): p. 75-90.
71. Mohiddin, S.A., et al., *Genomic organization, alternative splicing, and expression of human and mouse N-RAP, a nebulin-related LIM protein of striated muscle.* Cell Motil Cytoskeleton, 2003. **55**(3): p. 200-12.
72. Moncman, C.L. and K. Wang, *Nebulette: a 107 kD nebulin-like protein in cardiac muscle.* Cell Motil Cytoskeleton, 1995. **32**(3): p. 205-25.
73. Schreiber, V., et al., *Chromosomal assignment and expression pattern of the murine Lasp-1 gene.* Gene, 1998. **207**(2): p. 171-5.
74. Schreiber, V., et al., *Lasp-1, a novel type of actin-binding protein accumulating in cell membrane extensions.* Mol Med, 1998. **4**(10): p. 675-87.
75. Katoh, M., *Identification and characterization of LASP2 gene in silico.* Int J Mol Med, 2003. **12**(3): p. 405-10.
76. Terasaki, A.G., et al., *A novel LIM and SH3 protein (lasp-2) highly expressing in chicken brain.* Biochem Biophys Res Commun, 2004. **313**(1): p. 48-54.
77. Bang, M.L., et al., *Nebulin-deficient mice exhibit shorter thin filament lengths and reduced contractile function in skeletal muscle.* J Cell Biol, 2006. **173**(6): p. 905-16.
78. Gokhin, D.S., et al., *Reduced thin filament length in nebulin-knockout skeletal muscle alters isometric contractile properties.* Am J Physiol Cell Physiol, 2009. **296**(5): p. C1123-32.
79. Gokhin, D.S. and V.M. Fowler, *A two-segment model for thin filament architecture in skeletal muscle.* Nat Rev Mol Cell Biol, 2013. **14**(2): p. 113-9.
80. Littlefield, R.S. and V.M. Fowler, *Thin filament length regulation in striated muscle sarcomeres: Pointed-end dynamics go beyond a nebulin ruler.* Semin Cell Dev Biol, 2008. **19**(6): p. 511-9.
81. Ottenheijm, C.A., et al., *Thin filament length dysregulation contributes to muscle weakness in nemaline myopathy patients with nebulin deficiency.* Hum Mol Genet, 2009. **18**(13): p. 2359-69.
82. Pappas, C.T., P.A. Krieg, and C.C. Gregorio, *Nebulin regulates actin filament lengths by a stabilization mechanism.* J Cell Biol, 2010. **189**(5): p. 859-70.

83. Bang, M.L., et al., *Nebulin plays a direct role in promoting strong actin-myosin interactions.* Faseb J, 2009. **23**(12): p. 4117-25.
84. Ochala, J., et al., *Disrupted myosin cross-bridge cycling kinetics triggers muscle weakness in nebulin-related myopathy.* Faseb J, 2011. **25**(6): p. 1903-13.
85. Ottenheijm, C.A., et al., *Changes in cross-bridge cycling underlie muscle weakness in patients with tropomyosin 3-based myopathy.* Hum Mol Genet, 2011. **20**(10): p. 2015-25.
86. Ottenheijm, C.A., et al., *Sarcoplasmic reticulum calcium uptake and speed of relaxation are depressed in nebulin-free skeletal muscle.* Faseb J, 2008. **22**(8): p. 2912-9.
87. Tonino, P., et al., *Reduced myofibrillar connectivity and increased Z-disk width in nebulin-deficient skeletal muscle.* J Cell Sci, 2010. **123**(Pt 3): p. 384-91.
88. Wallgren-Pettersson, C., et al., *Mutations in the nebulin gene can cause severe congenital nemaline myopathy.* Neuromuscul Disord, 2002. **12**(7-8): p. 674-9.
89. Wallgren-Pettersson, C., et al., *Clinical and genetic heterogeneity in autosomal recessive nemaline myopathy.* Neuromuscul Disord, 1999. **9**(8): p. 564-72.
90. Maiellaro-Rafferty, K., et al., *Altered regional cardiac wall mechanics are associated with differential cardiomyocyte calcium handling due to nebulette mutations in preclinical inherited dilated cardiomyopathy.* J Mol Cell Cardiol, 2013. **60**: p. 151-60.
91. Purevjav, E., et al., *Nebulette mutations are associated with dilated cardiomyopathy and endocardial fibroelastosis.* J Am Coll Cardiol, 2010. **56**(18): p. 1493-502.
92. Mastrototaro, G., et al., *Nebulette knockout mice have normal cardiac function but show Z-line widening and upregulation of cardiac stress markers.* Cardiovascular research, 2015: p. cvv156.
93. Maruyama, K., et al., *Connectin, an elastic protein of muscle Characterization and Function.* Journal of biochemistry, 1977. **82**(2): p. 317-337.
94. Maruyama, K., F. MURAKAMI, and K. OHASHI, *Connectin, an Elastic Protein of Muscle Comparative Biochemistry.* Journal of biochemistry, 1977. **82**(2): p. 339-345.
95. Baharvand, H., et al., *The effect of extracellular matrix on embryonic stem cell-derived cardiomyocytes.* Journal of molecular and cellular cardiology, 2005. **38**(3): p. 495-503.
96. Camelliti, P., C. Green, and P. Kohl, *Structural and functional coupling of cardiac myocytes and fibroblasts*. Vol. 42. 2006: Karger Publishers.
97. Kostin, S., et al., *The internal and external protein scaffold of the T-tubular system in cardiomyocytes.* Cell and tissue research, 1998. **294**(3): p. 449-460.
98. Layland, J., R.J. Solaro, and A.M. Shah, *Regulation of cardiac contractile function by troponin I phosphorylation.* Cardiovascular research, 2005. **66**(1): p. 12-21.
99. McElhinny, A.S., et al., *Nebulin regulates the assembly and lengths of the thin filaments in striated muscle.* The Journal of cell biology, 2005. **170**(6): p. 947-957.
100. Schweitzer, S.C., et al., *Paranemin and the organization of desmin filament networks.* Journal of cell science, 2001. **114**(6): p. 1079-1089.
101. Solaro, R.J., *Remote control of A-band cardiac thin filaments by the IZI protein network of cardiac sarcomeres.* Trends in cardiovascular medicine, 2005. **15**(4): p. 148-152.
102. Gautel, M., et al., *The central Z-disk region of titin is assembled from a novel repeat in variable copy numbers.* Journal of Cell Science, 1996. **109**(11): p. 2747-2754.
103. Sorimachi, H., et al., *Tissue-specific expression and alpha-actinin binding properties of the Z-disc titin: implications for the nature of vertebrate Z-discs.* J Mol Biol, 1997. **270**(5): p. 688-95.

104. Ohtsuka, H., et al., *Binding of the N-terminal 63 kDa portion of connectin/titin to α-actinin as revealed by the yeast two-hybrid system.* FEBS letters, 1997. **401**(1): p. 65-67.
105. Turnacioglu, K.K., et al., *An N-terminal fragment of titin coupled to green fluorescent protein localizes to the Z-bands in living muscle cells: overexpression leads to myofibril disassembly.* Molecular biology of the cell, 1997. **8**(4): p. 705-717.
106. Young, P., et al., *Molecular structure of the sarcomeric Z - disk: two types of titin interactions lead to an asymmetrical sorting of α - actinin.* The EMBO journal, 1998. **17**(6): p. 1614-1624.
107. Gregorio, C.C., et al., *The NH2 terminus of titin spans the Z-disc: its interaction with a novel 19-kD ligand (T-cap) is required for sarcomeric integrity.* The Journal of cell biology, 1998. **143**(4): p. 1013-1027.
108. Mues, A., et al., *Two immunoglobulin-like domains of the Z-disc portion of titin interact in a conformation-dependent way with telethonin.* Febs Letters, 1998. **428**(1): p. 111-114.
109. D'Angelo, M. and M. Hetzer, *The role of the nuclear envelope in cellular organization.* Cellular and Molecular Life Sciences CMLS, 2006. **63**(3): p. 316-332.
110. Neunhäuserer, D., et al., *Human skeletal muscle: transition between fast and slow fibre types.* Pflügers Archiv-European Journal of Physiology, 2011. **461**(5): p. 537-543.
111. Thorstensson, A., et al., *Actomyosin ATPase, myokinase, CPK and LDH in human fast and slow twitch muscle fibres.* Acta Physiologica Scandinavica, 1977. **99**(2): p. 225-229.
112. Schiaffino, S. and C. Reggiani, *Myosin isoforms in mammalian skeletal muscle.* Journal of Applied Physiology, 1994. **77**(2): p. 493-501.
113. D'Antona, G., et al., *Skeletal muscle hypertrophy and structure and function of skeletal muscle fibres in male body builders.* The Journal of physiology, 2006. **570**(3): p. 611-627.
114. Harrison, B.C., D.L. Allen, and L.A. Leinwand, *IIb or not IIb? Regulation of myosin heavy chain gene expression in mice and men.* Skelet Muscle, 2011. **1**(1): p. 5.
115. Giger, J., et al., *Activity of the β-myosin heavy chain antisense promoter responds to diabetes and hypothyroidism.* American Journal of Physiology-Heart and Circulatory Physiology, 2007. **292**(6): p. H3065-H3071.
116. Luther, H.P., et al., *Characterization of naturally occurring myosin heavy chain antisense mRNA in rat heart.* Journal of cellular biochemistry, 1998. **70**(1): p. 110-120.
117. Pandorf, C.E., et al., *Dynamics of myosin heavy chain gene regulation in slow skeletal muscle role of natural antisense RNA.* Journal of Biological Chemistry, 2006. **281**(50): p. 38330-38342.
118. Rinaldi, C., et al., *Intergenic bidirectional promoter and cooperative regulation of the IIx and IIb MHC genes in fast skeletal muscle.* American Journal of Physiology-Regulatory, Integrative and Comparative Physiology, 2008. **295**(1): p. R208-R218.
119. Brown, D.M., T. Parr, and J.M. Brameld, *Myosin heavy chain mRNA isoforms are expressed in two distinct cohorts during C2C12 myogenesis.* Journal of muscle research and cell motility, 2012. **32**(6): p. 383-390.
120. Schiaffino, S. and C. Reggiani, *Fiber types in mammalian skeletal muscles.* Physiological reviews, 2011. **91**(4): p. 1447-1531.
121. Charge, S.B. and M.A. Rudnicki, *Cellular and molecular regulation of muscle regeneration.* Physiological reviews, 2004. **84**(1): p. 209-238.

122. Close, R., *Dynamic properties of mammalian skeletal muscles.* Physiol Rev, 1972. **52**(1): p. 129-197.
123. Huxley, H. and J. Hanson, *Changes in the cross-striations of muscle during contraction and stretch and their structural interpretation.* Nature, 1954(173): p. 973-6.
124. Huxley, A.F. and R. Niedergerke, *Structural changes in muscle during contraction.* Nature, 1954. **173**(4412): p. 971-973.
125. Holmes, K.C., *The actomyosin interaction and its control by tropomyosin.* Biophysical journal, 1995. **68**(4 Suppl): p. 2S.
126. Holmes, K.C., *The swinging lever-arm hypothesis of muscle contraction.* Current Biology, 1997. **7**(2): p. R112-R118.
127. Houdusse, A., et al., *Atomic structure of scallop myosin subfragment S1 complexed with MgADP: a novel conformation of the myosin head.* Cell, 1999. **97**(4): p. 459-470.
128. Cooke, R. and K.C. Holmes, *The Mechanism of Muscle Contractio.* CRC critical reviews in biochemistry, 1986. **21**(1): p. 53-118.
129. Gordon, A.M., E. Homsher, and M. Regnier, *Regulation of contraction in striated muscle.* Physiol Rev, 2000. **80**(2): p. 853-924.
130. Huxley, H., *The mechanism of muscular contraction.* Science, 1969. **164**(3886): p. 1356-1366.
131. Schmidt, T., *Lang (2000) Physiologie des Menschen*, Springer-Verlag. ISBN 3540667334.
132. Haselgrove, J. *X-ray evidence for a conformational change in the actin-containing filaments of vertebrate striated muscle*. in *Cold Spring Harbor Symposia on Quantitative Biology*. 1973. Cold Spring Harbor Laboratory Press.
133. Parry, D. and J. Squire, *Structural role of tropomyosin in muscle regulation: analysis of the x-ray diffraction patterns from relaxed and contracting muscles.* Journal of molecular biology, 1973. **75**(1): p. 33-55.
134. Al-Khayat, H.A., N. Yagi, and J.M. Squire, *Structural changes in actin-tropomyosin during muscle regulation: computer modelling of low-angle X-ray diffraction data.* Journal of molecular biology, 1995. **252**(5): p. 611-632.
135. Lehman, W., R. Craig, and P. Vibert, *Ca2+-induced tropomyosin movement in Limulus thin filaments revealed by three-dimensional reconstruction.* 1994.
136. Lehrer, S.S. and M.A. Geeves, *The muscle thin filament as a classical cooperative/allosteric regulatory system.* Journal of molecular biology, 1998. **277**(5): p. 1081-1089.
137. Zot, A.S. and J.D. Potter, *Structural aspects of troponin-tropomyosin regulation of skeletal muscle contraction.* Annual review of biophysics and biophysical chemistry, 1987. **16**(1): p. 535-559.
138. Bers, D.M., D.A. Eisner, and H.H. Valdivia, *Sarcoplasmic reticulum Ca2+ and heart failure roles of diastolic leak and Ca2+ transport.* Circulation Research, 2003. **93**(6): p. 487-490.
139. Hilgemann, D.W., *New insights into the molecular and cellular workings of the cardiac Na+/Ca2+ exchanger.* American Journal of Physiology-Cell Physiology, 2004. **287**(5): p. C1167-C1172.
140. Citi, S. and J. Kendrick - Jones, *Regulation of non - muscle myosin structure and function.* Bioessays, 1987. **7**(4): p. 155-159.
141. Sanger, J.W., et al., *How to build a myofibril.* J Muscle Res Cell Motil, 2005. **26**(6-8): p. 343-54.

142. Du, A., J.M. Sanger, and J.W. Sanger, *Cardiac myofibrillogenesis inside intact embryonic hearts.* Developmental biology, 2008. **318**(2): p. 236-246.
143. Sanger, J.W., et al., *Assembly and dynamics of myofibrils.* BioMed Research International, 2010. **2010**.
144. Frank, D., et al., *The sarcomeric Z-disc: a nodal point in signalling and disease.* J Mol Med, 2006. **84**(6): p. 446-68.
145. Luther, P.K., *The vertebrate muscle Z-disc: sarcomere anchor for structure and signalling.* J Muscle Res Cell Motil, 2009. **30**(5-6): p. 171-85.
146. Sheikh, F., et al., *"Z"eroing in on the role of Cypher in striated muscle function, signaling, and human disease.* Trends Cardiovasc Med, 2007. **17**(8): p. 258-62.
147. Epstein, H.F. and D.A. Fischman, *Molecular analysis of protein assembly in muscle development.* Science, 1991. **251**(4997): p. 1039-1044.
148. Holtzer, H., et al., *Independent Assembly of 1.6. MU. m Long Bipolar MHC Filaments and IZI Bodies.* Cell structure and function, 1997. **22**(1): p. 83-93.
149. Ojima, K., et al., *Initiation and maturation of IZI bodies in the growth tips of transfected myotubes.* Journal of Cell Science, 1999. **112**(22): p. 4101-4112.
150. Ehler, E., et al., *Myofibrillogenesis in the developing chicken heart: assembly of Z-disk, M-line and the thick filaments.* Journal of cell science, 1999. **112**(10): p. 1529-1539.
151. Blanchard, A., V. Ohanian, and D. Critchley, *The structure and function of α-actinin.* Journal of muscle research and cell motility, 1989. **10**(4): p. 280-289.
152. Goll, D.E., et al., *Studies on purified α-actinin: I. Effect of temperature and tropomyosin on the α-actinin/F-actin interaction.* Journal of molecular biology, 1972. **67**(3): p. 469-488.
153. Bang, M.L., C. Gregorio, and S. Labeit, *Molecular dissection of the interaction of desmin with the C-terminal region of nebulin.* J Struct Biol, 2002. **137**(1-2): p. 119-27.
154. Wright, J., Q.-Q. Huang, and K. Wang, *Nebulin is a full-length template of actin filaments in the skeletal muscle sarcomere: an immunoelectron microscopic study of its orientation and span with site-specific monoclonal antibodies.* Journal of Muscle Research & Cell Motility, 1993. **14**(5): p. 476-483.
155. Pappas, C.T., et al., *Nebulin interacts with CapZ and regulates thin filament architecture within the Z-disc.* Molecular biology of the cell, 2008. **19**(5): p. 1837-1847.
156. Conover, G.M., S.N. Henderson, and C.C. Gregorio, *A myopathy-linked desmin mutation perturbs striated muscle actin filament architecture.* Molecular biology of the cell, 2009. **20**(3): p. 834-845.
157. Luther, P.K., *Three-dimensional reconstruction of a simple Z-band in fish muscle.* J Cell Biol, 1991. **113**(5): p. 1043-55.
158. Luther, P.K., *Three-dimensional structure of a vertebrate muscle Z-band: implications for titin and alpha-actinin binding.* J Struct Biol, 2000. **129**(1): p. 1-16.
159. Yamaguchi, M., et al., *Fine structure of wide and narrow vertebrate muscle Z-lines: a proposed model and computer simulation of Z-line architecture.* Journal of molecular biology, 1985. **184**(4): p. 621-643.
160. Luther, P.K., J.S. Barry, and J.M. Squire, *The three-dimensional structure of a vertebrate wide (slow muscle) Z-band: lessons on Z-band assembly.* J Mol Biol, 2002. **315**(1): p. 9-20.
161. Luther, P.K., et al., *Heterogeneity of Z-band structure within a single muscle sarcomere: implications for sarcomere assembly.* Journal of molecular biology, 2003. **332**(1): p. 161-169.

162. Goldstein, M., et al., *Two structural states of Z-bands in cardiac muscle.* American Journal of Physiology-Heart and Circulatory Physiology, 1989. **256**(2): p. H552-H559.
163. Goldstein, M.A., et al., *Structural states in the Z band of skeletal muscle correlate with states of active and passive tension.* The Journal of general physiology, 1988. **92**(1): p. 113-119.
164. Pyle, W.G. and R.J. Solaro, *At the crossroads of myocardial signaling the role of Z-discs in intracellular signaling and cardiac function.* Circulation Research, 2004. **94**(3): p. 296-305.
165. Faulkner, G., G. Lanfranchi, and G. Valle, *Telethonin and other new proteins of the Z - disc of skeletal muscle.* IUBMB life, 2001. **51**(5): p. 275-282.
166. Clark, K.A., et al., *Striated muscle cytoarchitecture: an intricate web of form and function.* Annu Rev Cell Dev Biol, 2002. **18**: p. 637-706.
167. Frey, N., et al., *Mice lacking calsarcin-1 are sensitized to calcineurin signaling and show accelerated cardiomyopathy in response to pathological biomechanical stress.* Nature medicine, 2004. **10**(12): p. 1336-1343.
168. Knoll, R., et al., *The cardiac mechanical stretch sensor machinery involves a Z disc complex that is defective in a subset of human dilated cardiomyopathy.* Cell, 2002. **111**(7): p. 943-55.
169. Otey, C.A., et al., *Cytoplasmic Ig-domain proteins: cytoskeletal regulators with a role in human disease.* Cell Motil Cytoskeleton, 2009. **66**(8): p. 618-34.
170. Parast, M.M. and C.A. Otey, *Characterization of palladin, a novel protein localized to stress fibers and cell adhesions.* J Cell Biol, 2000. **150**(3): p. 643-56.
171. Rachlin, A.S. and C.A. Otey, *Identification of palladin isoforms and characterization of an isoform-specific interaction between Lasp-1 and palladin.* J Cell Sci, 2006. **119**(Pt 6): p. 995-1004.
172. Wang, H.V. and M. Moser, *Comparative expression analysis of the murine palladin isoforms.* Dev Dyn, 2008. **237**(11): p. 3342-51.
173. Ronty, M., et al., *Molecular analysis of the interaction between palladin and alpha-actinin.* FEBS Lett, 2004. **566**(1-3): p. 30-4.
174. Krcmery, J., et al., *Nucleocytoplasmic functions of the PDZ-LIM protein family: new insights into organ development.* Bioessays. **32**(2): p. 100-8.
175. Zheng, M., et al., *ALP/Enigma PDZ-LIM domain proteins in the heart.* J Mol Cell Biol. **2**(2): p. 96-102.
176. Gontier, Y., et al., *The Z-disc proteins myotilin and FATZ-1 interact with each other and are connected to the sarcolemma via muscle-specific filamins.* J Cell Sci, 2005. **118**(Pt 16): p. 3739-49.
177. Laure, L., et al., *A new pathway encompassing calpain 3 and its newly identified substrate cardiac ankyrin repeat protein is involved in the regulation of the nuclear factor-kappaB pathway in skeletal muscle.* FEBS J, 2010. **277**(20): p. 4322-37.
178. Salmikangas, P., et al., *Myotilin, the limb-girdle muscular dystrophy 1A (LGMD1A) protein, cross-links actin filaments and controls sarcomere assembly.* Human molecular genetics, 2003. **12**(2): p. 189-203.
179. Dixon, R.D., et al., *Palladin is an actin cross-linking protein that uses immunoglobulin-like domains to bind filamentous actin.* J Biol Chem, 2008. **283**(10): p. 6222-31.
180. Beck, M.R., et al., *Structure and function of palladin's actin binding domain.* Journal of molecular biology, 2013. **425**(18): p. 3325-3337.

181. Boukhelifa, M., et al., *A critical role for palladin in astrocyte morphology and response to injury.* Mol Cell Neurosci, 2003. **23**(4): p. 661-8.
182. Mykkanen, O.M., et al., *Characterization of human palladin, a microfilament-associated protein.* Mol Biol Cell, 2001. **12**(10): p. 3060-73.
183. Gammill, L.S. and M. Bronner-Fraser, *Genomic analysis of neural crest induction.* Development, 2002. **129**(24): p. 5731-5741.
184. Gultice, A.D., K.L. Selesniemi, and T.L. Brown, *Hypoxia inhibits differentiation of lineage-specific Rcho-1 trophoblast giant cells.* Biology of reproduction, 2006. **74**(6): p. 1041-1050.
185. Wall, M.E., et al., *Human adipose-derived adult stem cells upregulate palladin during osteogenesis and in response to cyclic tensile strain.* Am J Physiol Cell Physiol, 2007. **293**(5): p. C1532-8.
186. Alcorn, J.F., et al., *Jun N-terminal kinase 1 regulates epithelial-to-mesenchymal transition induced by TGF-β1.* Journal of cell science, 2008. **121**(7): p. 1036-1045.
187. Jin, L., et al., *Angiotensin II, focal adhesion kinase, and PRX1 enhance smooth muscle expression of lipoma preferred partner and its newly identified binding partner palladin to promote cell migration.* Circ Res, 2007. **100**(6): p. 817-25.
188. Jin, L., et al., *The actin-associated protein Palladin is required for development of normal contractile properties of smooth muscle cells derived from embryoid bodies.* J Biol Chem, 2009. **284**(4): p. 2121-30.
189. Goicoechea, S., et al., *Palladin binds to Eps8 and enhances the formation of dorsal ruffles and podosomes in vascular smooth muscle cells.* J Cell Sci, 2006. **119**(Pt 16): p. 3316-24.
190. Olson, E.N. and A. Nordheim, *Linking actin dynamics and gene transcription to drive cellular motile functions.* Nature reviews Molecular cell biology, 2010. **11**(5): p. 353-365.
191. Kolb, S.J. and J.T. Kissel, *Spinal muscular atrophy: a timely review.* Archives of neurology, 2011. **68**(8): p. 979-984.
192. Pollard, T.D., *Regulation of actin filament assembly by Arp2/3 complex and formins.* Annu. Rev. Biophys. Biomol. Struct., 2007. **36**: p. 451-477.
193. Posern, G. and R. Treisman, *Actin'together: serum response factor, its cofactors and the link to signal transduction.* Trends in cell biology, 2006. **16**(11): p. 588-596.
194. Vartiainen, M.K., et al., *Nuclear actin regulates dynamic subcellular localization and activity of the SRF cofactor MAL.* Science, 2007. **316**(5832): p. 1749-1752.
195. Miano, J.M., X. Long, and K. Fujiwara, *Serum response factor: master regulator of the actin cytoskeleton and contractile apparatus.* American Journal of Physiology-Cell Physiology, 2007. **292**(1): p. C70-C81.
196. Wang, Z., et al., *Myocardin and ternary complex factors compete for SRF to control smooth muscle gene expression.* Nature, 2004. **428**(6979): p. 185-189.
197. Zaromytidou, A.-I., F. Miralles, and R. Treisman, *MAL and ternary complex factor use different mechanisms to contact a common surface on the serum response factor DNA-binding domain.* Molecular and cellular biology, 2006. **26**(11): p. 4134-4148.
198. Buchwalter, G., C. Gross, and B. Wasylyk, *Ets ternary complex transcription factors.* Gene, 2004. **324**: p. 1-14.
199. Dalton, S. and R. Treisman, *Characterization of SAP-1, a protein recruited by serum response factor to the c-fos serum response element.* Cell, 1992. **68**(3): p. 597-612.
200. Hipskind, R., et al., *Ets-related protein Elk-1 is homologous to the c-fos regulatory factor p62TCF.* 1991.

201. Parmacek, M.S., *Myocardin-Related Transcription Factors Critical Coactivators Regulating Cardiovascular Development and Adaptation.* Circulation research, 2007. **100**(5): p. 633-644.
202. Pipes, G.T., E.E. Creemers, and E.N. Olson, *The myocardin family of transcriptional coactivators: versatile regulators of cell growth, migration, and myogenesis.* Genes & development, 2006. **20**(12): p. 1545-1556.
203. Wang, D.-Z., et al., *Activation of cardiac gene expression by myocardin, a transcriptional cofactor for serum response factor.* Cell, 2001. **105**(7): p. 851-862.
204. Wang, D.-Z., et al., *Potentiation of serum response factor activity by a family of myocardin-related transcription factors.* Proceedings of the National Academy of Sciences, 2002. **99**(23): p. 14855-14860.
205. Muehlich, S., et al., *Serum-induced phosphorylation of the serum response factor coactivator MKL1 by the extracellular signal-regulated kinase 1/2 pathway inhibits its nuclear localization.* Molecular and cellular biology, 2008. **28**(20): p. 6302-6313.
206. Gineitis, D. and R. Treisman, *Differential usage of signal transduction pathways defines two types of serum response factor target gene.* Journal of Biological Chemistry, 2001. **276**(27): p. 24531-24539.
207. Shaw, P.E., H. Schröter, and A. Nordheim, *The ability of a ternary complex to form over the serum response element correlates with serum inducibility of the human c-fos promoter.* Cell, 1989. **56**(4): p. 563-572.
208. Fielitz, J., et al., *Loss of muscle-specific RING-finger 3 predisposes the heart to cardiac rupture after myocardial infarction.* Proceedings of the National Academy of Sciences, 2007. **104**(11): p. 4377-4382.
209. Touvron, M., et al., *Locally expressed IGF1 propeptide improves mouse heart function in induced dilated cardiomyopathy by blocking myocardial fibrosis and SRF-dependent CTGF induction.* Disease models & mechanisms, 2012. **5**(4): p. 481-491.
210. Han, Z., et al., *A myocardin-related transcription factor regulates activity of serum response factor in Drosophila.* Proceedings of the National Academy of Sciences of the United States of America, 2004. **101**(34): p. 12567-12572.
211. Miralles, F., et al., *Actin dynamics control SRF activity by regulation of its coactivator MAL.* Cell, 2003. **113**(3): p. 329-342.
212. Kuwahara, K., et al., *Muscle-specific signaling mechanism that links actin dynamics to serum response factor.* Molecular and cellular biology, 2005. **25**(8): p. 3173-3181.
213. Jin, L., et al., *The actin associated protein palladin is important for the early smooth muscle cell differentiation.* PLoS One, 2010. **5**(9): p. e12823.
214. Hwang, P.M. and B.D. Sykes, *Targeting the sarcomere to correct muscle function.* Nature Reviews Drug Discovery, 2015. **14**(5): p. 313-328.
215. Bagnall, R.D., L. Yeates, and C. Semsarian, *Analysis of the Z-disc genes PDLIM3 and MYPN in Patients with Hypertrophic Cardiomyopathy.* International journal of cardiology, 2010. **145**(3): p. 601-602.
216. Maron, B.J., *Hypertrophic cardiomyopathy: a systematic review.* Jama, 2002. **287**(10): p. 1308-1320.
217. McNally, E.M., J.R. Golbus, and M.J. Puckelwartz, *Genetic mutations and mechanisms in dilated cardiomyopathy.* The Journal of clinical investigation, 2013. **123**(123 (1)): p. 19-26.
218. Morimoto, S., *Sarcomeric proteins and inherited cardiomyopathies.* Cardiovascular research, 2008. **77**(4): p. 659-666.

219. Huby, A.-C., et al., *Disturbance in Z-disk mechanosensitive proteins induced by a persistent mutant myopalladin causes familial restrictive cardiomyopathy.* Journal of the American College of Cardiology, 2014. **64**(25): p. 2765-2776.
220. Otey, C.A., et al., *The palladin/myotilin/myopalladin family of actin-associated scaffolds.* Int Rev Cytol, 2005. **246**: p. 31-58.
221. Parlakian, A., et al., *Targeted inactivation of serum response factor in the developing heart results in myocardial defects and embryonic lethality.* Molecular and cellular biology, 2004. **24**(12): p. 5281-5289.
222. Tanaka, N., et al., *Transthoracic echocardiography in models of cardiac disease in the mouse.* Circulation, 1996. **94**(5): p. 1109-1117.
223. Burkholder, T.J., et al., *Relationship between muscle fiber types and sizes and muscle architectural properties in the mouse hindlimb.* J Morphol, 1994. **221**(2): p. 177-90.
224. Hill, A.V., *The heat of shortening and the dynamic constants of muscle.* Proc R Soc Lond B Biol Sci, 1938. **126**: p. 136-195.
225. Linari, M., et al., *Stiffness and fraction of Myosin motors responsible for active force in permeabilized muscle fibers from rabbit psoas.* Biophys J, 2007. **92**(7): p. 2476-90.
226. Linari, M., et al., *The mechanism of the force response to stretch in human skinned muscle fibres with different myosin isoforms.* J Physiol, 2004. **554**(Pt 2): p. 335-52.
227. Vydyanath, A., et al., *Axial distribution of myosin binding protein-C is unaffected by mutations in human cardiac and skeletal muscle.* Journal of muscle research and cell motility, 2012. **33**(1): p. 61-74.
228. Zhang, J., et al., *Syncoilin is required for generating maximum isometric stress in skeletal muscle but dispensable for muscle cytoarchitecture.* American Journal of Physiology-Cell Physiology, 2008. **294**(5): p. C1175-C1182.
229. Barash, I.A., et al., *Structural and regulatory roles of muscle ankyrin repeat protein family in skeletal muscle.* American Journal of Physiology-Cell Physiology, 2007. **293**(1): p. C218-C227.
230. Brodie, C. and S.R. Sampson, *Nerve growth factor and fibroblast growth factor influence post-fusion expression of Na-channels in cultured rat skeletal muscle.* J Cell Physiol, 1990. **144**(3): p. 492-7.
231. Salic, A. and T.J. Mitchison, *A chemical method for fast and sensitive detection of DNA synthesis in vivo.* Proceedings of the National Academy of Sciences, 2008. **105**(7): p. 2415-2420.
232. Breinbauer, R. and M. Köhn, *Azide–alkyne coupling: a powerful reaction for bioconjugate chemistry.* ChemBioChem, 2003. **4**(11): p. 1147-1149.
233. Kolb, H.C., M. Finn, and K.B. Sharpless, *Click chemistry: diverse chemical function from a few good reactions.* Angewandte Chemie International Edition, 2001. **40**(11): p. 2004-2021.
234. Rostovtsev, V.V., et al., *A stepwise huisgen cycloaddition process: copper (I) - catalyzed regioselective "ligation" of azides and terminal alkynes.* Angewandte Chemie, 2002. **114**(14): p. 2708-2711.
235. Wang, Q., et al., *Bioconjugation by copper (I)-catalyzed azide-alkyne [3+ 2] cycloaddition.* Journal of the American Chemical Society, 2003. **125**(11): p. 3192-3193.
236. Chien, C.-T., et al., *The two-hybrid system: a method to identify and clone genes for proteins that interact with a protein of interest.* Proceedings of the National Academy of Sciences, 1991. **88**(21): p. 9578-9582.
237. Fields, S. and O.-k. Song, *A novel genetic system to detect protein protein interactions.* 1989.

238. Abazov, V.M., et al., *Search for Wbb and WH production in pp collisions at square root [s]=1.96 TeV.* Phys Rev Lett, 2005. **94**(9): p. 091802.
239. Studier, F.W., *Protein production by auto-induction in high-density shaking cultures.* Protein expression and purification, 2005. **41**(1): p. 207-234.
240. Dixon, R.D., et al., *Palladin is an actin cross-linking protein that uses immunoglobulin-like domains to bind filamentous actin.* Journal of Biological Chemistry, 2008. **283**(10): p. 6222-6231.
241. Spudich, J.A. and S. Watt, *The regulation of rabbit skeletal muscle contraction I. Biochemical studies of the interaction of the tropomyosin-troponin complex with actin and the proteolytic fragments of myosin.* Journal of Biological Chemistry, 1971. **246**(15): p. 4866-4871.
242. Abràmoff, M.D., P.J. Magalhães, and S.J. Ram, *Image processing with ImageJ.* Biophotonics international, 2004. **11**(7): p. 36-42.
243. Cooper, J.A., S.B. Walker, and T.D. Pollard, *Pyrene actin: documentation of the validity of a sensitive assay for actin polymerization.* Journal of Muscle Research & Cell Motility, 1983. **4**(2): p. 253-262.
244. Livak, K.J. and T.D. Schmittgen, *Analysis of relative gene expression data using real-time quantitative PCR and the 2− ΔΔCT method.* methods, 2001. **25**(4): p. 402-408.
245. Gentleman, R.C., et al., *Bioconductor: open software development for computational biology and bioinformatics.* Genome biology, 2004. **5**(10): p. R80.
246. Robinson, M.D., D.J. McCarthy, and G.K. Smyth, *edgeR: a Bioconductor package for differential expression analysis of digital gene expression data.* Bioinformatics, 2010. **26**(1): p. 139-140.
247. Benjamini, Y. and Y. Hochberg, *Controlling the false discovery rate: a practical and powerful approach to multiple testing.* Journal of the Royal Statistical Society. Series B (Methodological), 1995: p. 289-300.
248. Eisen, M.B., et al., *Cluster analysis and display of genome-wide expression patterns.* Proceedings of the National Academy of Sciences, 1998. **95**(25): p. 14863-14868.
249. Bradford, M.M., *A rapid and sensitive method for the quantitation of microgram quantities of protein utilizing the principle of protein-dye binding.* Analytical biochemistry, 1976. **72**(1): p. 248-254.
250. Towbin, H., T. Staehelin, and J. Gordon, *Electrophoretic transfer of proteins from polyacrylamide gels to nitrocellulose sheets: procedure and some applications.* Proceedings of the National Academy of Sciences, 1979. **76**(9): p. 4350-4354.
251. Yuan, J.S., et al., *Statistical analysis of real-time PCR data.* BMC bioinformatics, 2006. **7**(1): p. 85.
252. Endlich, N., et al., *Palladin is a dynamic actin-associated protein in podocytes.* Kidney Int, 2009. **75**(2): p. 214-26.
253. Huxley, A.F. and R.M. Simmons, *Proposed mechanism of force generation in striated muscle.* Nature, 1971. **233**(5321): p. 533-538.
254. Sells, M.A., et al., *Human p21-activated kinase (Pak1) regulates actin organization in mammalian cells.* Current Biology, 1997. **7**(3): p. 202-210.
255. Boukhelifa, M., et al., *A critical role for palladin in astrocyte morphology and response to injury.* Molecular and Cellular Neuroscience, 2003. **23**(4): p. 661-668.
256. Edwards, D.C., et al., *Activation of LIM-kinase by Pak1 couples Rac/Cdc42 GTPase signalling to actin cytoskeletal dynamics.* Nature cell biology, 1999. **1**(5): p. 253-259.
257. Sotiropoulos, A., et al., *Signal-regulated activation of serum response factor is mediated by changes in actin dynamics.* Cell, 1999. **98**(2): p. 159-169.

258. Gerilechaogetu, F., et al., *Mechanosensing and Regulation of Cardiac Function.* J Clin Exp Cardiolog, 2014. **5**(314): p. 2.

# ACKNOWLEDGMENTS

This study was carried out at the Sarcomeres in Cardiac Pathologies laboratory at the Humanitas Research Hospital in Rozzano (Milan), Italy from September 2012 to November 2015. The work was financially supported by the Telethon Foundation, Italy (GGP1228) and the Italian Ministry of Education, Universities and Research (PRIN 2010-2011 no. 2010R8JK2X_006).

I wish to thank all the people, who have supported me and made the completion of this thesis possible.

First of all, I would like to express my gratitude to my tutor Dr. Marie-Louise Bang, who gave me the opportunity to work in her group and who guided me throughout my PhD studies. Her intensive support and scientific knowledge were precious for the success of my work.
I am also grateful to Prof. Gianlugi Condorelli and Prof. Massimo Locati for agreeing to be my supervisors at the University of Milan

Thanks to all the past and present members of the laboratory for the their help, support, and pleasant working atmosphere. Especially, I wish to thank Dr. Daniel Yamamoto, who performed the initial analyses of the myopalladin knockout mice before I joined the lab, my colleague Dr. Giuseppina Mastrototaro, who helped me with the cell culture experiments, and the animal surgeon Pierluigi Carullo for performing the numerous *in vivo* experiments.

I am very grateful to our collaborators, without whom this project would not have been possible. Especially, I would like to thank Prof. Ju Chen at the University of California San Diego in whose lab the myopalladin knockout mice were originally generated, Prof. Marco Linari at the University of Florence for the muscle biomechanical analyses, and Prof. Vincenzo Nigro at the Second University of Naples and the Telethon Institute of Genetics and Medicine (TIGEM) in Pozzuoli (Naples) for the RNA-sequencing

I would also like to thank to my thesis reviewers Prof. Mathias Gautel and Prof. Wolfgang Linke for assigning your precious time to evaluate my thesis.

I thank my parents for the strength and education that you provide me. I am sincerely grateful for the hard work and fighting spirit inherited from them. Vittoria, thank you for your friendship, never-ending patience, and support in these years. I'll never forget it!

Finally, I would like to dedicate this work to the memory of my aunt Gina. I miss you so lot!